Universitat Autònoma de Barcelona

Functional characterization of the connection between the circadian clock and the DNA damage and repair response in Arabidopsis thaliana

Sergio Gil Rodríguez

Universitat Autònoma de Barcelona

CRAG CENTRE FOR RESEARCH IN AGRICULTURAL GENOMICS

Functional characterization of the connection between the circadian clock and the DNA damage and repair response in *Arabidopsis thaliana*

PhD Thesis

Sergio Gil Rodríguez

Barcelona, 2019

Universitat Autònoma de Barcelona

CRAG CENTRE FOR RESEARCH IN AGRICULTURAL GENOMICS

Facultad de Biociencias

Departamento de Biología Animal, Biología Vegetal y Ecología

Programa de Doctorado en Biología y Biotecnología Vegetal

Functional characterization of the connection between the circadian clock and the DNA damage and repair response in *Arabidopsis thaliana*

Memoria presentada por Sergio Gil Rodríguez para optar por el título de doctor por la Universitat Autònoma de Barcelona

Directora

Dra. Paloma Mas Martínez

Doctorando

Sergio Gil Rodríguez

Barcelona, 2019

“Would you tell me, please, which way I ought to go from here?’
‘That depends a good deal on where you want to get to’, said the Cat.
‘I don't much care where…’said Alice.
‘Then it doesn't matter which way you go’, said the Cat.
‘…so long as I get SOMEWHERE’, Alice added as an explanation.
‘Oh, you're sure to do that’, said the Cat, ‘if you only walk long enough.”

Alice in Wonderland, Lewis Carroll 1865

ACKNOWLEDGMENTS

Durante estos 4 años de tesis doctoral que he desarrollado en el CRAG he aprendido muchas cosas del gran mundo de la ciencia tanto a nivel académico como personal. No me cabe la menor duda que nada de esto habría sido posible sin el papel fundamental que han tenido muchas personas durante mi doctorado. Gracias a ellos he podido disfrutar de esta etapa a pesar de los momentos agrios y difíciles.

Primero de todo me gustaría agradecer a mi directora de tesis la Prof. Dra. Paloma Mas por su apoyo y dedicación incondicional a este gran proyecto en el que hemos trabajado conjuntamente. Por todas las ideas e inquietudes científicas que hemos compartido en nuestras largas reuniones. Gracias por permitirme hacer ciencia.

A mis compañeros Gastón Pizzio, Luis Manuel Cervela y Jorge Alberto Fung. Casi comenzamos esta aventura al mismo tiempo y desde entonces me habéis ayudado y acompañado en todo momento, sobre todo cuando las cosas no han ido como esperábamos. Gracias por todos los momentos que hemos compartido dentro y fuera del lab. Recordaré todos aquellos *time courses* que hemos realizado juntos y que acabábamos sin saber dónde estábamos. Por amenizar el ambiente en el laboratorio y por todas aquellas interminables conversaciones intentando arreglar el mundo. Gracias por hacerme sentir parte del grupo. Ya decían que si quieres llegar rápido camina solo, pero si quieres llegar lejos hazlo en grupo.

Special thanks to Manjul Singh and Aditi Gupta. You both came at later stages of my PhD but slowly became one of the most important supports in my PhD. Thanks for all the great scientific discussions, and all the funny activities we shared outside of the lab including escape rooms and cool journeys. I'm sure you both will become great head-researchers very soon and I'll be there to see it.

A mis amigos de otros laboratorios en especial a Marisa Domingo, Cristina Vives, Crina Popa y Laura Ossorio. Gracias por todas las reuniones, celebraciones, cafés y escapadas rurales que hemos compartido y por todos los consejos.

Gracias a todas las personas que me han ayudado desde los servicios del CRAG de invernaderos, genómica, microscopia y compras especialmente a Glòria, Pilar, Sergio, Alejandro, Joanna, Montse y Mario.

Por último, agradecer el papel crucial de mi familia y mis amigos en todo momento durante estos 4 años. En especial, a mis padres Ana Rodríguez y Vicente Gil, mi hermano Vicente Gil y a Kora por el apoyo incondicional, los ánimos y la paciencia que han tenido y tienen conmigo. Gracias por estar siempre ahí, por aguantarme y por no dejar de creer en mí.

TABLE OF CONTENTS

Table of contents

INTRODUCTION

Introduction

1. Overview of circadian rhythms

From the beginning of life in our planet, nearly all living organisms have been exposed to external environmental changes imposed by the daily rotation of the Earth. In order to properly adapt to these environmental changes, organisms have developed an internal timekeeping mechanism known as the circadian clock ("*circa*"≈ approximately, "*diēs*"≈ day) (Gerhart-Hines & Lazar, 2015). The circadian clock is present in practically all organisms and synchronizes growth, physiology and metabolism in tune with the 24-hour environmental changes. This synchronization has been proposed to enhance the organism's fitness and survival (Takahashi, 2017, Dubowy & Sehgal, 2017, Nohales & Kay, 2016). Dysfunction of this internal clock has severe defects in the proper synchronization of many biological processes including among many others the sleep/wake cycles in mammals or the stomatal movements in plants (Figure 1) (Zhu & Zee, 2012, Hassidim et al., 2017).

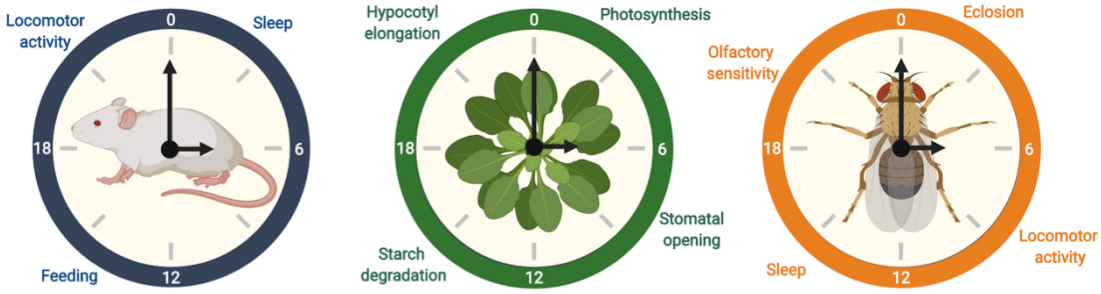

Figure 1. Schematic diagram of the biological processes controlled by the circadian clock in different model organisms. *Mus musculus* (left), *Arabidopsis thaliana* (center), *Drosophila melanogaster* (right). Created with BioRender.

One of the first reported descriptions of the circadian rhythmicity was made in the 18th century by the French astronomer Jean-Jacques Dortous de Mairan, who realized that when the plant *Mimosa Pudica* was deprived of the light:dark cycles, the leaves still continued moving rhythmically (J., 1729). This observation suggested the existence of an endogenous mechanism responsible of the rhythmic movements. Research over the years have confirmed the presence of this internal mechanism or circadian clock

and have led to the identification of the main components and mechanisms of function in many organisms (Kumar & Sharma, 2018). Moreover, several studies have established common features shared among the clocks display in different organisms: 1) circadian rhythms describe oscillations on a 24-hour basis even in absence of rhythmic environmental cues; 2) the rhythms are daily synchronized or entrained by the environmental changes throughout the light/dark cycles, and 3) the endogenous clock buffers a wide range of physiological temperatures and thus maintains robust rhythms with similar period, what is known as temperature compensation (Bodenstein et al., 2012).

2. Circadian clock organization and function

The circadian clocks are classically divided into three main pathways: input, the central oscillator and output. The input pathway senses the daily changes in the surrounding environment through specific clock components and transmits the information to the central oscillator. The central oscillator in turn generates 24-h oscillations in multiple biological processes known as outputs, including among many others, feeding behavior, nutrient transport or cell growth (Nohales & Kay, 2016, Takahashi, 2017). These three functional pathways are a rather simplified view of the circadian system as the real functioning of the clock is much more complex. Overall, the basis of the circadian timekeeping relies on the accurate regulation among key clock components, which regulate each other following transcription-translation feedback loops (Brown et al., 2012). Genetic and molecular studies have shown that this regulation by negative feedback loops is present in many but not all organisms (Kumar & Sharma, 2018, Doherty & Kay, 2010).

Relevant studies have uncovered the organization of the circadian system within cells, tissues and organs all the way to the whole organism. In mammals and also in plants, the circadian clock has a hierarchical organization, coordinated by a master clock (Honma, 2018, Inoue et al., 2018). The master clock cells located at the suprachiasmatic nucleus (SCN) in mammals (Mohawk et al., 2012) and at the shoot apex in plants (Takahashi et al., 2015) display a very strong communication or coupling

that provides robustness to the rhythms. Clock function at the master clocks is important in the control of the circadian rhythms in distal parts of the organisms (Takahashi et al., 2015, Endo et al., 2014).

3. The plant circadian clock

As sessile organisms, plants have developed unique strategies to rapidly adapt to their surrounding environment (Sanchez & Kay, 2016). In this context, the circadian clock in plants has been shown to play a crucial role for optimum fitness and survival (Sanchez & Kay, 2016). The plant circadian clock has been extensively studied in the model system *Arabidopsis thaliana* (Sanchez & Kay, 2016). However, over the past recent years, numerous studies have begun to unravel the circadian function in other plant species, including crops of agronomical interest (Bendix et al., 2015). Similar to other circadian systems, the Arabidopsis circadian central oscillator is synchronized every day by environmental input pathways and controls the rhythms of multiple clock outputs (Figure 2).

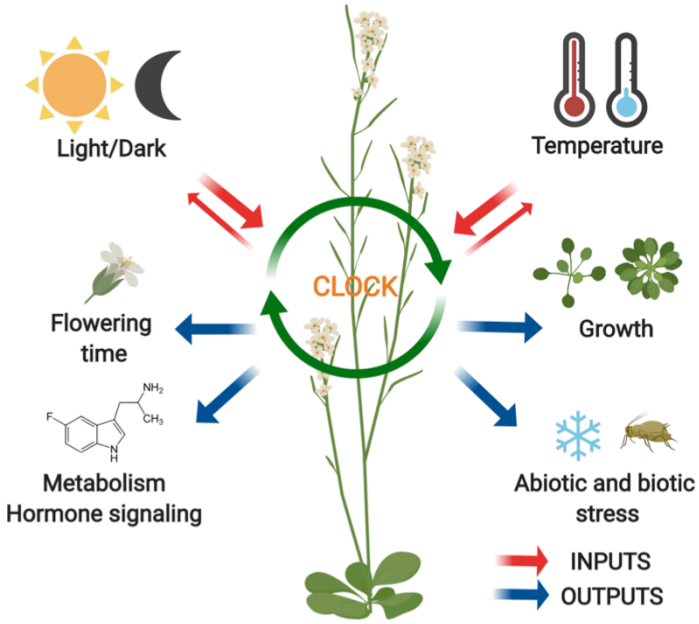

Figure 2. Schematic diagram of the circadian clock in *Arabidopsis thaliana*. Daily environmental changes in light and temperature are perceived and transmitted to the central oscillator by the input pathways. In turn, the central oscillator generates proper rhythms in many different output pathways to synchronize the organism with the surrounding environment. Created with BioRender

3.1. Circadian input pathways in plants

The plant circadian clock is entrained by diurnal changes in light and temperature, which provide crucial information to daily reset the endogenous clock (Inoue et al., 2017). Other cues, such as metabolic signals might also act as inputs to the clock (Haydon et al., 2015). The central oscillator can in turn modulate the way these input signals are perceived (Figure 2), and thus enabling accurate synchrony of the biological processes. In the following sections, we particularly focus on the light input to the clock and the function of *CRY2* regulating plant growth and circadian rhythms.

3.1.1. Light input to the clock

The light entrainment of the clock is a well-established feature in nearly all diurnal organisms (Yoshii et al., 2016, Hastings et al., 2019), and in the context of plants is mediated via specific photoreceptors, including phytochromes, cryptochromes, phototropins and members of the ZEITLUPE (ZTL) family (Inoue et al., 2017). These photoreceptors perceive and respond to specific light stimuli: while phytochromes mostly sense red/far-red light changes; cryptochromes, phototropins and the ZTL family are involved in the blue/ultraviolet A (UV-A) light responses (Figure 3) (Inoue et al., 2017). In addition, plants can also respond to the UV-B radiation through the UV RESISTANCE LOCUS 8 (UVR8) photoreceptor (Tilbrook et al., 2013). In tune with their function synchronizing the clock, the specific light perception by the photoreceptors directly regulates crucial light-dependent biological processes such as shade-avoidance, germination, and phototropism (Mawphlang & Kharshiing, 2017). The interaction among different photoreceptors has been shown to be essential for accurate light-responses (Inoue et al., 2017).

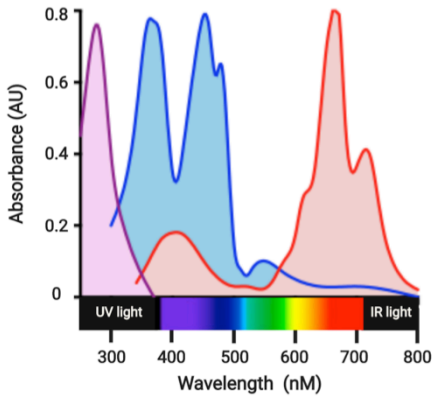

Figure 3. Diagram showing absorption spectra of the different plant photoreceptors. Shade colored areas correlate with the specific photoreceptors absorption spectra; phytochromes (red), cryptochromes and phototropins (blue), and UVR8 (purple). UV: Ultraviolet. IR: Infrared

In addition to their oscillatory pattern of expression (Harmer et al., 2000), cryptochromes and phytochromes are involved in the daily resetting of the central oscillator by regulating the period length of the clock in a light intensity-dependent manner (McWatters & Devlin, 2011). This direct correlation was initially observed by the biologist Jürgen Aschoff (Aschoff), who enunciated the Aschoff's rule: as the light intensity increases, the period length of the clock shortens (Figure 4).

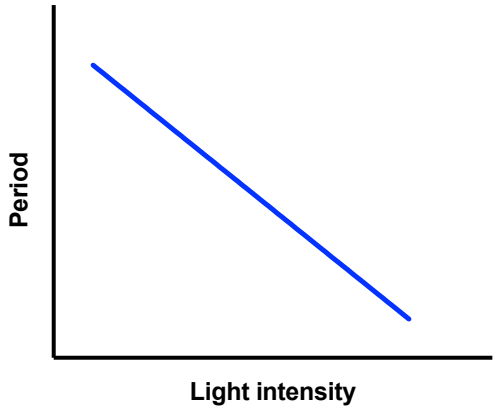

Figure 4. Diagram showing the Aschoff's rule. Increasing light intensities shortens the period length, while decreasing light intensity results in lengthening of the circadian rhythms.

Changes in the light fluence rate promote phase shifts (shift to an earlier or later phase), as a result of altered input signals of the photoreceptors to the clock (McWatters & Devlin, 2011). Mutations in the cryptochromes and phytochromes lead to period lengthening under blue and red light, respectively (Devlin & Kay, 2000, Bauer

et al., 2004). The responses of the clock to light differ between diurnal and nocturnal organisms, displaying particular resetting responses in a time-dependent manner. In Arabidopsis, as a diurnal organism, light perturbations during the morning promote an advanced phase of the clock, whereas light pulses at night lead to a delayed phase. The clock displays a particular feature known as gating that allows specific responses to diurnal changes or stresses depending on the moment of the day. Light responses are also gated by the clock in tune with the rhythmic expression of the plant photoreceptors (Toth et al., 2001). The specific light sensitivity of the clock maximizes light perception during the day-time and mitigates resetting of the clock to unexpected external stimuli (Oakenfull & Davis, 2017). This response is mainly regulated by the photoreceptor ZTL and the clock components EARLY FLOWERING 3 (ELF3) and ELF4 in the late day and early night (Mas et al., 2003, Liu et al., 2001, McWatters et al., 2000, McWatters et al., 2007). Additionally, TIME FOR COFFEE (TIC) is proposed to regulate the gated light response during the mid-late night (Ding et al., 2007).

The expression of several clock components is directly or indirectly regulated by light. Several studies demonstrated a major role of the CONSTITUTIVELY PHOTOMORPHOGENIC 1 (COP1) promoting the proteasomal degradation of the clock proteins ELF3 and GIGANTEA (GI) (Yu et al., 2008). Moreover, *ELF4* expression and protein stabilization is regulated indirectly by COP1 through the abundance of the light-related components: ELONGATED HYPOCOTYL 5 (HY5), FAR RED ELONGATED HYPOCOTYL 3 (FHY3) and FAR RED IMPAIRED RESPONSE 1 (FAR1) (Li et al., 2011). Around dawn, these transcription factors bind to the *ELF4* promoter and activate its expression, while is repressed at dusk by the morning clock components CIRCADIAN CLOCK-ASSOCIATED (CCA1) and LATE ELONGATED HYPOCOTYL (LHY). This coordinated interaction promotes the proper *ELF4* expression and function (Li et al., 2011). On the other hand, several well-characterized components of the BASIC HELIX-LOOP-HELIX (bHLH) transcription factor family known to modulate the photoreceptors activity, named PHYTOCHROME-INTERACTING FACTORs (PIFs), are shown to interact with the core clock component TIMING OF CAB2 EXPRESSION 1/ PSEUDO RESPONSE REGULATOR 1 (TOC1 or PRR1), and thus synchronizing relevant biological processes

such as growth (Soy et al., 2016). Additionally to PIFs, light also triggers the proteasomal degradation of two proteins of the PRR family TOC1 and PRR5 through light-dependent E3 ubiquitin ligases including ZTL (Mas et al., 2003, Nakamichi et al., 2005, Kiba et al., 2007). ZTL ubiquitinates PRR5 and TOC1 and thus targeting them for 26S proteasomal degradation.

3.1.1.1 Light-mediated responses controlled by photoreceptors

Among the five members of the phytochrome family in Arabidopsis, the PHYTOCHROME A (PHYA) and PHYB are responsible of the red light entrainment of the circadian clock whereas other phytochromes display relevant functions under specific stress conditions, or at different developmental stages (Strasser et al., 2010). The activity of the phytochromes relies in a reversible reaction upon red/far-red light (R/FR) changes: red light promotes the active form of the phytochromes (Pfr) whereas far-red light converts the active phytochromes in their inactive form (Pr). This reversible photoswitch enables quick biological responses to even small changes in the R/FR ratio or very low fluence of light, including developmental processes as the germination and de-etiolation (Strasser et al., 2010). In addition, several studies have pointed out the crucial role of the PHYB regulating the circadian clock in a red/far red light-dependent manner (Yeom et al., 2014). PHYB physically interacts with morning clock components such as CCA1 and LHY, and evening components like ELF3, GI and LUX ARRHYTHMO/PHYTOCLOCK 1 (LUX/PCL1) and thus integrating red/far red light information to the central oscillator. Phytochromes also interact with the blue light photoreceptors CRYPTOCHROME 1 (CRY1) and CRY2. PHYA and PHYB interact and regulate the activity of CRY1 and CRY2, respectively, and hence mediating proper blue light responses including photoperiodic time, hypocotyl elongation and the pace of the circadian clock (Mas et al., 2000, Ahmad et al., 1998).

Cryptochromes display a major role controlling blue light-induced physiological responses (Yang et al., 2017). Consistently, approximately 5-25% of the transcriptional changes upon blue light exposure are due to the cryptochrome signaling. In Arabidopsis CRY1 and CRY2 are functionally active as dimers and undergo blue light

photoreduction of oxidized FAD to FADH triggering dynamic conformational changes in CRYs (Bouly et al., 2007). CRY1 and CRY2 display redundant functions entraining the plant circadian clock (Inoue et al., 2017). However, these two flavoproteins exhibit different behavior and cell localization. Upon blue light exposure, CRY1 protein is stable and is homogeneously distributed within the cell, whereas CRY2 is restricted to the nucleus and undergoes rapid degradation by the 26S proteasomal system (Yang et al., 2017). In response to blue light, CRY2 function correlates with the formation of compact nuclear speckles named photobodies (Yu et al., 2009). The photoexcitation of the cryptochromes requires a rapid phosphorylation of the C-terminal tail, promoting conformational changes that are essential for the downstream CRY signaling pathways (Figure 5). Interestingly, CRY1 has been found to catalyze its own phosphorylation by direct binding to ATP while CRY2 required protein kinases to undergo phosphorylation (Bouly et al., 2003, Ozgur & Sancar, 2006).

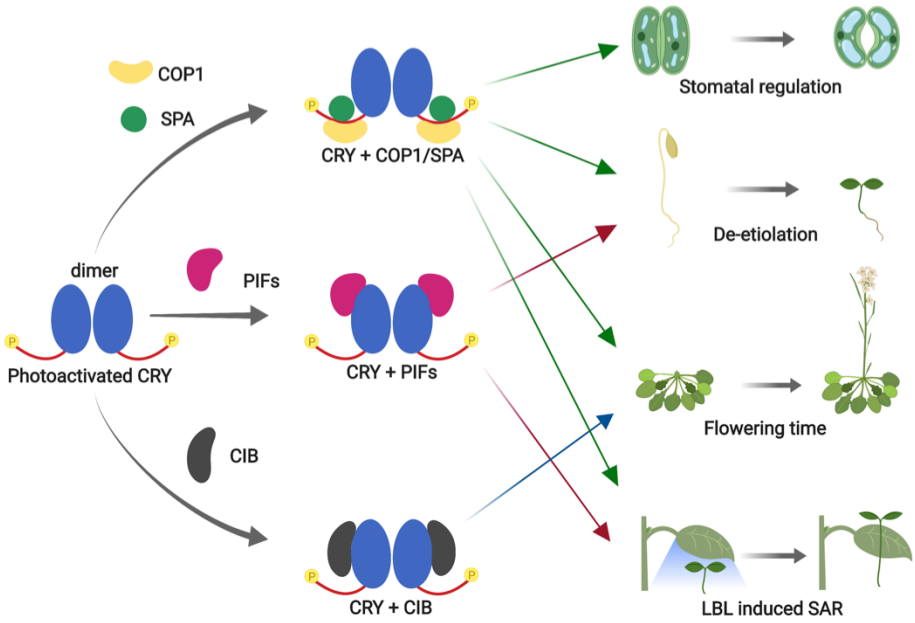

Figure 5. Schematic network depicting CRY-regulated processes. CRY dimer is phosphorylated in the C-terminal tails (left), and can then interact with several factors. Three main CRY-complexes can be potentially formed (center), in order to display specific biological outputs (right). Created with BioRender.

Cryptochrome promotion of transcriptional changes is mediated by their interaction with a wide array of proteins. COP1 and the SUPRESSOR OF *PHYA-105* (SPA) form an E3 ubiquitin ligase complex, which regulates, in a CRY-dependent manner, the turnover of

transcription factors involved in the regulation of photomorphogenesis (Yang et al., 2017), and stomatal development and closure (Mao et al., 2005). Phytochromes also interact with COP1 contributing to the downstream responses (Sheerin et al., 2015). Blue light also triggers CRY2 interaction with two members of the bHLH transcription factor family: the CRYPTOCHROME-INTERACTING BASIC HELIX-LOOP-HELIX (CIB) and the PHYTOCHROME-INTERACTING FACTORs (PIFs). Upon blue light, the coordinated function of CRY2 and PHYB induces flowering under long days by activating a cascade of downstream transcription factors including GI, CONSTANS (CO) and ultimately 5 different CIB proteins that redundantly up-regulate the *FLOWERING LOCUS T (FT)* promoting the floral transition (Liu et al., 2008, Yang et al., 2018). CRYs also stabilize PIF proteins by direct binding and hence regulating several developmental processes such as the Low Blue Light (LBL)-induced Shade Avoidance Response (SAR) and warm temperature-induced hypocotyl elongation (Pedmale et al., 2016). Under low blue light, accumulation of CRY2 co-localizes with PIF4/5 and PIF4/5-related genes suggesting a direct repressing function of CRY2 of the PIF-related processes (Fraser et al., 2016). Moreover, several studies have demonstrated the specific degradation and sequestration of the PIFs by direct binding of photoactivated PHYB (Park et al., 2018). The CRY2-dependent photo-responses are inhibited by direct interaction with the BLUE-LIGHT INHIBITOR OF CRYPTOCHROMES 1 (BIC1) factor (Yang et al., 2017, Weidler et al., 2012).

CRYs share protein sequence homology with a specific family of proteins named photolyases (Mei & Dvornyk, 2015), which all together form the cryptochrome/photolyase family (CPF) (Yang et al., 2017). DNA photolyases are enzymes found in many organisms, display DNA repair activity in a blue light-dependent manner, and respond to UV light-induced damage generated by solar radiation (Manova & Gruszka, 2015). UV light promotes pyrimidine dimers (PPs) in the DNA known as photoproducts that potentially alter gene transcription (Tornaletti et al., 1999, Tornaletti & Hanawalt, 1999). Photolyases are classically divided in two main groups in tune with the two major photoproducts: photolyases that can repair 6-4 PPs (photolyase I) and cyclobutane pyrimidine dimers (CPDs, photolyase II). The energy

provided by the blue light activates the photolyases which in turn bind to the photoproducts and mediate DNA repair of the PPs known as photoreactivation (Manova & Gruszka, 2015). The different photolyases exhibit different repair reactions but common error-free DNA repair results providing a very effective and ancient DNA repair mechanism against UV light-induced damage (Manova & Gruszka, 2015, Mei & Dvornyk, 2015). However, due to the nuclear distribution of the photolyases, photoproducts generated in the mitochondria or chloroplast can not be photoreactivated (Kaiser et al., 2009). In Arabidopsis, two genes codify for the two existing photolyases: *UV REPAIR DEFECTIVE 3 (UVR3)* encoding the photolyase I, and *PHOTOLYASE 1* or *UV RESISTANCE 2 (PHR1/UVR2)* for the photolyase II (Ahmad et al., 1997, Nakajima et al., 1998). Additional studies have provided evidence of other enzymes of the CPF named *Drosophila, Arabidopsis, Synechocystis,* Human (DASH) – type cryptochromes (CRY-DASHs) (Mei & Dvornyk, 2015). CRY-DASH enzymes exhibit similar DNA binding domain and photorepair activity as photolyases, but are only involved in ssDNA repair of the CPDs (Kavakli et al., 2017). In Arabidopsis, CRY3 is a CRY-DASH that mediates repair of UV-induced damage in cell organelles including mitochondria and chloroplasts (Liu et al., 2016). In other plant species as tomato, the *CRY-DASH* gene describes robust diurnal expression patterns controlled by the interaction among CRY1 and CRY2 with the circadian clock (Facella et al., 2006).

CRYs in mammals are shown to be part of the core circadian clock and to retain photorepair activity, showing a functional coupling of the circadian clock and DNA repair (Kavakli et al., 2017). However, plant cryptochromes lack the characteristic photolyase activity despite of their similar photolyase DNA binding domain (Manova & Gruszka, 2015). However, studies performed in mammalian cells expressing *AtCRY2* artificially showed photobody formation and constitutively enhanced DNA damage signaling pathway in absence of genotoxic stress (Ozkan-Dagliyan et al., 2013).

3.1.2. Temperature input to the clock

Entrainment of the circadian clock is also mediated by changes in ambient temperature. Recent studies have shown the crucial role of phytochromes as thermal

timers integrating temperature information to the clock (Jung et al., 2016). Increasing temperature releases the repressing role of PHYB in several temperature response genes as the *ARABIDOPSIS THALIANA HOMEOBOX 2 (ATHB2)*, by dark conversion of active PHYB to its inactive form and thus enabling hypocotyl elongation (Jung et al., 2016). The key role of PHYB integrating the temperature and light input signals to the circadian clock suggests a synergic input regulation (Legris et al., 2016). Diurnal variations under a physiological range of temperatures (16-28ºC) as small as 4ºC directly modulate the plant clock function, inducing alternative splicing events and thermomorphogenic adjustments (Filichkin & Mockler, 2012, Quint et al., 2016). Changes in temperature have been shown to regulate clock genes at different levels. For instance, proper balance between the two existing *CCA1* splicing isoforms is shown to be essential for proper cold adaptation by the circadian clock (Dong et al., 2011). Analogously, high temperatures also regulates the alternative splicing events in clock components such as *TOC1, ELF3, CCA1, PRR7* and *PRR9* (Filichkin & Mockler, 2012). Under heat stress, the HEAT SHOCK TRANSCRIPTION FACTOR B2B (HSFB2B) regulates hypocotyl growth by repressing the activity of *PRR7* (Kolmos et al., 2014). Moreover, the interaction of ZTL with the Heat Shock Protein 90 (HSP90) and HSP70 would provide a second thermal adaptive mechanism by regulating insoluble protein aggregates formed under heat stress (Gil et al., 2017). In addition to clock entraining by diurnal changes in temperature, the circadian clock also displays a property known as temperature compensation. The clock sustains robust and constant periodicity of the circadian rhythms in a wide range of physiological temperatures (Gould et al., 2006). Classically, PRR7 and PRR9 are shown to be crucial for this adaptive mechanism, but several studies have also support the role of CCA1, LHY, GI and the EVENING COMPLEX (EC)(Salome et al., 2010). The antagonistic interplay between CCA1 transcriptional activity and its phosphorylation by CASEIN KINASE 2 (CK2) has been also shown to be an essential mechanism controlling temperature compensation in Arabidopsis (Portoles & Mas, 2010).

3.2. Molecular network at the core of the central oscillator in plants

The endogenous clock consists of a complex regulatory network based on feedback loops (Figure 6) (Shalit-Kaneh et al., 2018). The first components identified to be part of the central oscillator in Arabidopsis included CCA1 and LHY, two single MYB-like transcription factors (Wang & Tobin, 1998, Schaffer et al., 1998). These two components form a heterodimer and transcriptionally repress evening-expressed clock genes in the morning by binding to specific cis-regulatory elements (Priest et al., 2009). A third component identified to be part of the oscillator was a member of the PSEUDO RESPONSE REGULATOR family (PRR) known as TOC1 or PRR1 with a peak of expression around dusk (Figure 6) (Huang et al., 2012). CCA1 and LHY increase during the morning and repress *TOC1* gene expression (Alabadi et al., 2001). In turn, activation of TOC1 contributes to the repression of *CCA1* and *LHY* in the evening (Gendron et al., 2012). TOC1 not only represses *CCA1* and *LHY* but nearly all of the components of the oscillator (Figure 6) (Nagel et al., 2015, Huang et al., 2012, Adams et al., 2015). Consistently with their important function within the clock, mutation or over-expression of these components lead to clear phenotypes of clock outputs including flowering time, hypocotyl elongation, proper stomatal responses or the cell cycle (Lu et al., 2012, Niwa et al., 2007, Park et al., 2016, Hassidim et al., 2017, Fung-Uceda et al., 2018).

Over the last years, an increasing number of studies have uncovered additional components and their complex regulatory network within the Arabidopsis oscillator. During the morning, three members of the PRR family known as *PRR9*, *PRR7* and *PRR5* are sequentially expressed (Nakamichi et al., 2005) and repressed by the heterodimer CCA1/LHY, and by each other: *PRR9* is repressed by PRR7, which in turns is repressed by PRR5 and all by TOC1 (Nakamichi et al., 2010, Ito et al., 2008) (Figure 6). Moreover, PRRs down-regulate the expression of *CCA1* and *LHY* (Nakamichi et al., 2005). Mutations of the *PRRs* exhibit developmental defects in flowering time, abiotic responses and mitochondrial metabolism (Martin et al., 2018, Nakamichi et al., 2010, Ito et al., 2007, Fukushima et al., 2009). *PRR9* and *PRR7* expression is also regulated by a set of evening expressed clock components ELF3, ELF4 and LUX. The proteins form a

complex known as the Evening Complex (EC). Through the DNA binding domain of LUX, the EC repress morning clock genes like *PRR9* and *PRR7* and indirectly activates *CCA1* and *LHY* expression, which in turn repress the EC (Ezer et al., 2017, Helfer et al., 2011, Nusinow et al., 2011). The transcriptional activity of the EC is regulated in a light- and temperature-dependent manner (Ezer et al., 2017). GI is also expressed at the evening, activating *TOC1* expression and forming a complex in a light-dependent manner with ZTL (Sanchez & Kay, 2016).

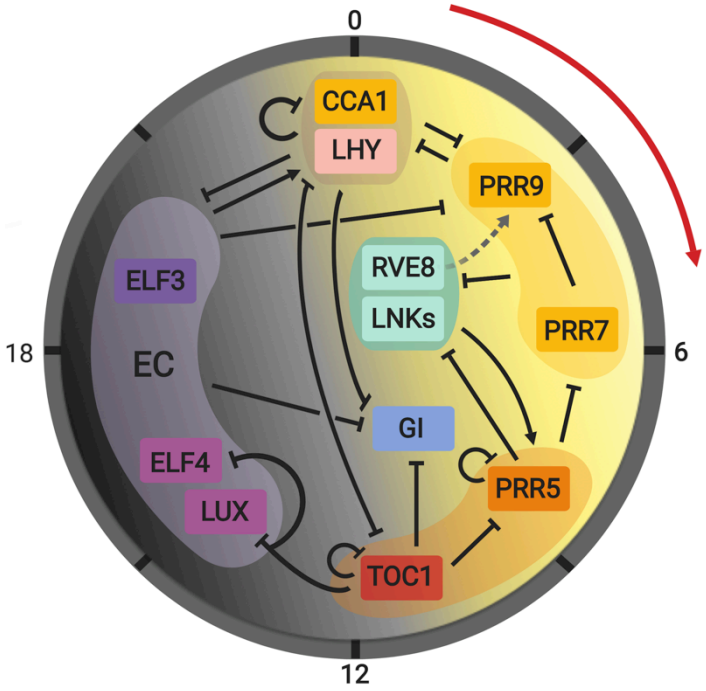

Figure 6. Schematic organization of the molecular network of the plant central oscillator. Circadian rhythms in plants rely in negative feedback loops among the clock components in a time-dependent manner. The red line shows the direction of the clock throughout the day. Time is represented in hours. Shade areas indicate functional groups. The broken grey line indicates hypothetical relationship. Created with BioRender.

In addition to CCA1 and LHY, other MYB-related transcription factors function as direct regulators of circadian gene expression. The clock components REVEILLE 8/ LHY CCA1 LIKE 5 (RVE8/LCL5), RVE4/LCL1 AND RVE6/LCL2 regulate *PRR5* and *TOC1* activity by direct binding to their gene promoters (Farinas & Mas, 2011, Xie et al., 2014). Despite the sequence similarity with CCA1/LHY and binding to *TOC1*, RVEs and CCA1/LHY display antagonistic regulatory functions *of TOC1* by modulating the acetylated state of

the histone 3 (H3) at the *TOC1* promoter. While CCA1 repress *TOC1* by inducing H3 deacetylation, RVE8 promotes hyper-acetylation of the H3 and thus activates *TOC1* expression (Farinas & Mas, 2011). The RVEs interact with other clock components known as NIGHT LIGHT-INDUCIBLE AND CLOCK-REGULATED GENES (LNKs) and together co-activate evening-expressed clock genes including *PRR5*, *TOC1, LUX, ELF4* and *GI* (Xie et al., 2014, Hsu et al., 2013, Rugnone et al., 2013). Moreover, LNK1 and LNK2 mediate red-light responses connecting phytochrome signaling with the circadian clock (Rugnone et al., 2013). Over-expression or mutation of RVE or LNK components displays developmental defects in plant growth, hypocotyl elongation and anthocyanin accumulation (Rawat et al., 2011, Perez-Garcia et al., 2015, Rugnone et al., 2013). A recent study has also reported the mechanism by which RVE8 and LNK1 and LNK2 co-activate circadian gene expression (Ma et al., 2018). The specific binding of RVE8 at the *PRR5* and *TOC1* promoters followed by its interaction with LNKs is essential for the recruitment of the transcriptional machinery at the clock gene promoters. The RNA polymerase II and the transcription elongation factor STRUCTURE-SPECIFIC RECOGNITION PROTEIN 1 (SSRP1) from the FACILITATES CHROMATIN TRANSCRIPTION (FACT) complex are thus rhythmically recruited by LNKs at the clock promoters to trigger the transcription initiation and elongation of the nascent RNAs of *PRR5* and *TOC1* (Ma et al., 2018).

3.3. Circadian clock outputs in plants

The circadian clock allows adaptive responses in physiology, metabolism and behavior to be in-tune with the surrounding environment (Dodd et al., 2015, Lu et al., 2005, Niwa et al., 2009, Endo et al., 2016). Circadian regulation of clock outputs relies in some cases on the transcriptional regulation of genes involved in the clock output pathways (Covington et al., 2008). In the following sections, we briefly describe the circadian outputs including photosynthesis, cell growth and cell cycle as well as flowering time and leaf senescence. Finally, we briefly focus on the stress responses controlled by the clock.

3.3.1. Photosynthesis, cell growth and cell cycle

Photosynthesis is a key essential process in plants that is controlled by the circadian clock. Most of the protein-coding genes involved in the light-harvesting complexes including the photosystems, and approximately 70% of the chloroplast-encoded genes are circadianly regulated (Harmer et al., 2000, Noordally et al., 2013). The mRNA of the LIGHT-HARVESTING CHLOROPHYLL A/B PIGMENT-PROTEIN COMPLEX OF THE PHOTOSYSTEM II (LHCII), the promoter activity of the *CHLOROPHYLL A/B BINDING PROTEIN 2:LUC (CAB2)* and the chlorophyll content of the chloroplasts diurnally oscillate with a peak during the day, suggesting a role for the circadian clock regulating photosynthesis (Busheva et al., 1991, Millar et al., 1992). In chloroplasts, the nuclear-encoded *SIGMA FACTOR (SIG)* genes, whose gene products are required for the transcriptional regulation in chloroplasts, display a circadian regulation in a light-dependent manner and it is controlled by phytochromes and cryptochromes (Noordally et al., 2013, Belbin et al., 2017). In addition, CCA1 is essential for the transcriptional activation of the *LIGHT-HARVESTING CHLOROPHYLL A/B BINDING (LHCB)* genes in a red-light dependent manner through the phytochrome action (Wang & Tobin, 1998). Analogously, other metabolic pathways linked with the CO_2 fixation such as the photorespiration and starch mobilization also display circadian rhythms (McClung et al., 2000, Farre & Weise, 2012). PRR5, PRR7 and PRR9 regulate metabolic intermediates including for example, intermediates of the Calvin cycle and citric acid cycle (Fukushima et al., 2009). Similarly, mutation or over-expression of core clock genes as *TOC1* and *CCA1* display negative effects in photosynthesis and CO_2 fixation (Dodd et al., 2005). The circadian function has been proposed to be essential for proper photosynthetic activity (Dodd et al., 2005).

The circadian clock also plays an essential role controlling plant growth and development. At the cellular level, recent studies have provided evidence for the functional connection between the circadian clock and the cell cycle. TOC1 controls the proper timing of the cell cycle by regulating the rhythmic expression of the *CELL DIVISION CONTROL 6 (CDC6)* gene, encoding a component of the DNA pre-replication complex essential DNA licensing during the S-phase (Fung-Uceda et al., 2018). Direct

repression of *CDC6* by TOC1 prevents the G1-to-S phase transition. Thus, over-expression of TOC1 lengthens the G1-phase and delays the entry into the S-phase. Overall, proper expression and function of TOC1 was shown to be important for cell proliferation and differentiation by controlling both the mitotic cycle and the endocycle (Fung-Uceda et al., 2018). The MYB factors RVEs also regulate size and growth of mesophyll cells by setting appropriate circadian phases of *PIF4* and *PIF5* gene expression (Gray et al., 2017). Mutant plants of *RVEs* display developmental defects in hypocotyl elongation, leaf growth and flowering time due to enhanced cell growth rate.

3.3.2. Flowering time and leaf senescence

The clock also regulates the proper timing of the floral transition and leaf senescence. The expression of *FT* in leaves and the movement of the FT protein from leaves to the shoot apical meristem mediates the initiation of flowering (Amasino & Michaels, 2010). *FT* is mainly induced by CO, which is in turn regulated by photoreceptors, the circadian clock and E3 ubiquitin ligases (Suarez-Lopez et al., 2001, Song et al., 2012). As mentioned above (section “Light Input to the clock”), the interaction of phytochromes and CRY2 with the COP1/SPA complex gates the *FT* accumulation by regulating CO stability (Liu et al., 2008, Endo et al., 2013, Hajdu et al., 2015). The temporal regulation of *CO* is also controlled by direct regulation of the CYCLING DOF FACTORs (CDF), which bind at the *CO* promoter and repress its expression in the morning. In turn, *CDF* expression is circadianly regulated and it is activated in the morning by CCA1 and LHY and repressed by PRR9, PRR7 and PRR5 in the afternoon (Niwa et al., 2007). In addition, CO protein stability is regulated by the complex formed by GI, the FLAVIN-BINDING KELCH REPEAT F-BOX (FKF1) and ZTL in a blue light-dependent manner under long days. In the morning, the ZTL-GI complex promotes CO degradation while CO is stabilized in the evening by the targeted degradation of CDFs by the FKF1-GI complex (Song et al., 2014). Several factors also repress CO by inactivating its function at the *FT* promoter. The MICROPROTEIN 1A/B-BOX 30 (miP1a/BBX30), the TARGET OF EAT 1 (TOE1) and TOE2 are transcription factors that also recruit TOPLESS (TPL) and co-repress *FT* expression by sequestering CO (Graeff et al., 2016, Zhang et al., 2015a). CO

not only controls *FT* expression but the FT long-distance movement from leaves to the shoot apical meristem (SAM) (Zhu et al., 2016). The regulation of the movement occurs through induction of the well-known transporter SODIUM POTASSIUM ROOT DEFECTIVE (NaKR1), (Zhu et al., 2016) which interacts with FT and mediates the FT-long-distance movement throughout the phloem to deliver FT at the SAM (Zhu et al., 2016). Additionally to NaKR1, the transporter FT-INTERACTING PROTEIN 1 (FTIP1) regulates the cell-to-cell transport of FT from the companion cells to the sieve elements (Shim et al., 2017).

Another process controlled by the circadian clock is leaf senescence. The process relies on the circadian regulation of the master aging regulator *ORESARA 1 (ORE1)* by PRR9 and PIFs (Kim et al., 2018, Sakuraba et al., 2014). PRR9 also regulates *ORE1* by repressing its negative regulator *MIR164B.* ORE1 activity modulates the expression of *SENESCENCE ASSOCIATED GENES (SAGs)*, whose gene products are involved in cell death responses (Sakuraba et al., 2014). In addition, recent studies have shown a direct correlation between CCA1 and the initiation of leaf senescence (Song et al., 2018b). At the juvenile state, CCA1 strongly represses *ORE1* and activates negative regulators of senescence such as *GOLDEN2-LIKE (GLKs)* genes. As plants age, *CCA1* expression dampens and weakness *ORE1* inhibition (Song et al., 2018b). Progressive *ORE1* expression and accumulation neutralizes the function of GLKs and thus triggers leaf senescence (Rauf et al., 2013).

3.3.3. Stress responses

The responses to stress conditions such as osmotic stress and pathogen resistance are also controlled by the circadian clock (Goodspeed et al., 2012, Legnaioli et al., 2009). The endogenous clock rhythmically controls approximately 40-50% of the basal expression of stress related-genes (Atamian & Harmer, 2016). Circadian regulation of the stress responses relies on the regulation of the expression of phytohormones including abscisic acid (ABA), ethylene (ET), salicylic acid (SA) and jasmonic acid (JA) (Figure 7) (Grundy et al., 2015, Singh & Mas, 2018). Under drought conditions, ABA regulates many responses including the stomatal closure and thus enhances plant

tolerance to osmotic stress (Singh & Mas, 2018). The circadian clock rhythmically controls ABA-related genes and ABA receptors, contributing to ABA accumulation in the evening (Singh & Mas, 2018). This gated regulation relies on the coordinated regulation of ABA-related genes by TOC1. TOC1 directly represses the expression of the ABA receptor *ABA-RELATED (ABAR)* and interacts with ABA INSENSITIVE 3 (ABI3) preventing ABA accumulation at night (Kurup et al., 2000, Legnaioli et al., 2009). In turn, ABA regulates *TOC1* in the morning through ABAR and the transcription factor MYB96 (Lee et al., 2016). Moreover, CCA1 and LHY also contribute to the gated response regulating the ABA biosynthesis and MYB96 during the morning and thus increasing ABA levels (Adams et al., 2015, Lee et al., 2016). ABA-induced stomatal closure under stress also relies on the cytosolic levels of Ca^{2+} induced by the circadian regulation of the cyclic adenosine diphosphate ribose (cADPR), which rhythmically controls the Ca^{2+} release (Dodd et al., 2007). The small gaseous phytohormone ET also functions in response to osmotic stress and in other plant defense responses including cold tolerance and host-pathogen responses (Broekaert et al., 2006, Broekgaarden et al., 2015). ET emission and biosynthesis is regulated by ET-related genes such as *ACC SYNTHASE (ACS),* which are gated by CCA1 and PIF5 at the midday in a light-dependent manner (Song et al., 2018a). In addition, the role of ET in plant immunity is mediated by the rhythmic expression of *XAP5 CIRCADIAN TIMEKEEPER (XCT)* that in turn mediates the down-stream of the factor ETHYLENE-INSENSITIVE 3 (EIN3) in the ET signaling (Ellison et al., 2011).

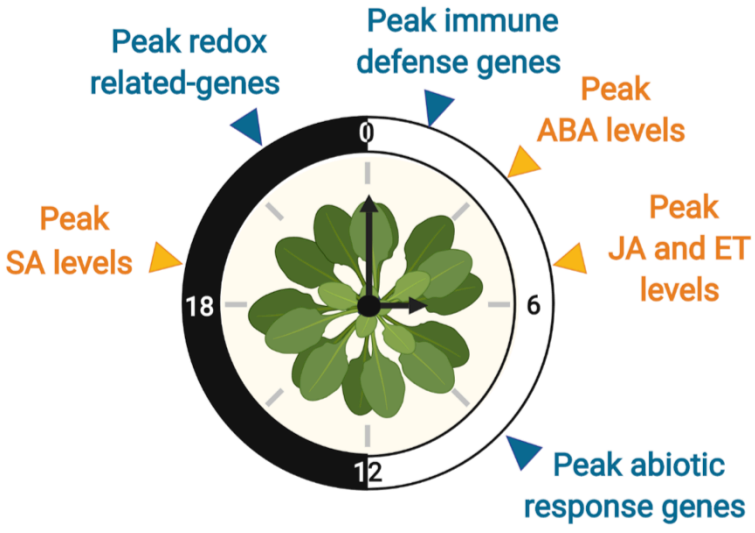

Figure 7. Schematic timing of the phytohormones and stress-related genes. Phytohormone levels (orange) and induction of stress related-genes (blue) are gated at specific times by the circadian clock.

The defense phytohormones SA and JA display plant responses to biotic stresses (Karapetyan & Dong, 2018). Immune receptors from the SA like *RECOGNITION OF PERONOSPORA PARASITICA 4 (RPP4)* are circadianly regulated by CCA1, which promotes *RPP4* expression in the early morning anticipating potential pathogen infections (Wang et al., 2011). Similarly, the evening-phase clock gene *CCA1 HIKING EXPEDITION (CHE)* gates the SA biosynthesis by regulating the activity of the *ISOCHORISMATE SYNTHASE 1 (ICS1*) gene, and thus promoting SA accumulation at night (Figure 7) (Zheng et al., 2015). Although SA and JA play synergic roles in plant defense (Goodspeed et al., 2012), JA accumulation peaks in the middle of the day due to the circadian regulation of the clock component TIME FOR COFFEE (TIC) (Figure 7) (Kazan & Manners, 2013). At night, TIC mediates the proteasomal degradation of a key component of the JA pathway named MYC2 and promotes the expression of *CORONATINE INSENSITIVE 1 (COI1)* at dawn (Shin et al., 2012). Plant immunity is also related to the cellular redox state and reactive oxygen species (ROS) accumulation within the cells. CCA1 maintains a proper redox state and ROS homeostasis by regulating plant catalases including *CATALASE 2 (CAT2)* (Lai et al., 2012). In addition, immune responses are sensed by the master immune regulator NON-EXPRESSOR OF PATHOGENESIS-RELATED GENE 1 (NPR1), which in turn transcriptionally regulates core clock genes including *LHY* and *TOC1* (Zhou et al., 2015). NPR1 plays a crucial role reinforcing the circadian rhythms in response to redox perturbations (Zhou et al., 2015).

4. Overview of the DNA Damage and Repair (DDR) response

Stresses may lead to deleterious effects on genome integrity, and inducing DNA damage (Spampinato, 2017). DNA lesions can arise from different endogenous and external stresses including UV light, ionizing radiation, free radicals and intrinsic metabolic malfunctions (Manova & Gruszka, 2015). Typically, damaged DNA generates chemical and physical defects in the DNA structure that can be classically organized in two different categories depending if the DNA lesions affect one or both DNA strands. Single-stranded lesions include mismatch, intra-strand cross-links, DNA photoproducts and Single-Strand Breaks (SSBs) while double-stranded lesions mainly involve Double

strand breaks (DSB) (Figure 8) (Spampinato, 2017). Among the different DNA lesions, the DSBs are the most cytotoxic due to their direct effects on DNA replication and transcription that lead to aberrant chromosomal structures and eventually to the inhibition of cell growth (Waterworth et al., 2011). If the DNA is not repaired, the DSBs can promote activation of several pathways leading to cell cycle arrest and programmed cell death (PCD) (Roy, 2014). Upon severe DNA damage, cells preferentially undergo PCD rather than DNA repair in order to not propagate undesirable genetic information to next generations (Nowsheen & Yang, 2012, Latrasse et al., 2016).

Due to its relevance for fitness and survival, organisms have developed a wide-range of mechanisms to efficiently detect and repair particular DNA lesions in order to maintain genome integrity. The set of all of these responsive mechanisms is known as DNA Damage and Repair (DDR) response. Single stranded DNA lesions related to damaged bases and nucleotides are recognized and repaired through the base excision repair (BER) and nucleotide excision repair (NER) pathways, respectively. The BER pathway involves damage-specific DNA glycosylases, which recognize and remove damaged bases and then permits the incorporation of a single nucleotide by DNA polymerases (Roldan-Arjona & Ariza, 2009, Balestrazzi et al., 2011). Lesions in nucleotides are mainly produced by UV light and trigger the interaction of numerous factors from the NER pathway that remove the damaged nucleotides through endonuclease activities (Singh et al., 2010, Alekseev & Coin, 2015). A different repair mechanism named mismatch repair (MMR) directly participates in the cell cycle, and corrects mutations generated during DNA replication (Lario et al., 2013). This high-fidelity mechanism is ubiquitous in all organisms and is essential for proper genome integrity (Spampinato et al., 2009). Specific endonucleases from the MutS endonuclease family (MSH) recognize and excise mismatches with the EXONUCLEASE 1 (EXO1) in an ATP-dependent manner followed by DNA re-synthesis and ligation by DNA polymerases (Spampinato et al., 2009). In response to DNA damage, factors involved in the cell cycle and DNA replication as the E2 promoter-binding factors (E2Fs) mediate the proper expression of

cell cycle genes through direct-targeted regulation of the MSH activity (Lario et al., 2011).

In plants, a number of conserved DDR mechanisms are triggered under stressful conditions that can affect the plant DNA integrity. Environmental factors such as light and temperature are able to modulate DDR in plants (Boyko et al., 2005). A number of studies have shown that in response to DNA damage, the amount of DNA lesions is different among organs and the DNA repair activity is mainly found in leaves and roots, suggesting a tissue-specificity of the DDR (Yang et al., 2010, Boyko et al., 2006, Golubov et al., 2010). As plants age, the genome instability and mutation rates increase compared to younger plants due to more frequent contribution of error-prone DDR mechanisms and progressive accumulation of older cells (Golubov et al., 2010). In addition to the common mechanisms shared with other organisms, plants exhibit unique genes that are not present in other eukaryotic organisms (Beemster et al., 2005). In plants, the p53 function on DDR appears to rely on SUPPRRESSOR OF GAMMA RESPONSE 1 (SOG1). SOG1 functions as a master regulator of the DDR in plants, and is essential for cell cycle arrest, programmed cell death as well as for the rapid transcriptional changes in over a hundred of genes upon DNA damage (Yoshiyama, 2016). Despite the functional similarities between SOG1 and p53, the amino acid sequences of both proteins are not conserved (Yoshiyama et al., 2014).

Responses to particular UV-induced damage are known to be transcriptionally coupled with the circadian clock. In mammals the clock components CRY (CRYPTOCHROME) and PER1 (PERIOD 1) modulate the DDR signaling and cell cycle progression (Sancar et al., 2010). Similarly, in plants, the DDR to UV-B light is circadianly regulated by the EC during the evening through direct binding to UV-B-induced response loci. (Takeuchi et al., 2014). Recent studies have shown that around 10-30% of the total DDR genes involved in the UV-B response show rhythmic gene expression (Oztas et al., 2018). In the next sections, we describe the different mechanisms involved in the detection and repair of the DSBs that are known in plants.

4.1. DNA repair of the double strand breaks

Rapid recognition of the DSBs is essential to mitigate the detrimental effects of the DSBs. The initial detection of the DSBs is common in all organisms and is driven by two master regulators from the phosphoinositide-3-kinase-related protein kinases (PIKKs) family known as ATAXIA TELANGIECTASIA MUTATED (ATM) and ATAXIA TELANGIECTASIA MUTATED AND RAD3-RELATED (ATR) (Bradbury & Jackson, 2003). Although these kinases display partial redundancy, they show different activities depending on the source of the DNA damage (Waterworth et al., 2011). ATM is more prone to be activated by DSBs whereas ATR mainly responds to alterations in DNA replication that lead to SSBs (Friesner et al., 2005). Both ATM and ATR rapidly initiate the DNA damage signaling by phosphorylating and recruiting numerous factors to the DNA lesions and thus initiating the DSB repair (Friesner et al., 2005, Yoshiyama et al., 2013). Rapid co-localization of the DDR components is essential to maintain the stability and protect the DNA against further DNA damage (Amiard et al., 2011, Amiard et al., 2013). The ATM/ATR-phosphorylation mediates the activity of key DDR factors such as the master regulator SOG1 and the histone variant H2AX (Yoshiyama et al., 2009, Paull et al., 2000). In response to DSBs, phosphorylated H2AX (γH2AX) binds to the DSBs serving as a DNA damage signal for the cell (Paull et al., 2000). The accumulation of the γH2AX directly correlates with the number of DSBs within the cells (Lobrich et al., 2010). This feature has been extensively used in many studies as a method to monitor and analyze DSB damage and repair in cells (Friesner et al., 2005, Kinner et al., 2008).

The initial events of DSB detection establish specific DSB repair pathways. The cells display different repair mechanisms that are specific and appropriate to particular developmental stages and cell cycle progression (Delacote & Lopez, 2008, Waterworth et al., 2015, Waterworth et al., 2011, Grabarz et al., 2012, Kakarougkas & Jeggo, 2014, Golubov et al., 2010). In order to avoid mutagenic effects, DSBs repair require a precise balance between genomic stability, energy demand and processing time. Typically, DSB repair is mediated by two different DNA repair pathways: homologous recombination (HR) and non-homologous end-joining (NHEJ) (Spampinato, 2017).

Although these repair systems can act simultaneously, they display important differences. The HR provides a high-fidelity repair mechanism to accurately fix DSBs but requires a lot of energy. On the other hand, the NHEJ is a faster and more frequent repair mechanism than the HR (Puchta & Fauser, 2014) but is more prone to introduce DNA errors and genome instability (Puchta, 2005, Spampinato, 2017). Many studies indicate that the NHEJ pathway has significantly contributed to the genome diversity in all organisms due to the intrinsic elevated mutation rate (Puchta, 2005). The HR also has the potential to introduce genomic instability by crossing over non-homologous sequences. Additionally, the HR and NHEJ differ in their function throughout the cell cycle. The NHEJ is mainly restricted to G1, G2 phases and to cells entering in the S-phase whereas the HR is favored from the S phase to the G2/M checkpoint of the cell cycle (Spampinato, 2017). We next describe the mechanisms and genes underlying the HR and NHEJ pathways.

4.1.1. Homologous recombination (HR)

The HR mechanism requires homolog sequences in the genome as templates in order to repair DSBs (Figure 9). The initial step involves the recruitment to the DSB of the protein complex MRN formed by MEIOTIC RECOMBINATION 11 (MRE11), RAD ASSOCIATED WITH DIABETES 50 (RAD50), and NIJMEGEN BREAKAGE SYNDROME 1 (NBS1) (Waterworth et al., 2011). The MRN complex binds to the DNA and together with the protein GAMMA RESPONSE GENE 1 (GR1 or COM1) (Uanschou et al., 2007) initiates the resection of the DSB ends generating 3’ overhangs (Manova & Gruszka, 2015). This long single-stranded DNA is protected by direct binding of the trimeric replication protein A (RPA) complex. Recent studies in yeast indicate that the DNA polymerase is also recruited and promotes the transient hybrid formation between the ssDNA overhang and newly synthetized RNA (known as R-loop) stabilizing the DNA and leading to a proper RPA recruitment (Ohle et al., 2016). Subsequently, RAD51 and RAD51-like proteins replace the RPA complexes forming a long protein filament and promoting homology search and invasion into the intact DNA (Waterworth et al., 2011). Mutation of *RAD51* shows severe effects including chromosomal instability and sterility (Li et al., 2004). In addition to RAD51, other factors like the HOMOLOG OF X-

RAY REPAIR CROSS COMPLEMENTING 2 (XRCC2), XRCC3, BREAST CANCER ASSOCIATED 1 (BRCA1) and BRCA2 form a different complex and act synergistically in the strand invasion process (Osman et al., 2011). Strand invasion of the 3'overhang displaces the heteroduplex forming a D loop that is followed by DNA synthesis of the homolog sequence and duplex extension (Waterworth et al., 2011). At this point, HR pathway displays different DNA repair sub-pathways: synthesis-dependent strand-annealing (SDSA), double-strand break repair (DSBR) and single-strand annealing (SSA) (Waterworth et al., 2011). In the SDSA pathway, the migrating overhang recombines with the intact chromatid and dissociates without disturbing the original DNA of the sister chromatid (Waterworth et al., 2011). In contrast, in the DSBR pathway, the overhang invasion promote the recombination of both chromatids forming Holliday junctions (HJs) (Waterworth et al., 2011). Recombination can lead to the formation of one or two HJs, which are successively cleaved by the resolvases GEN1 HOLLIDAY JUNCTION 5' FLAP ENDONUCLEASE (GEN1), the CROSSOVER JUNCTION ENDONUCLEASE MUS81 (MUS81) (Chan & West, 2015, Hartung et al., 2006) and other helicases and DNA topoisomerases (Manova & Gruszka, 2015). Ultimately, the SSA is a highly active pathway that mediates the annealing of DSBs that occur between repeated sequences (Waterworth et al., 2011). Typically, The SSA pathway involves DNA deletions that occur during the ligation of the DNA ends (West et al., 2004). Interestingly, several studies indicate that the SSA accomplishes for most of the DNA repair between repeated sequences (Siebert & Puchta, 2002).

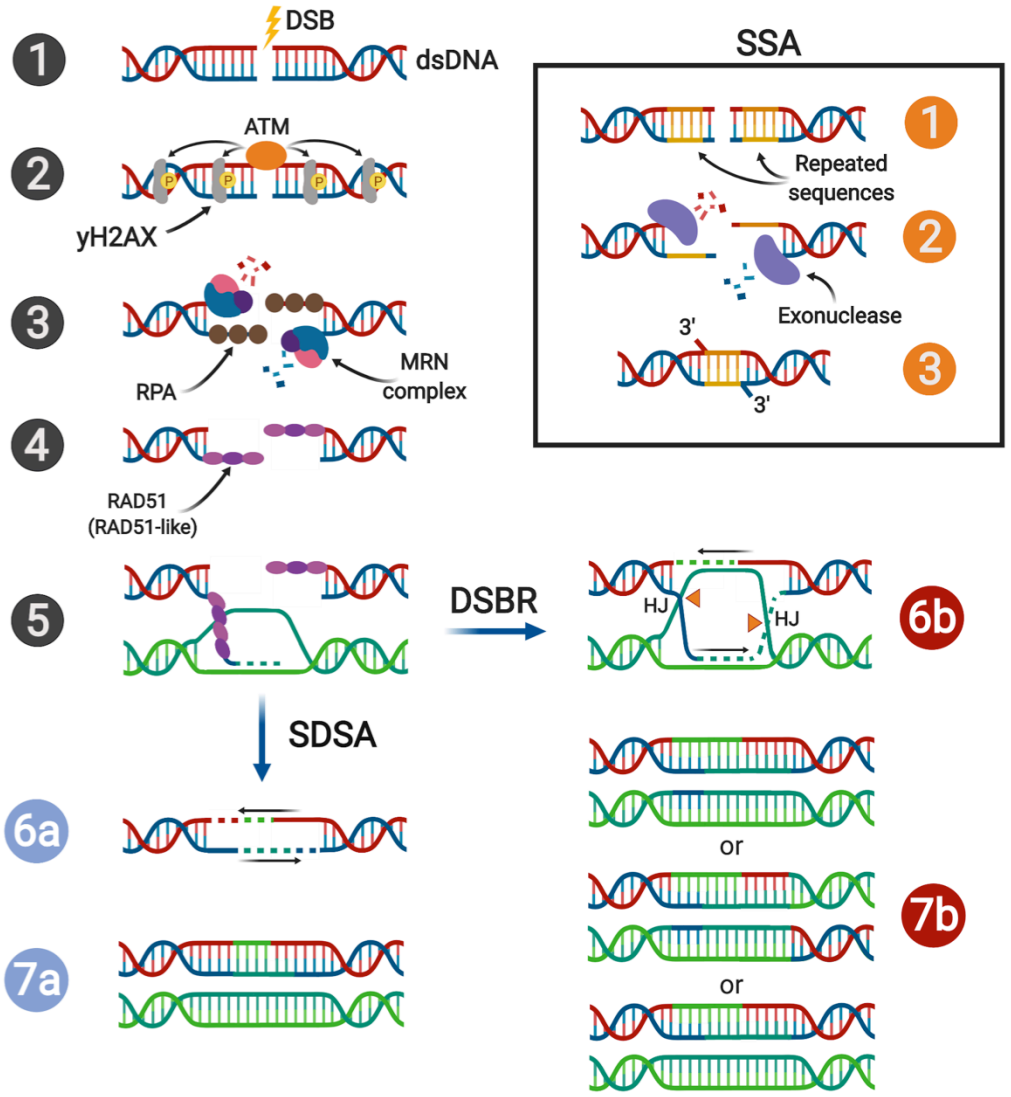

Figure 9. Diagram depicting the homologous recombination pathway in *Arabidopsis thaliana*. (1) DSBs are recognized by ATM (2), which in turn phosphorylated downstream factors including the H2AX and the recruitment of the MRN complex (3). This complex mediates the resection of the DNA producing 3' overhangs protected by the interaction with RPA proteins (3). RAD51 replace RPA proteins (4) and mediate the ssDNA invasion and recombination with sister chromatid (5). Final resection of the DNA can lead to recombination without disturbing sister chromatin (SDSA, 6a and 7a) or formation of Holliday junctions that lead to rearrangements of both chromatids (DSBR, 6b and 7b). DSB damage between repeated DNA sequences is efficiently repaired through direct resection and ligation of the DNA (SSA, upper-right panel). Created with BioRender.

4.1.2. Non-homologous end-joining (NHEJ)

As mentioned above, the NHEJ is more frequent than the HR pathway. The NHEJ does not require sequence homology, and rapidly rejoins DNA ends in order to maintain DNA stability (Figure 10). Several reports have shown the high induction of the NHEJ pathway in response to several stresses that lead to increased programmed cell death and mutation events (West et al., 2004). The NHEJ is divided into at least two different sub-pathways that compete for DSB repair: canonical-NHEJ (C-NHEJ) and alternative-NHEJ (A-NHEJ) (Mladenov & Iliakis, 2011). In the C-NHEJ, the initial DSB detection relies in the activity of a complex formed by the Ku heterodimer, Ku70-Ku80, which displays high affinity for exposed DNA ends and protect broken DNA against nuclease activity (Mannuss et al., 2012). Subsequently, the ku70-ku80 complex promotes the recruitment of XRCC4 and the LIGASE IV (LIG4) which ligate the DNA in a ATP-dependent manner (West et al., 2004). The A-NHEJ or microhomology-mediated end-joining (MMEJ) is independent of the ku heterodimer and involves the function of the MRN complex, XRCC1 and members of the poly ADP-ribose polymerase (PARP) family (Roy, 2014). The C-NHEJ is up to 2 times more frequent than A-NHEJ, involves minimal DNA lost but requires similar structural DNA ends. On the other hand, the A-NHEJ only requires microhomology of sequences as short as 2-14 bp distant from the DSBs to undergo the DNA repair, but involves a long resection process that ultimately leads to DNA deletions similarly as the SSA pathway (Figure 9 and 10) (Mladenov & Iliakis, 2011). Moreover, several studies have proposed an additional NHEJ sub-pathway (Osakabe et al., 2010). However, the nature of this third NHEJ pathway remains unclear and is proposed to be only relevant as a “back-up repair pathway” when both NHEJ and HR are artificially disrupted (Charbonnel et al., 2011).

PARP are enzymes present in all organisms that are involved in the covalent post-translational modification named poly (ADP-ribosyl) ation or parylation, which transfers ADP-ribose (PAR) groups from NAD^+ to target proteins (Briggs & Bent, 2011). Multiple PAR groups can be incorporated to proteins promoting very long and branched PAR chains (Pellegrino & Altmeyer, 2016). Parylation promotes many important changes in protein-protein and protein-DNA interactions, changes in protein

affinity, cell localization (Pellegrino & Altmeyer, 2016), and facilitates other post-translational modifications such as SUMOylation and ubiquitination in response to DNA damage (Pellegrino & Altmeyer, 2016). In response to DSBs, PARPs bind to DNA and parylate themselves and other DNA associated factors in order to recruit them to the DSB point (Briggs & Bent, 2011). Parylation is a reversible modification that can be removed by specific enzymes of the Poly (ADP-ribose) glycohydrolase (PARG) family (Briggs & Bent, 2011). Among the three PARPs and two PARG enzymes existing in Arabidopsis, PARP2 and PARG1 or TEJ display the most relevant function in response to DNA damage (Song et al., 2015, Rissel et al., 2014). Mutation of *TEJ* promotes dramatic defects in growth and survival when plants are exposed to genotoxic stress (Zhang et al., 2015b). Furthermore, *TEJ* mutant plants display a long circadian period phenotype in a light-dependent manner, suggesting that TEJ function is important for proper circadian regulation (Panda et al., 2002). In mammals, parylation follows a rhythmic pattern that is entrained by the feeding behavior. In turn, this circadian regulation promotes the parylation of the mammalian core component CLOCK (Asher et al., 2010).

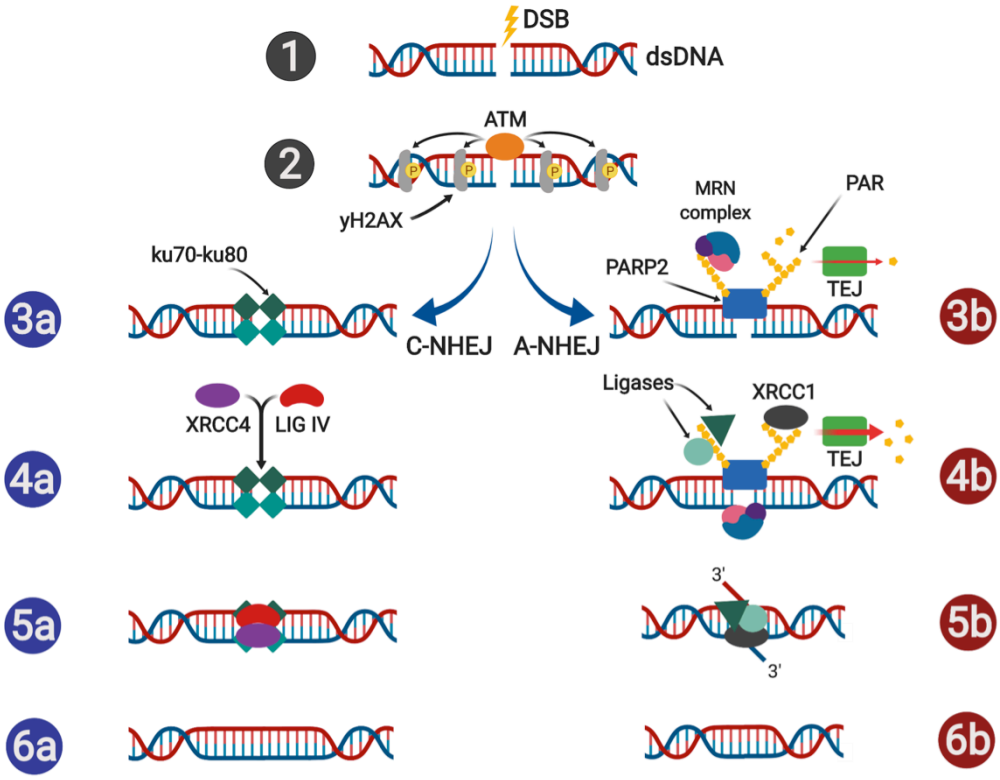

Figure 10. Diagram depicting the non-homologous end-joining pathway in *Arabidopsis thaliana*. (1) Similarly to HR, ATM mediates the phosphorylation of downstream factors such as H2AX (2). Then, if DSB maintain similar DNA ends (C-NHEJ), ku70-ku80 heterodimer binds to the DSB (3a) and recruit XRCC4 and LIG IV (4a) to repair and ligate the DNA (5a-6a). On the other hand, DSBs with different DNA ends are repaired through the A-NHEJ. PARP enzymes bind to the DSB and self-parylate to recruit the MRN complex (3b) and subsequent ligases and XRCC1 to the lesion (4b). TEJ maintains a proper balance of the PAR levels. MRN complex promote DNA overhangs and DNA is re-ligated by microhomology (5b) resulting in DNA deletions (6b). Created with BioRender.

OBJECTIVES

Objectives

In this Doctoral Thesis we aim to uncover the functional connection between the circadian clock and plant responses to double strand breaks (DSBs) in *Arabidopsis thaliana.* This main objective was achieved through the following specific objectives:

1. **To examine the possible diurnal regulation of DNA double strand break (DSB) formation.** By implementing the comet assay technique, we aimed to quantify DSBs generated by bleomycin (BLM) treatment applied at different times during the day.

2. **To analyze the circadian regulation of promoter activity and gene expression of key DNA Damage and Repair genes involved in the DNA double strand break repair.** We aimed to examine the oscillatory patterns of gene expression and promoter activities by Real Time-Quantitative Polymerase Chain Reaction (RT-QPCR) and bioluminescence assays, respectively using WT plants treated with BLM at different times during the day.

3. **To study whether the circadian clock function is affected by DNA double strand breaks and whether altering the circadian clock affects the DNA Damage and Repair response.** We analyzed transcriptional changes in core clock genes by RT-QPCR and examined gene expression and promoter activity of key DNA Damage and Repair genes using loss-of-function and over-expressing plants of key clock components.

4. **To explore the role of the photoreceptor CRY2 regulating DNA double strand breaks and the expression of key DNA Damage and Repair genes.** We quantified double strand breaks and studied the transcriptional changes of DNA Damage Repair genes in plants miss-expressing *CRY2* upon BLM treatment under different light conditions.

5. **To examine the changes of DNA-RNA hybrid (R-loops) formation in response to double strand breaks.** We aimed to examine R-loop enrichment and distribution in DNA Damage Repair gene loci upon BLM treatment using WT and CRY2 miss-expressing plants using DNA-RNA immunoprecipitation (DRIP) assays.

6. **To analyze the regulation of DNA Damage Response genes by the direct binding of CRY2 to the DNA Damage Repair loci.** By performing chromatin immunoprecipitation (ChIP) assays, we aimed to identify direct DNA Damage Response target genes of CRY2.

7. **To identify the role of CRY2 regulating biological responses triggered by double strand breaks.** We monitored changes in programmed cell death responses and true leaf emergence in WT and CRY2 miss-expressing plants following BLM treatment.

RESULTS

Results

1. Differential diurnal accumulation of double strand breaks after bleomycin treatment

In order to examine a possible diurnal regulation of the DNA damage and repair responses in *Arabidopsis thaliana*, we performed the so-called comet assays with samples treated with 1 µM of the drug bleomycin (BLM). BLM is a glycopeptide that produces DNA double strand breaks (DSBs). The DSBs have a direct impact on transcription, cell cycle and programmed cell death due to their cell toxicity and deleterious effects (Chen & Umeda, 2015, Roy, 2014).

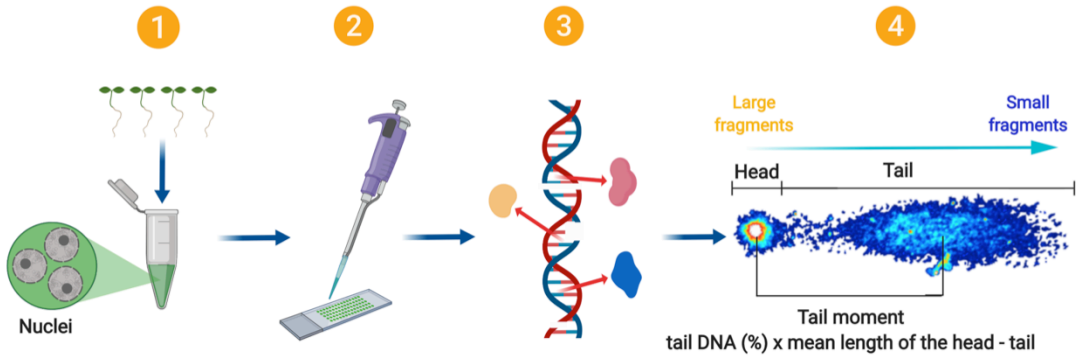

Figure 11. Schematic diagram depicting the Comet assay in *Arabidopsis thaliana*. Nuclei extracts from control and BLM-treated plants are embedded with low melting point agarose (1) and fixed in a slide pre-coated with agarose (2). Proteins and membranes are removed (3) and the isolated DNA is then subjected to electrophoresis and stained with a DNA dye (4). Created with BioRender.com.

The comet assays are based on single-cell gel electrophoresis that allows quantifying the DNA damage generated in isolated nuclei (Figure 11) (Glei et al., 2016, Santos et al., 2015). Following the electrophoresis, the DNA is spatially distributed in a "comet" shape, with a head and a tail. The DNA breaks are proportional to the amount of DNA in the tail in comparison with the intact DNA in the head (Hovhannisyan, 2010). The comet shape permits the measurement of different parameters of the DNA breaks (Santos et al., 2015) including the tail moment (Olive & Durand, 2005). The tail moment takes into account the distribution of migrating DNA (mean length of the head-tail) and the amount of DNA in the tail (tail DNA (%)) (Figure 11). The tail moment thus represents a reliable measurement of the DNA damage (Olive & Banath, 2006).

For our studies, 10-12 day-old Wild-Type (WT) seedlings were grown under 12h light/ 12h dark (LD) conditions and treated for 1 and 6 hours with BLM. Samples were then collected during the day at ZT7 (Zeitgeber Time 7: 7 hours after lights-on) and during the night at ZT19 (Figure 12A). Analyses of the tail moment showed a significant increase of DNA damage after BLM treatment at both 1h and 6h compared to Control (Ctrl) non-treated seedlings (Figure 12B). Comparisons of 1h versus 6h of BLM treatments indicated a slight but reproducible reduction of the tail moments at 6h (Figure 12B-C), suggesting that the DNA repair mechanism might be more efficient after 6h with BLM than after 1h. The statistical analyses also revealed significantly increased tail moments for BLM treatments at ZT7 compared to ZT19 (Figure 12B-C). These results indicate a higher accumulation of DSBs during the day and open the possibility that DNA repair mechanisms might be enhanced during the night.

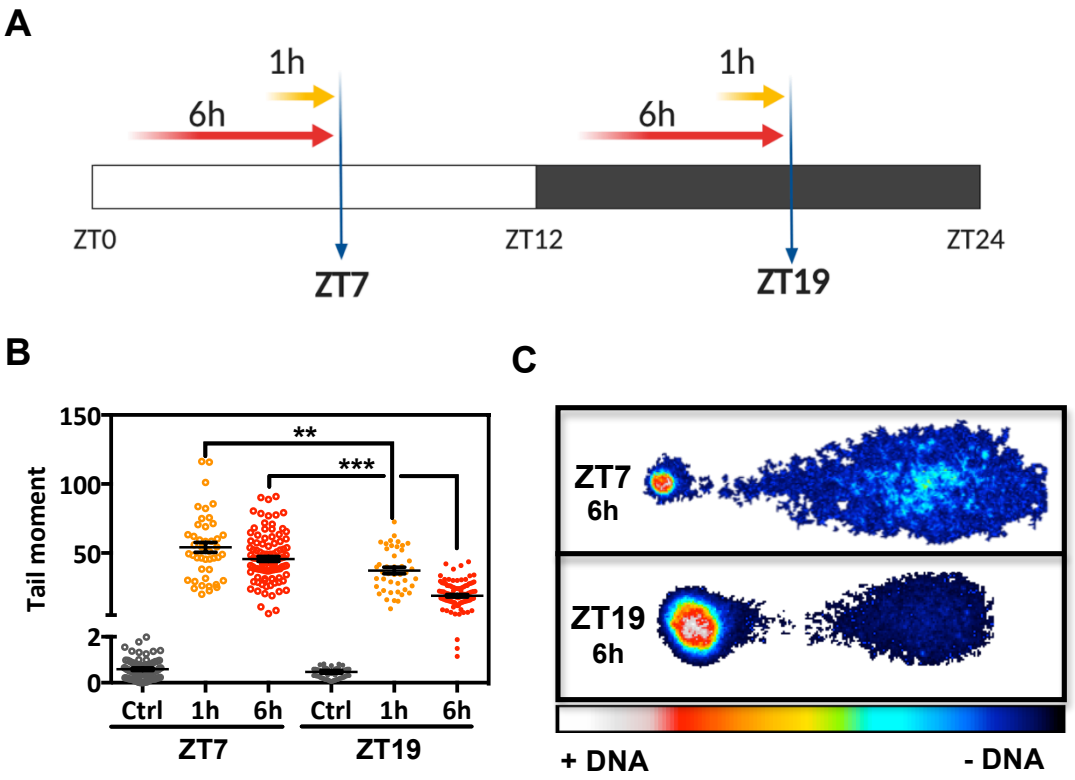

Figure 12. The DSB accumulation is higher during the day than at night. (A) Schematic diagram depicting the BLM treatments for the Time course. White and grey boxes represent light and dark periods, respectively. (B) Tail moment of WT untreated plants and BLM treated plants. (C) Confocal images of Comets from 6h treatments at ZT7 and ZT19 (coloured with Image J). Data is represented as the mean + SEM of n ≥ 50 Comets. All experiments were repeated at least three times independently, with similar results. Unpaired t-test was performed to evaluate the statistical significance of differences between each condition. ** P-value ≤ 0,01, *** P-value ≤ 0,001. Diagram created with BioRender.

2. Circadian patterns in the transcriptional induction of the DNA damage and Repair (DDR) related genes

In order to examine whether transcriptional changes following DNA damage were regulated by the clock, we analyzed the expression of key DNA Damage and Repair (DDR) genes (Spampinato, 2017) by Real Time-Quantitative Polymerase Chain Reaction (RT-qPCR). Samples were collected every 2h over a 24h diurnal cycle following BLM treatment for 24h (Figure 13A). Analyses of *BRCA1, PARP2* and *RAD51,* whose gene products function at different stages of the DDR pathway (Spampinato, 2017) showed a significant induction after BLM treatment compared to mock-treated (Ctrl) plants (Figure 13B-D). Notably, gene induction was not constant throughout the day but followed a rhythmic pattern, reaching a peak around ZT15-17 (Figure 13B-D). In contrast, BLM treatment leads to slight phase delay of *TEJ* expression (Figure 13E).

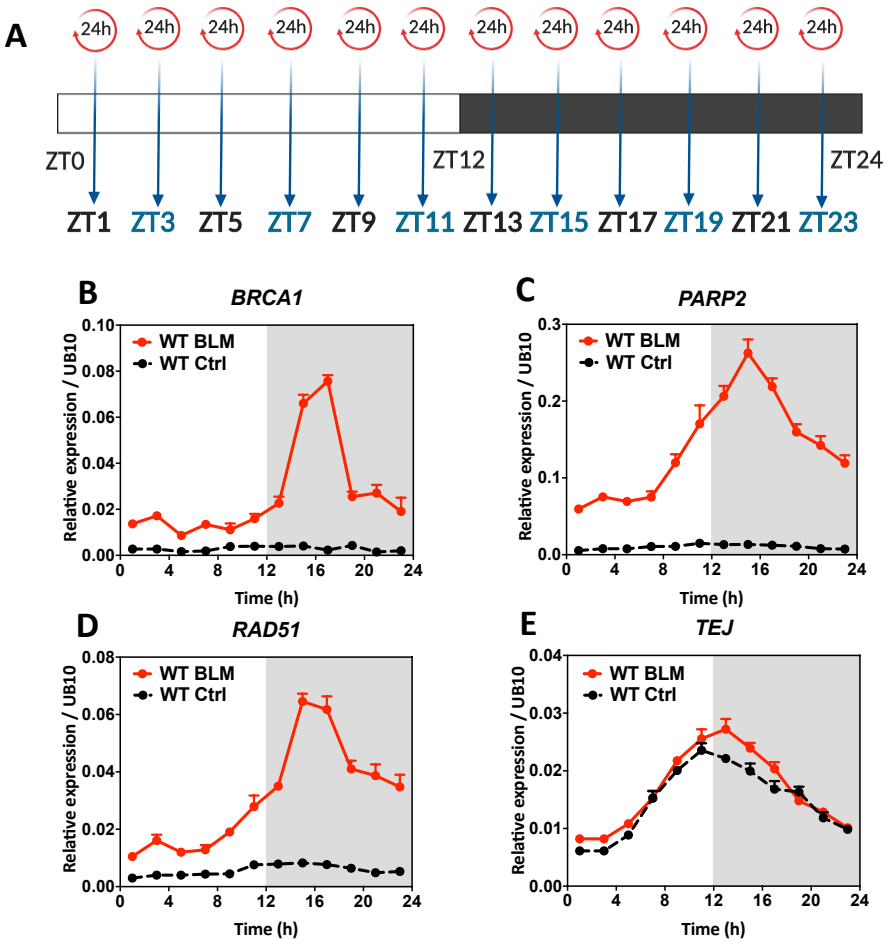

Figure 13. The circadian clock regulates the transcriptional response following DNA damage under entraining conditions. (A) Schematic drawing depicting the experimental design for the time course analyses of BLM treatment for 24h. Gene expression analyses by RT-qPCR of (B) *BRCA1,* (C) *PARP2,* (D) *RAD51* and (E) *TEJ* in untreated WT plants (Ctrl) and BLM treated plants. Values are represented as the mean + SEM of at least two biological replicates. White and dark grey boxes represent the day (light) and night (dark) periods, respectively.

Similar time course analyses but with plants synchronized under LD cycles followed by two days under constant light conditions (LL) also revealed a rhythmic pattern in the transcriptional induction of the DDR genes (Figure 14). The amplitude of the rhythms was slightly decreased compared to the one observed under LD but the rhythms were still evident (compare Figure 13 and 14). The delayed phase of *TEJ* expression was also observed under LL (Figure 14D). Altogether, the results indicate that the transcriptional induction of the DNA damage related genes is regulated by the clock and suggest that the increased gene expression during the night or subjective night might be correlated with the reduced DNA damage observed around this time in the Comet assays (Figure 12B-C).

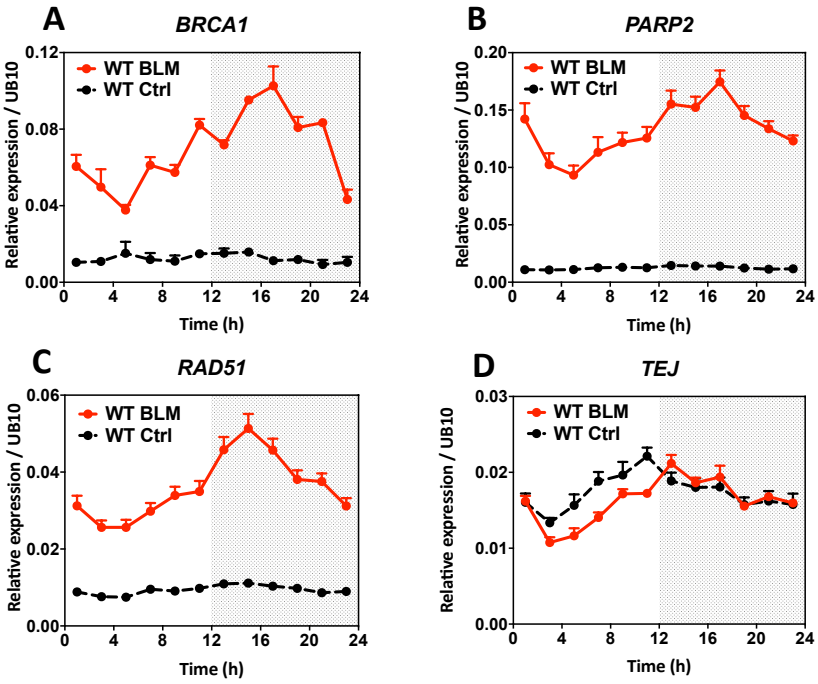

Figure 14. The circadian clock regulates the transcriptional response following DNA damage under constant light conditions. (A) Gene expression analyses by RT-qPCR of (A) *BRCA1,* (B) *PARP2,* (C) *RAD51* and (D) *TEJ* in untreated WT plants (Ctrl) and BLM treated plants. Values are represented as the mean + SEM of at least two biological replicates. White and grey boxes represent the subjective day and subjective night periods, respectively.

3. The promoter activities of DNA Damage and Repair (DDR) genes are controlled by the circadian clock

To further examine the rhythmic response by the circadian clock, we next analyzed the promoter activity of a subset of DDR genes. We generated reporter lines expressing the promoters of *BRCA1* and *RAD51* fused to the *LUCIFERASE* (*LUC*) gene (*pBRCA1:LUC* and *pRAD51:LUC*) and monitored their activities by *in vivo* bioluminescence assays. In mock-treated plants, *pBRCA1:LUC* and *pRAD51:LUC* remained very low under entraining and free-running conditions (Figure 15 and 16). These results are consistent with our transcriptional analysis by RT-qPCR (Figure 13 and 14) and with previous reports (Chen et al., 2003) showing the low expression of the DDR genes in the absence of BLM treatment. Following BLM treatment, the promoter activities were significantly induced particularly the first day following the treatment (Figure 15 and 16), reaching values around 100-fold to those of mock-treated plants (Figure 15 and 16). In subsequent days, the LUC signals dampened low but still remained significantly higher than the mock-treated plants. Notably, the induction was not constant but followed a rhythmic oscillation (Figure 15). Treatments at two different times during the diel cycle (ZT3 and ZT15) showed that the induction and the rhythms occurred following BLM treatment at both time points (Figure 15). The peak on the promoter activities appeared to be slightly advanced compared to their mRNA expression (compare Figure 13 and 15). BLM treatments of seedlings transferred to constant light conditions also lead to increased promoter activity that followed a rhythmic pattern (Figure 16). Altogether, the results indicate that the promoter activities and mRNA expression of DNA damage response genes are rapidly induced and this induction is rhythmically controlled by the clock.

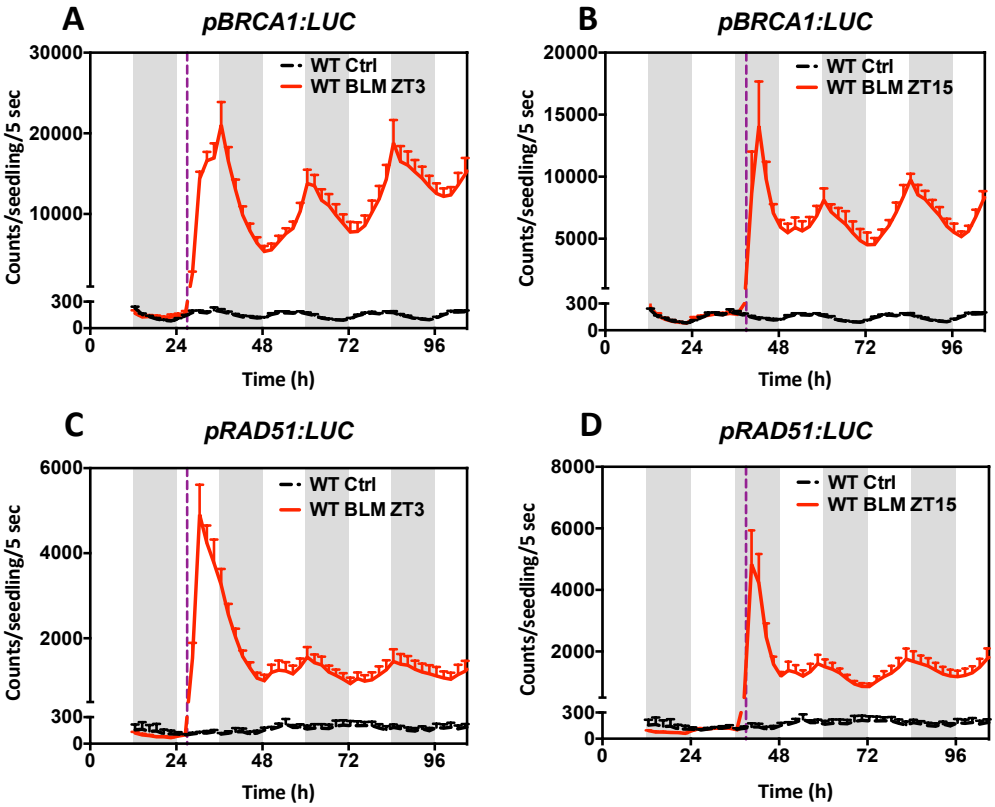

Figure 15. The promoter activity of the DDR genes describes rhythmic oscillations in response to DNA damage under entraining conditions. Bioluminescence assays for (A, B) p*BRCA1:LUC* and (C, D) *pRAD51:LUC* in untreated WT plants (Ctrl) and BLM treated plants. Dotted purple line indicates the BLM treatment. Data represents the means + SEM of the luminescence of 5-6 seedlings. White and grey boxes represent light and dark periods, respectively.

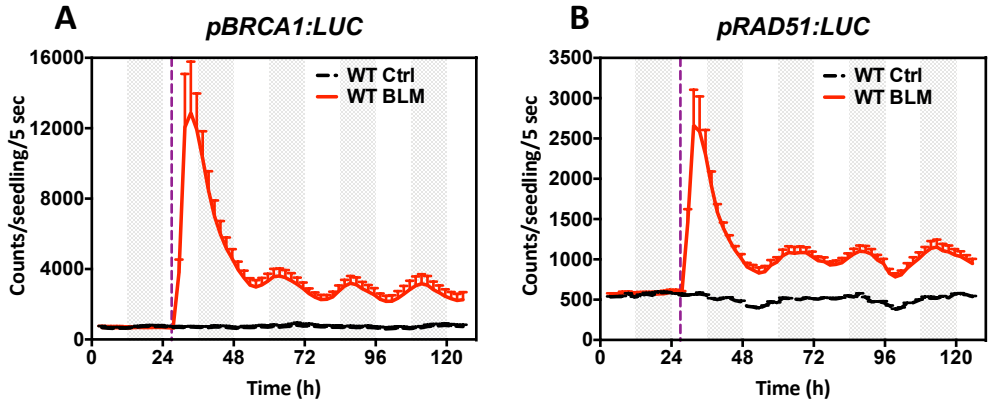

Figure 16. The promoter activity of the DDR genes describes rhythmic oscillations in response to DNA damage under constant light conditions. Bioluminescence assays for (A) p*BRCA1:LUC* and (B) *pRAD51:LUC* in untreated WT plants (Ctrl) and BLM treated plants. Dotted purple line indicates the BLM treatment. Data represents the means + SEM of the luminescence of 5-6 seedlings. White and grey boxes represent subjective light and subjective dark periods, respectively.

4. The expression of core clock genes is not severely affected by bleomycin treatment

Based on the rhythmic regulation of the transcriptional response to DNA damage, we next examined whether DNA damage also affected the expression of core oscillator genes. To that end, control and BLM-treated samples were assayed by RT-qPCR for expression analyses of selected oscillator genes. The morning- and evening-expressed clock genes exhibited the expected oscillations in mock-treated samples under both LD (Figure 17) and LL (Figure 18) conditions. The oscillatory patterns were also sustained in BLM-treated plants with slightly reduced amplitude for *TOC1* and *PRR9* (under LD and LL) and *CCA1* (under LL) around their respective peaks of expression (Figure 17A-C and Figure 18A-C). In contrast, the expression of *PRR5, PRR7* and *LUX* appeared to be rapidly and transiently induced by the BLM-treatment (Figure 17D-F and Figure 18D-F). These results suggest that a subset of clock genes is induced following DNA damage.

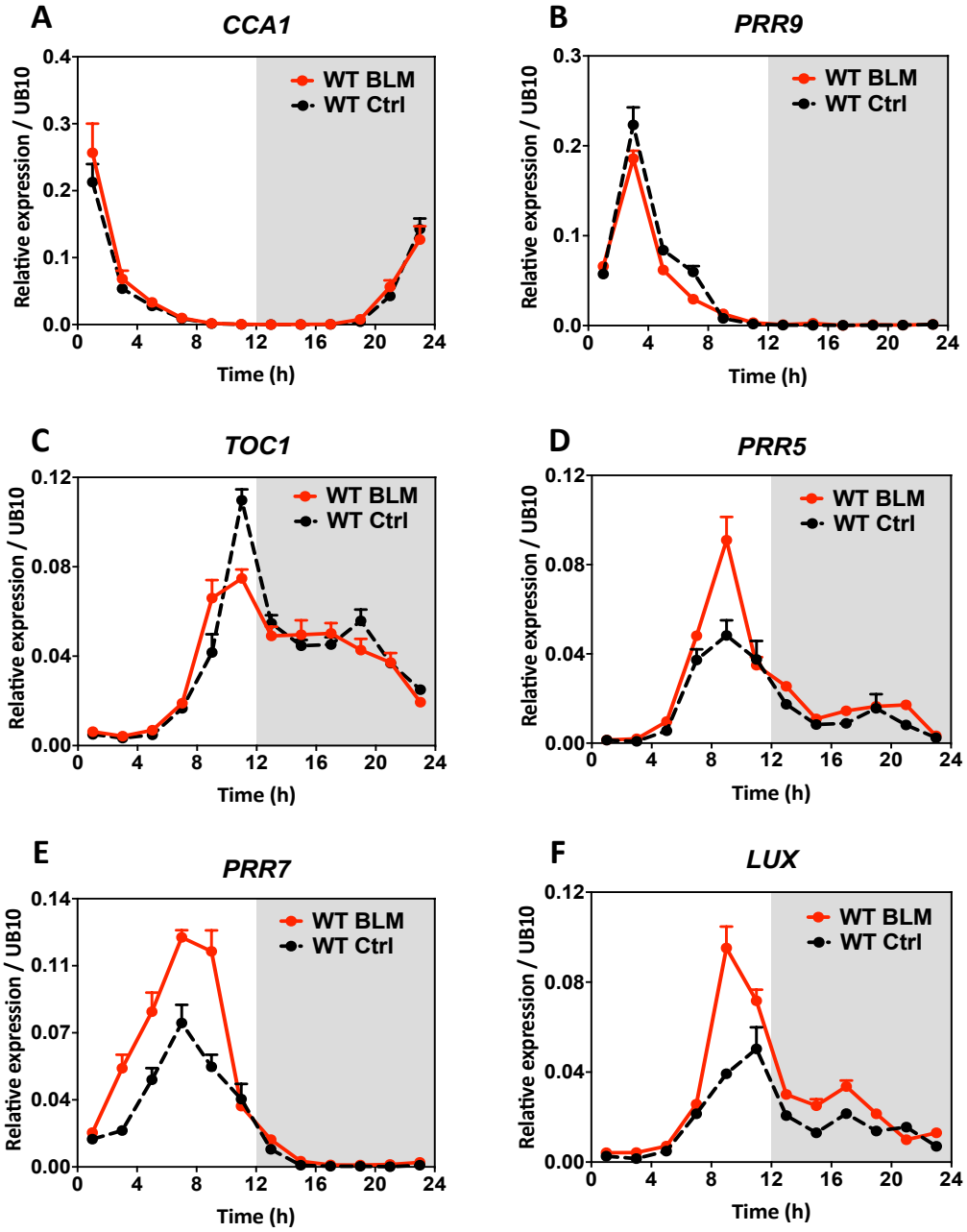

Figure 17. The clock components sustain similar circadian rhythms in response to BLM under entraining conditions. Gene expression analyses by RT-qPCR of (A) CCA1, (B) PRR9, (C) TOC1, (D) PRR5, (E) PRR7 and (F) LUX in untreated WT plants (Ctrl) and BLM treated plants. Values are represented as the mean +SEM of at least two biological replicates. White and grey boxes represent light and dark periods, respectively.

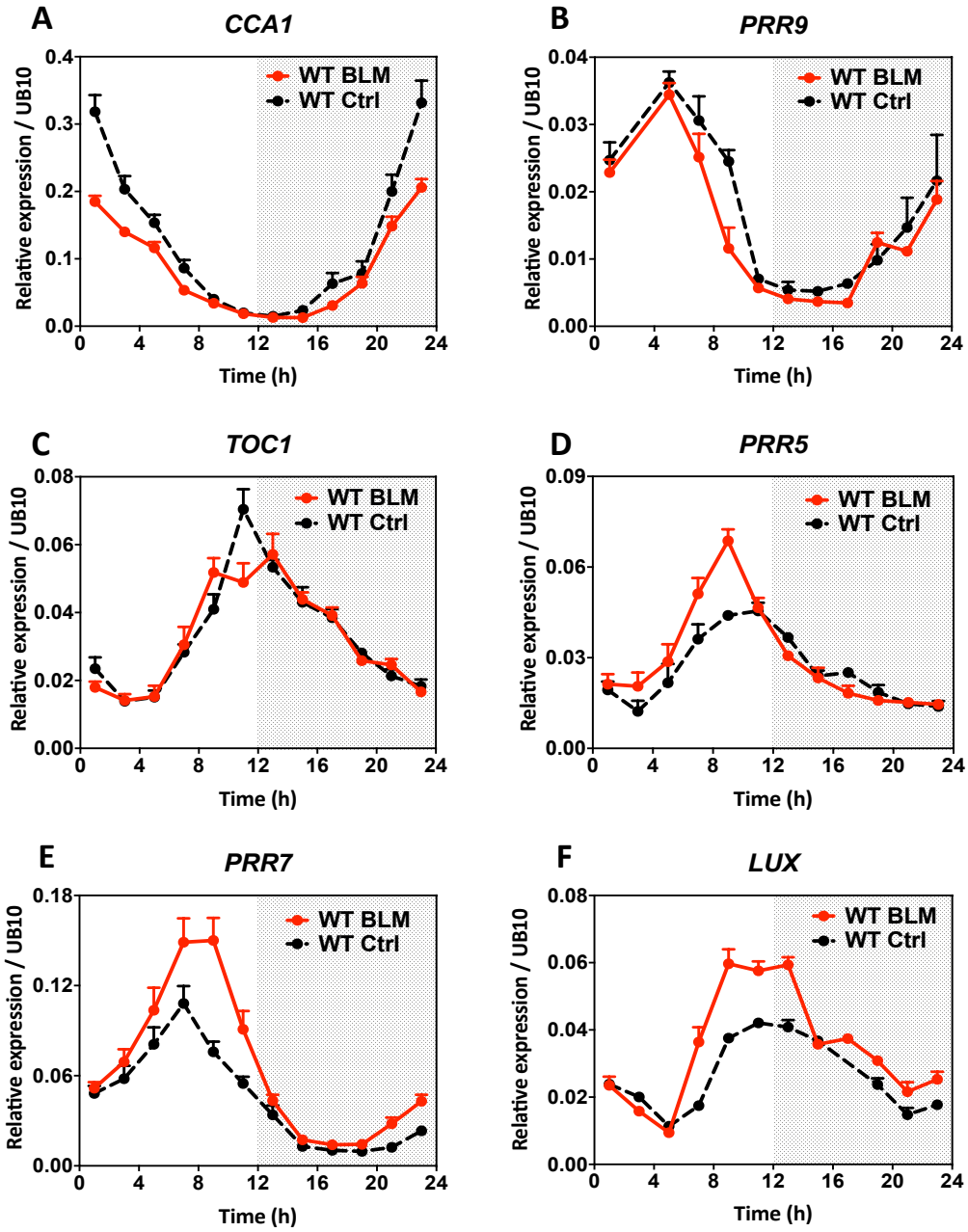

Figure 18. The clock components sustain similar circadian rhythms in response to BLM under constant light conditions. Gene expression analyses by RT-qPCR of (A) CCA1, (B) PRR9, (C) TOC1, (D) PRR5, (E) PRR7 and (F) LUX in untreated WT plants (Ctrl) and BLM treated plants. Values are represented as the mean +SEM of at least two biological replicates. White and grey boxes represent subjective light and subjective dark periods, respectively.

To further examine the effect of BLM on clock genes, we monitored the promoter activities of *PRR9*, *PRR7, CCA1* and *TOC1* (*pPRR9:LUC, pPRR7:LUC, pCCA1:LUC* and *pTOC1:LUC*). The promoters of *CCA1* and *TOC1* displayed no apparent changes in response to BLM compared to the mock-treated plants under both LD and LL conditions (Figure 19 and 20). The promoter activity of *PRR9* also did not change under LD (Figure 19C). Under LL, the *PRR7* promoter activity slightly increased after 24-h of BLM treatment to afterwards sustain the oscillations albeit with reduced amplitude (Figure 20C). Together, our results indicate that the oscillation of promoters and mRNAs of clock genes are still rhythmic despite the DNA damage. The changes in mRNA induction of *PRR7* by RT-qPCR were not fully recapitulated in the bioluminescence assays of promoter activity.

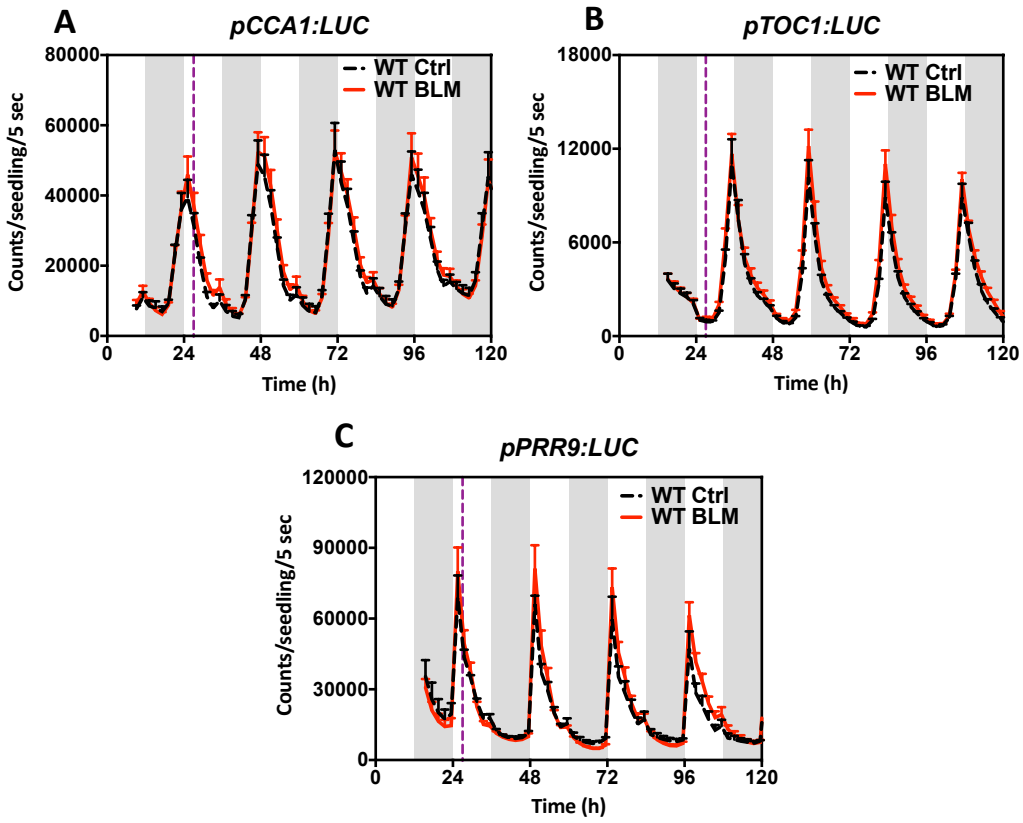

Figure 19. The promoter activity of the clock components sustains similar rhythms in response to DSBs under entraining conditions. Bioluminescence assays for (A) p*CCA1:LUC*, (B) *pTOC1:LUC* and (C) *pPRR9:LUC* in untreated WT (Ctrl) and BLM treated plants. Dotted purple line indicates the BLM treatment. Data represents the means +SEM of the luminescence of 8-10 seedlings. White and grey boxes represent light and dark periods, respectively.

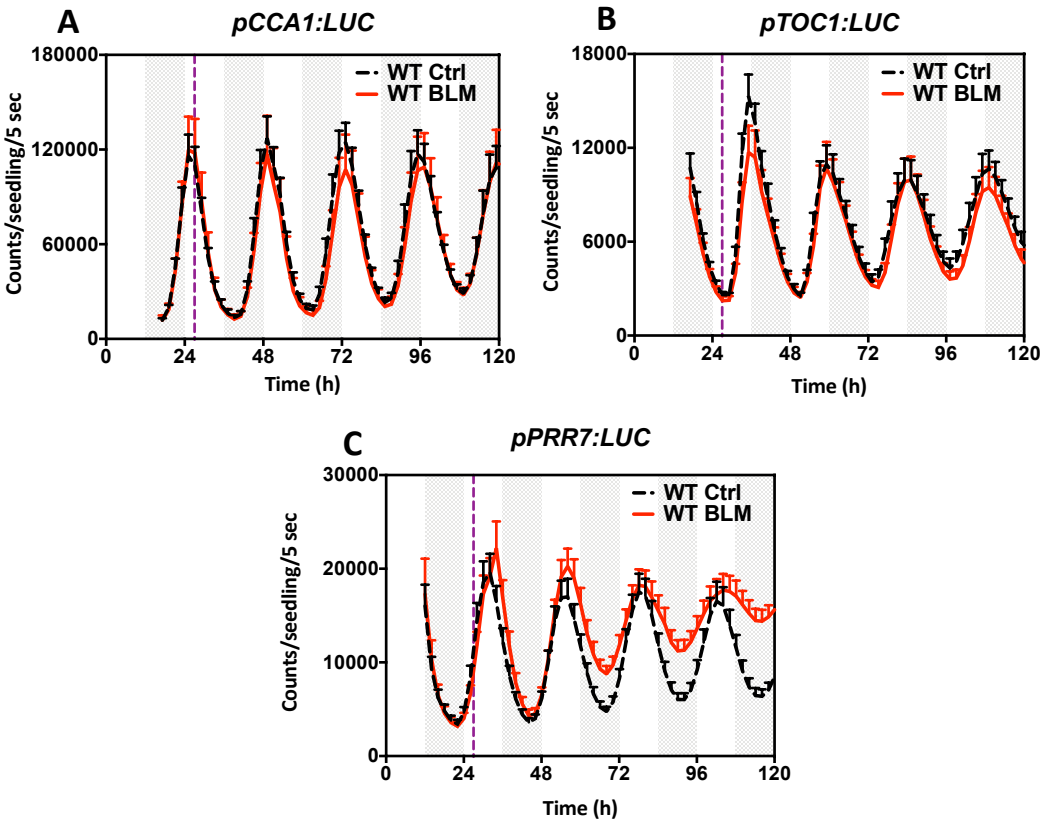

Figure 20. The promoter activity of the clock components sustains similar rhythms in response to DSBs in constant light conditions. Bioluminescence assays for (A) p*CCA1:LUC,* (B) *pTOC1:LUC* and (C) *pPRR7:LUC* in untreated WT plants (Ctrl) and BLM treated plants. Dotted purple line indicates the BLM treatment. Data represents the means +SEM of the luminescence of 8-10 seedlings. White and grey boxes represent subjective light and subjective dark periods, respectively.

5. Proper expression of *CCA1* is important for the rhythmic induction of the DNA Damage and Repair (DDR) response

Based on the observed rhythmic induction of DDR genes, we next examined bioluminescence rhythms of *pBRCA1:LUC* and *pRAD51:LUC* in plants in which the clock is not properly functioning. To that end, we transformed the *pBRCA1:LUC* and *pRAD51:LUC* constructs into the CCA1 over-expressing plants (CCA1-ox) (Wang & Tobin, 1998) and analyzed rhythms following BLM treatment under LD and LL conditions. Our results showed that BLM-induced rhythms persisted in CCA1-ox plants but *pBRCA1:LUC* and *pRAD51:LUC* induction was clearly reduced in CCA1-ox compared to WT (Figure 21). The high induction after BLM treatment in WT was particularly reduced for *pRAD51:LUC* (Figure 21B). However, the promoter oscillations were still sustained albeit with low amplitude (inset on Figure 21B).

Consistent with the lack of proper functioning of the clock, rhythms were severely compromised in CCA1-ox under LL conditions (Figure 22A and inset of Figure 22B). The promoter activity showed dampening of rhythms observed under LD particularly for *pRAD51:LUC* (compare insets of Figure 21B and Figure 22B). These results suggest that the circadian clock controls the rhythms of DDR promoter induction following BLM treatment.

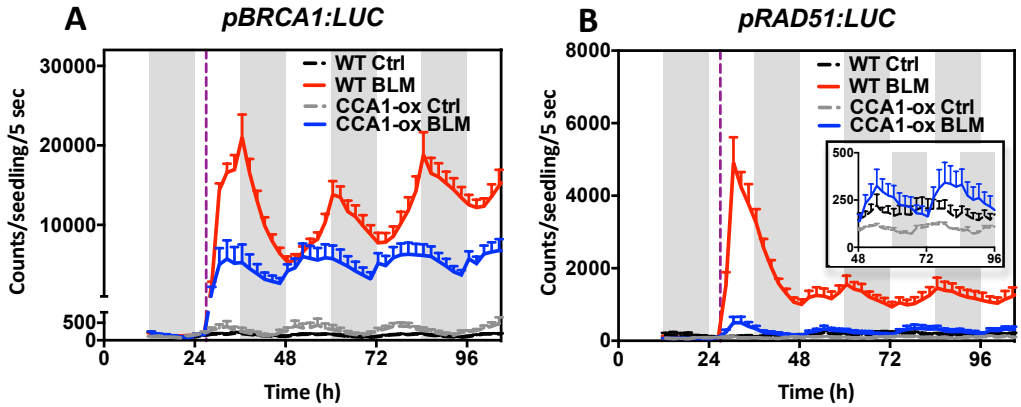

Figure 21. The clock regulates the induction and followed rhythms of the DDR promoters under entraining conditions. Bioluminescence assays for (A) p*BRCA1:LUC* and (B) *pRAD51:LUC* in WT and CCA1-ox lines in untreated plants (Ctrl) and BLM treated plants. (B) The inset figure shows a magnification of the promoter activity of *pRAD51:LUC* below 500 counts/seedling/5sec and from 48 to 96h. Dotted purple line indicates the BLM treatment. Data represents the means +SEM of the luminescence of 5-6 seedlings. White and grey boxes represent light and dark periods, respectively.

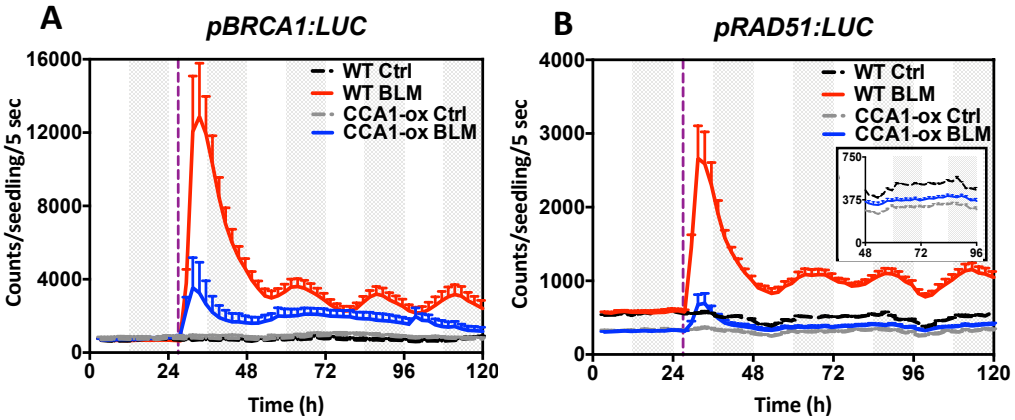

Figure 22. The clock regulates the induction and followed rhythms of the DDR promoters under constant light conditions. Bioluminescence assays for (A) p*BRCA1:LUC* and (B) *pRAD51:LUC* in WT and CCA1-ox lines in untreated plants (Ctrl) and BLM treated plants. (B) The inset figure shows a magnification of the promoter activity of *pRAD51:LUC* below 750 counts/seedling/5sec and from 48 to 96h. Dotted purple line indicates the BLM treatment. Dotted purple line indicates the BLM treatment. Data represents the means +SEM of the luminescence of 5-6 seedlings. White and grey boxes represent subjective light and subjective dark periods, respectively. .

Our results indicate that the circadian clock rhythmically regulates the transcriptional response to BLM, at least for a subset of DDR genes. Based on the altered DDR promoter activity in CCA1-ox (Figure 17 and 18), we next performed time course analyses of DDR gene expression in WT and CCA1-ox plants. Consistent with the promoter activity results, our analyses showed a reduced BLM-dependent rhythmic induction of *PARP2* and particularly of *RAD51* in CCA1-ox compared to WT under LD conditions (Figure 23). The regulation seemed to be specific after DNA damage by BLM, as DDR gene expression in mock-treated (Ctrl) plants was not significantly affected by *CCA1* over-expression (Figure 23).

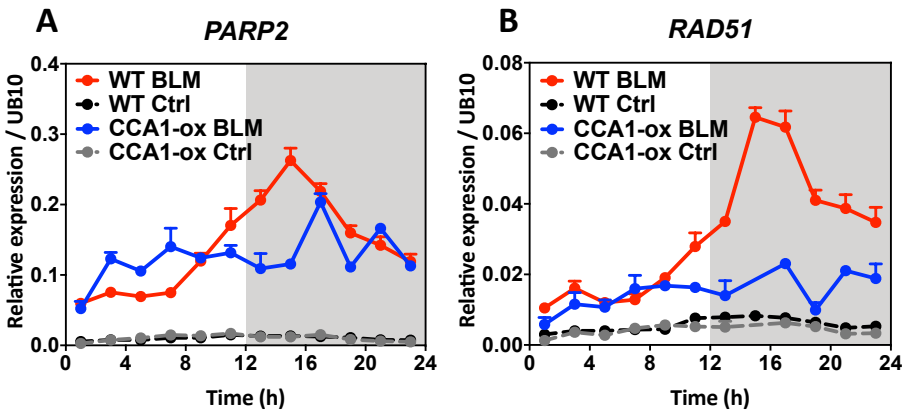

Figure 23. Over-expression of *CCA1* severely affects the DDR induction and the rhythmic response under entraining conditions. Gene expression analyses by RT-qPCR of (A) *PARP2* and (B) *RAD51* in untreated WT and CCA1-ox plants (Ctrl) and BLM treated plants. Values are represented as the mean + SEM of at least two biological replicates. White and grey boxes represent the day and night periods,

The reduced induction in *PARP2* and *RAD51* was also observed when CCA1-ox plants were treated under LL conditions (Figure 24). Analogously to the luminescence assays (Figure 22), over-expression of *CCA1* showed a more severe effect in the induction of *PARP2* and *RAD51* (Figure 24). Our results indicate that CCA1 may play a key role in the rhythmic DDR response.

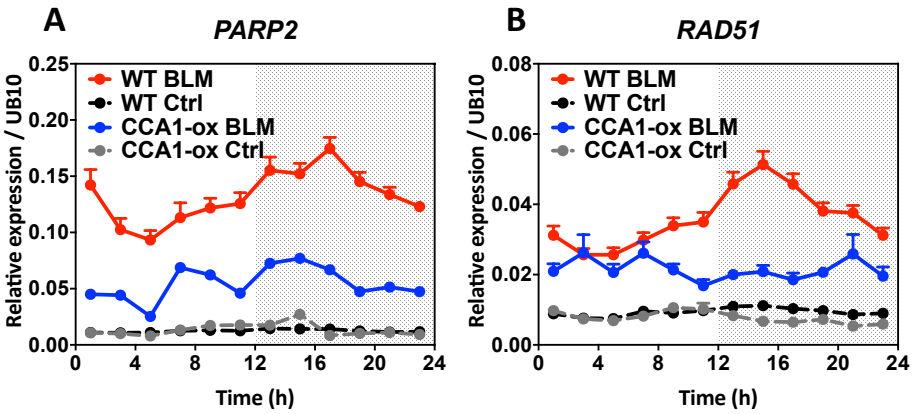

Figure 24. Over-expression of *CCA1* severely affects the DDR induction and the rhythmic response under constant light conditions. Gene expression analyses by RT-qPCR of (A) *PARP2* and (B) *RAD51* in untreated WT and CCA1-ox plants (Ctrl) and BLM treated plants. Values are represented as the mean + SEM of at least two biological replicates. White and grey boxes represent subjective day and subjective night periods, respectively.

6. The miss-regulation of *PRR7* and other PRRs alters the DNA Damage and Repair (DDR) response

As *PRR7* mRNA expression was induced following BLM treatment (Figure 17, 18 and 20), we also examined DDR induction in PRR7 over-expressing plants (PRR7-ox) and PRR7 knock-out mutant (*prr7-11)* plants. Our results showed that contrarily to the effect of CCA1-ox, the BLM-dependent induction was increased in PRR7-ox compared to WT (Figure 25A-B). The phase of *PARP2* induction appeared to be advanced in PRR7-ox (Figure 25A) but this phase shift was not so evident for *RAD51* (Figure 25B). Analyses of *prr7-11* mutant plants showed a similar induction compared to WT but with and advanced phase for *PARP2* (Figure 25C). Due to the partial redundant roles of PRR7 with other members of the PRR family (Farre et al., 2005, Nakamichi et al., 2005), we also examined *PARP2* and *RAD51* expression in the *prr5prr7prr9* triple mutant (*prr579)* (Fukushima et al., 2009). The results showed an important reduction of the BLM-dependent expression in the triple mutant compared to WT (Figure 25E-F). The reduction was particularly severe for *RAD51*, showing nearly similar accumulation to that of non-treated plants. Together, the results confirm that proper expression of *CCA1* and *PRR7* and other PRR genes is important for the DDR activation following BLM treatment.

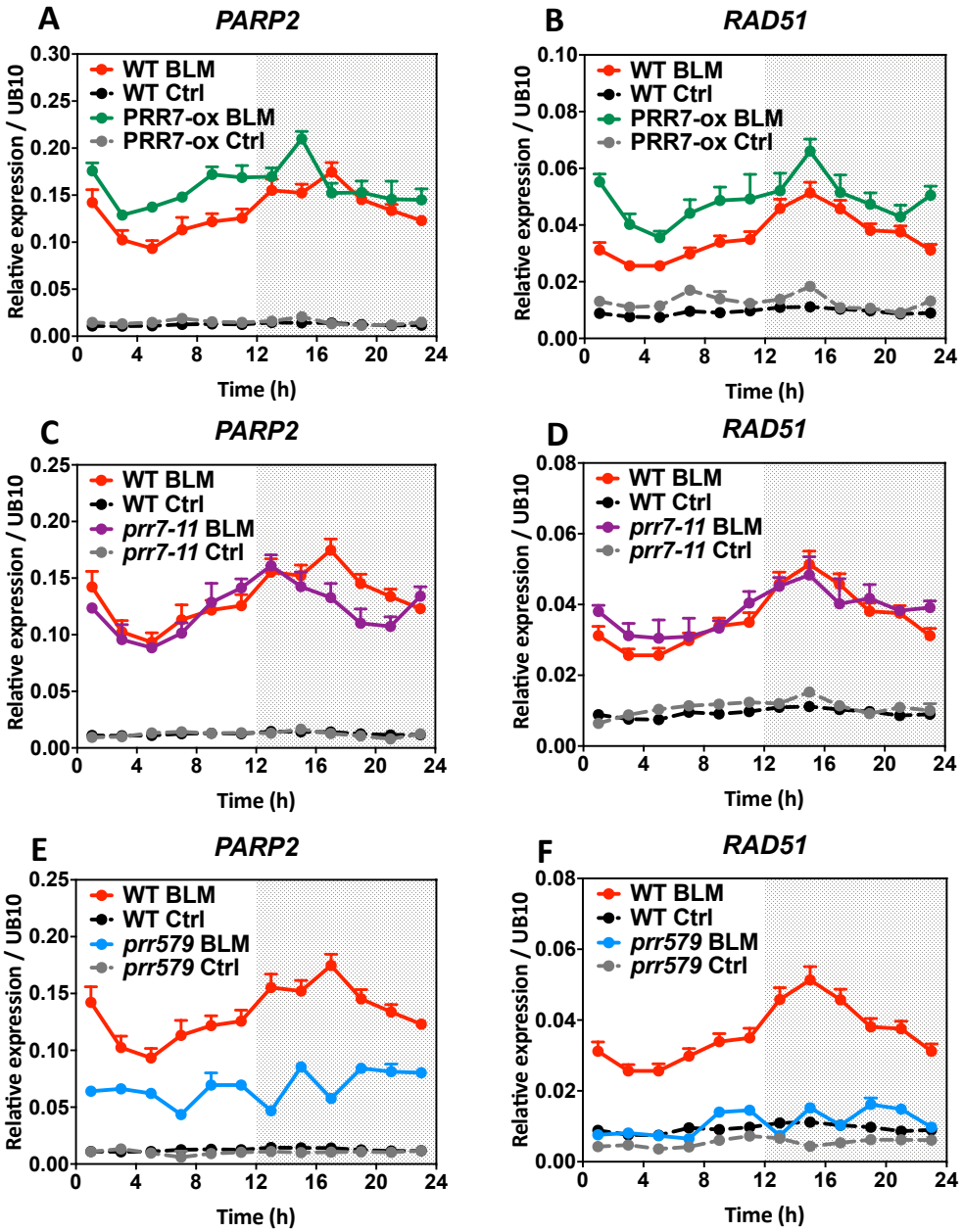

Figure 25. The proper expression of *PRR7* and other PRRs modulate the induction and rhythmic oscillations of the DDR genes under constant light conditions. Gene expression analyses by RT-qPCR of (A, C, E) *PARP2* and (B, D, F) *RAD51* in untreated WT, PRR7-ox, *prr7-11* and *prr579* plants (Ctrl) and BLM treated plants. Values are represented as the mean + SEM of at least two biological replicates. White and grey boxes represent subjective day and subjective night periods, respectively.

7. Diurnal regulation of parylated proteins accumulation upon bleomycin treatment

A number of different protein post-translational modifications are triggered following DNA damage. Among them, parylation (poly-ADP ribosylation, PAR) has been shown to

be key for the DDR pathway (Bartolomei et al., 2016). To determine whether the accumulation of the PAR modification in response to DNA damage is regulated by the clock, we performed Western-blot analyses using an antibody that specifically detects parylated proteins (anti-PAR antibody). Twelve day-old seedlings of WT and *CCA1* over-expressing lines (CCA1-ox) were grown under entraining LD cycles, and then treated with 10 μM of BLM at two different time points: during the day (ZT3) and during the night (ZT15). Total protein extracts were prepared after 24h of treatment, separated by SDS-PAGE and analyzed by immunoblotting with the anti-PAR antibody.

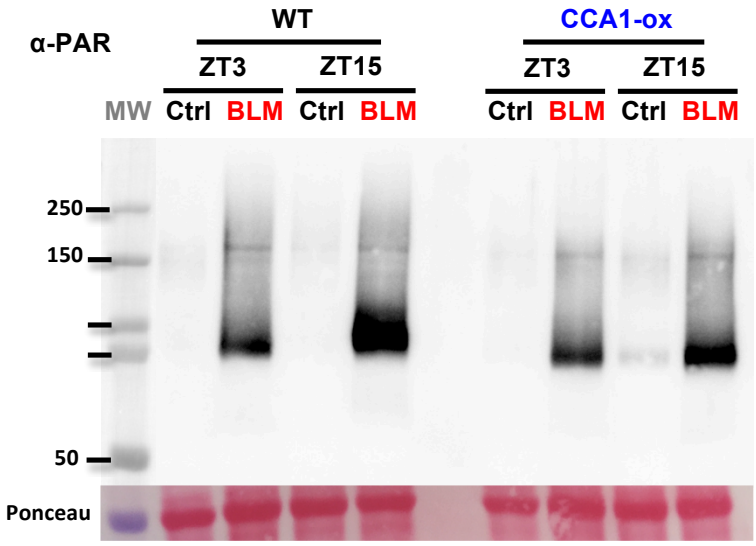

Figure 26. The circadian clock regulates the accumulation of parylated proteins. Western blot analysis of PAR deposition in untreated WT and CCA1-ox plants and BLM treated plants in LD. Equivalent loading of lanes was verified by Ponceau staining. Similar results were obtained in at least two independent experiments. MW: Molecular Weight, KDa: Kilodaltons.

Our results showed a clear accumulation of parylated proteins upon BLM treatment whereas no detectable parylation was found in mock-treated control samples (Figure 26). Parylated proteins appeared as a high molecular weight smear, with a strong band around 75-100 kDa. The distribution pattern correlated with the one described in previous studies (Caruso et al., 2018, Song et al., 2015). The bulk of parylated proteins appeared to be higher at ZT15 compared to ZT3 in WT plants treated with BLM (Figure 26) suggesting a differential regulation depending on the time of sampling. In contrast, and compared to WT, the strong band around 75-100 kDa was importantly reduced in CCA1-ox plants, particularly at ZT15 but not at ZT3 (Figure 26). These results suggest

that protein parylation might be also regulated by the clock and that proper expression and function of CCA1 directly or indirectly contributes to this rhythmic response.

8. The photoreceptor CRY2 regulates the circadian response to double strand breaks

CRYs share sequence homology with the photolyase protein family (Kavakli et al., 2017, Mei & Dvornyk, 2015). Although CRYs lack the photorepair activity of the photolyase enzymes (Selby & Sancar, 2006, Yang et al., 2017), a number of studies have implied a connection of CRYs with DNA repair (Selby & Sancar, 2006). Based on the circadian response of the DDR pathway that we observe in our studies and due to the connection of CRYs with the circadian clock (Devlin & Kay, 2000), we examined the transcriptional changes upon BLM treatment in WT and CRY2 mutant plants (*cry2-1*) (Lin et al., 1998). Time course analyses by RT-qPCR following 24h BLM treatment showed a clear reduction of the induction of DDR genes, particularly evident for *RAD51* but also clear for *PARP2* (Figure 27). The altered induction suggests that CRY2 activity might be important for the DDR rhythmic response by the clock.

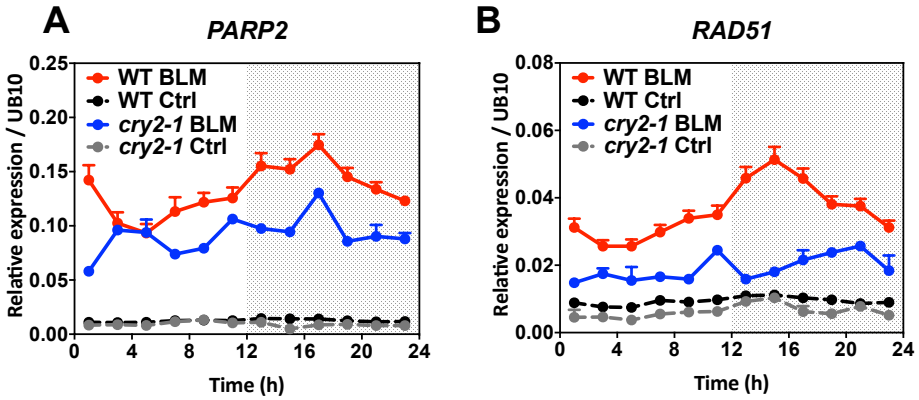

Figure 27. CRY2 regulates the rhythmic induction of the DDR genes. Gene expression analyses by RT-qPCR of (A) *PARP2* and (B) *RAD51* in untreated WT and *cry2-1* plants (Ctrl) and BLM treated plants. Values are represented as the mean + SEM of at least two biological replicates. White and grey boxes represent subjective day and subjective night periods, respectively.

9. Proper *CRY2* expression is essential for the transcriptional regulation of the DNA Damage and Repair (DDR) response

To examine early DDR responses and the role of CRY2 in these responses, we analyzed the transcriptional changes upon short BLM treatments of 1h, 2h, 4h and 8h with

samples collected at ZT9 (Figure 28A). Time course analyses by RT-qPCR showed that in WT plants, BLM treatment increased DDR gene expression, reaching a peak around 2h-4h with BLM (Figure 28B-D). Compared to WT, DDR gene induction was decreased in *cry2-1* and increased in CRY2 over-expressing plants (CRY2-ox) (Yu et al., 2009) (Figure 28B-D). As CRY2 is a blue light photoreceptor (BL) (Yu et al., 2009), we checked DDR gene expression in plants growing under blue light:dark cycles (BLD). Our results showed that the increased (CRY2-ox) and decreased (*cry2-1*) induction of DDR genes compared to WT was lost under BLD (compare Figure 28B-D and Figure 28E-G).

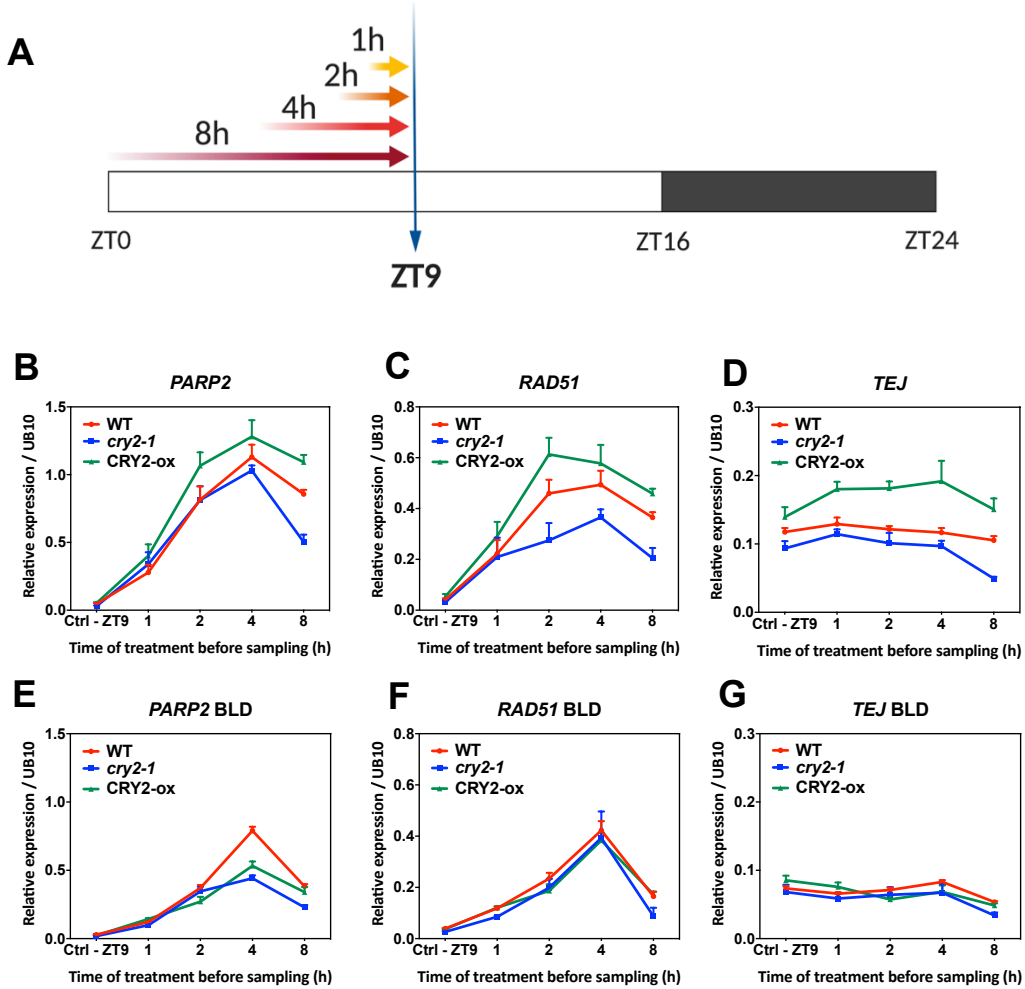

Figure 28. CRY2 plays a crucial role in the rapid induction of the DDR genes under entraining conditions and under blue light:dark conditions (BLD). (A) Schematic drawing depicting the experimental design for the time course analyses of BLM treatments. Gene expression analyses by RT-qPCR of (B, E) *PARP2,* (C, F) *RAD51* and (D, G) *TEJ* in untreated WT, *cry2-1* and CRY2-ox plants and BLM treated plants. Values are represented as the mean + SEM of at least two biological replicates. Diagram created with BioRender.

10. Double strand break accumulation is affected in CRY2 miss-expressing plants

To analyze if the accumulation of DSBs is also regulated by CRY2, we performed comet assays with samples collected at ZT9, following 8h treatment with BLM as described in Figure 28A. Our results showed that compared to WT, the tail moment was significantly reduced in *cry2-1* and increased in CRY2-ox (Figure 29A-B). Analyses of mutant plants of TEJ (*parg1-2*) confirmed the increased damage by BLM. Altogether, the comet assay data suggest that DNA damage is reduced in the absence of a functional CRY2 and conversely, over-expression of CRY2 renders plants more susceptible to DNA damage.

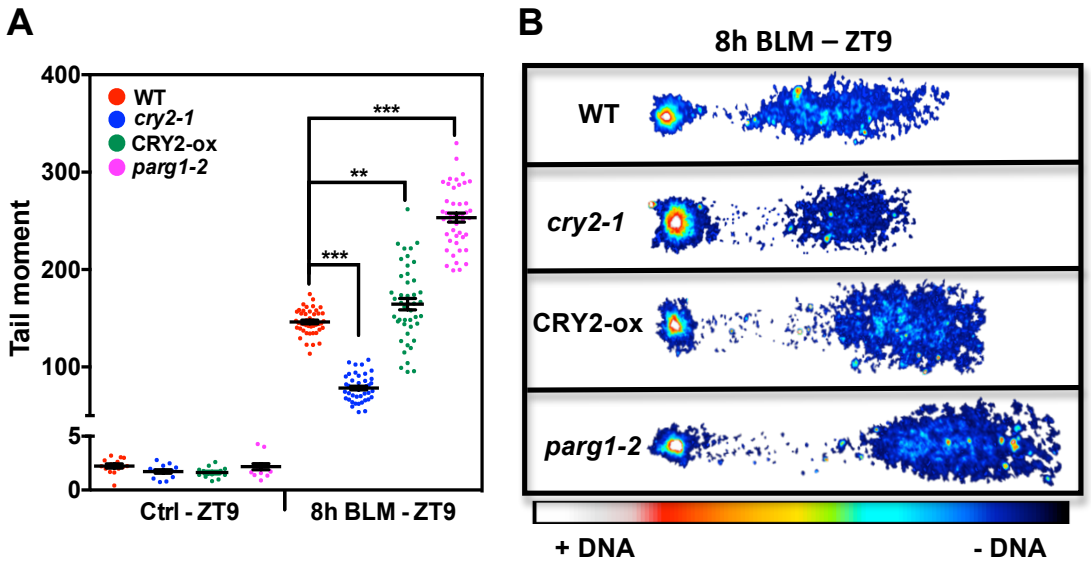

Figure 29. DSB accumulation is regulated by CRY2 under entraining conditions. Analyses of the comet assays in untreated WT, *cry2-1,* CRY2-ox and *parg1-2* plants and BLM treated plants. (B) Confocal images of Comets from BLM treatments (coloured with Image J). Data are represented as the mean + SEM of n ≥ 40 Comets of at least two biological replicates. Unpaired t-test was performed to evaluate the statistical significance of differences between each condition. ** P-value ≤ 0,01, *** P-value ≤ 0,001.

11. DNA-RNA hybrids are increased in response to DNA damage and their formation requires a functional CRY2

CRY2 has been implicated in the regulation of chromatin conformation (van Zanten et al., 2010). Therefore, we explored possible changes in chromatin structure in WT

plants treated with BLM. We also examined whether CRY2 has a functional role regulating these changes. To that end, we focused on the formation of DNA-RNA hybrids known as R-loops (Xu et al., 2017). The DNA-RNA hybrids are transient secondary structures formed during transcription, resulting in a displaced single stranded DNA (ssDNA) and the stable formation of a hybrid between the nascent RNA and the second ssDNA (DNA-RNA hybrid, Figure 30). R-loops have been previously connected with DSB localization, stabilization and repairing (Skourti-Stathaki & Proudfoot, 2014, Ohle et al., 2016).

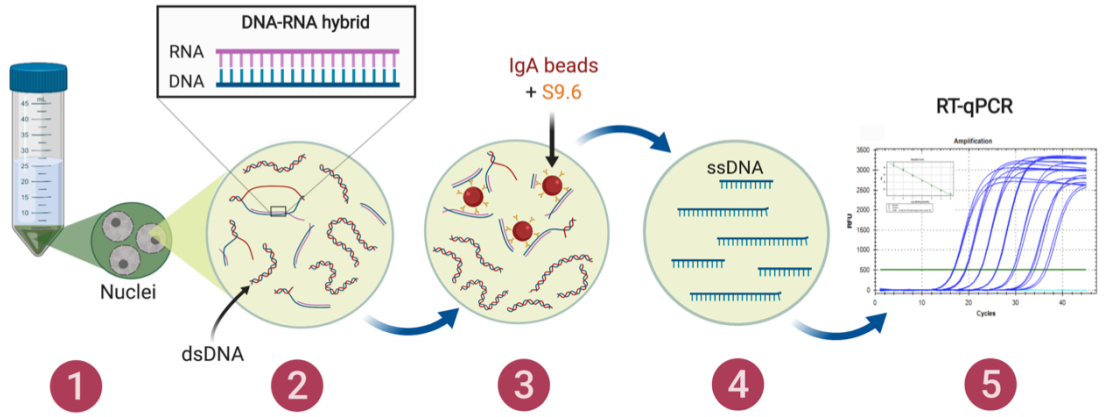

Figure 30. Schematic diagram depicting the DRIP-qPCR assay in *Arabidopsis thaliana*. Genomic DNA from purified nuclei extracts (1) is fragmented by sonication or enzyme digestion (2), and then the DNA-RNA hybrids are immunoprecipitated with the S9.6 antibody (3). ssDNAs are purified (4) and analyzed by RT-qPCR (5). Created with BioRender.com.

In our studies, R-loop formation was analyzed by DNA-RNA hybrid immunoprecipitation followed by qPCR (DRIP-qPCR) (Xu et al., 2017). The R-loops were immunoprecipitated using a specific antibody (S9.6) that recognizes DNA-RNA hybrids (Xu et al., 2017). The RNA from the immunoprecipitated hybrids was then removed and the ssDNA analyzed by RT-qPCR (Figure 30). Upon BLM treatment, R-loops were formed for a subset of the DDR loci analyzed. Enrichment of the DNA-RNA hybrids was particularly evident around the 5´ region and the transcriptional start sites of the genes (Figure 31A-B). The R-loop formation was clear for *PARP2, TEJ* and *RAD51* but also for other DDR genes such as *LIG4* and *MRE11*. No clear R-loop formation was observed in the 3´region of *PARP2* or the *LIG4*, suggesting that BLM does not pervasively and unspecifically induce R-loop formation.

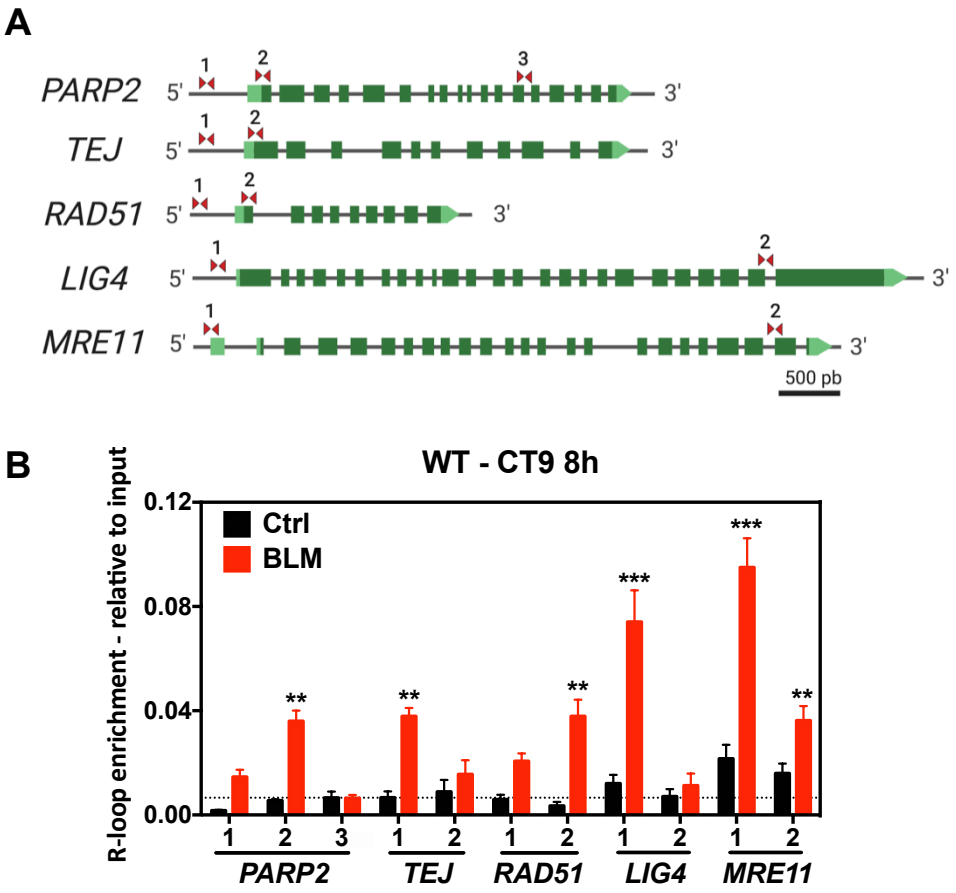

Figure 31. DSBs induce R-loop enrichment at the transcription start sites of the DDR genes. (A) Diagram depicting amplification regions; double arrowheads indicate primer positions. (B) DRIP-qPCR analyses of untreated and BLM treated plants for WT. The region 3 of *PARP2* was used as a negative control. Enrichment is represented as the mean + SEM relative to 10% of Input of at least two biological replicates. Dotted line represents threshold enrichment. Unpaired t-test was performed to evaluate the statistical significance of differences between each condition and the region 3 of PARP2. ** P-value ≤ 0,01, *** P-value ≤ 0,001. Diagram created with BioRender.

We next compared R-loops in WT and *cry2-1* mutant plants. Overall, there were not significant changes in R-loop formation in WT and *cry2-1* non-treated plants (Figure 32). However, in BLM-treated samples, R-loops in *cry2-1* plants were significantly reduced or even reached levels of non-treated plants (Figure 32). These results suggest that R-loop formation requires directly or indirectly proper CRY2 function. It is possible that the reduced DDR response observed in *cry2-1* might be mediated at least in part by the decreased R-loop formation.

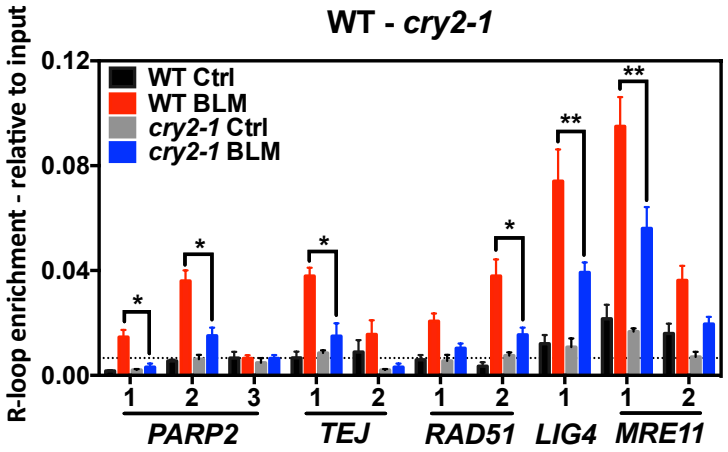

Figure 32. R-loop formation in response to DSB is mediated by CRY2. DRIP-qPCR analyses of untreated WT and *cry2-1* plants and BLM treated plants. The region 3 of *PARP2* was used as a negative control. Enrichment is represented as the mean + SEM relative to 10% of Input of at least two biological replicates. Dotted line represents threshold enrichment. Unpaired t-test was performed to evaluate the statistical significance of differences between BLM treated WT and *cry2-1* data. * P-value ≤ 0,05, ** P-value ≤ 0,01.

12. CRY2 binds to DNA Damage and Repair (DDR) loci in response to double strand breaks

Our results of gene expression, comet assays and R-loop formation all point out to a role of CRY2 in the DDR pathway. We next examined whether this CRY2 function might occur through direct binding to DDR genes. We thus performed Chromatin Immunoprecipitation assays (ChIP) followed by q-PCR analyses of selected DDR genes using CRY2-ox plant samples collected at ZT9. Our results showed CRY2 specific binding to the *TEJ* and *PARP2* loci (Figure 33A), a binding that was significantly increased upon BLM treatment (Figure 33A). The use of a transgenic line expressing *CRY2* under its own promoter in the *cry2-1* mutant background (CRY2 minigene) confirmed that the binding was not due to artefactual over-expression of CRY2 (Figure 33B) although CRY2 binding to region 2 of *PARP2* was not observed in CRY2 minigene plants (Figure 33B). Together, the results suggest that the phenotypes in gene expression and comet assays in plants miss-expressing CRY2 might be due to alterations in R-loop formation and the direct binding of CRY2 to *TEJ* and *PARP2* loci.

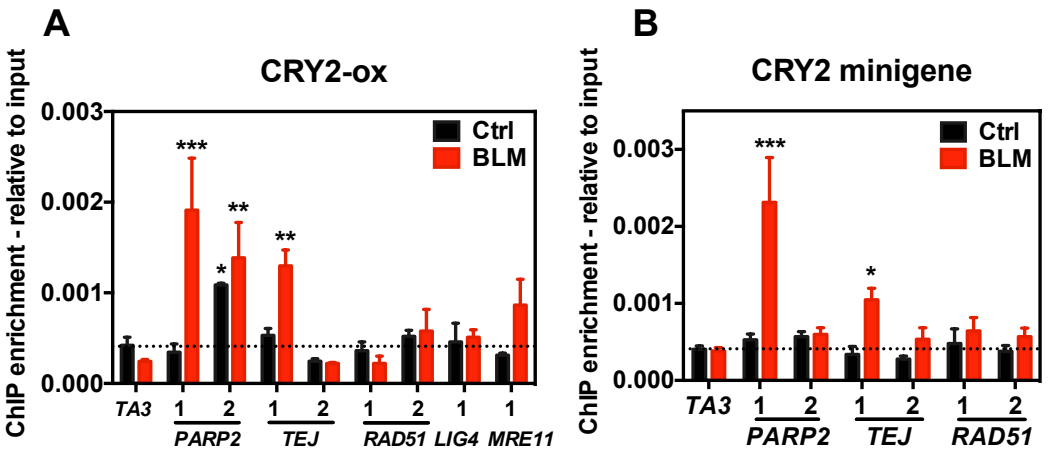

Figure 33. CRY2 binds to important DDR gene promoters in response to DSBs. Chromatin Immunoprecipitation (ChIP) assays for (A) CRY2-ox and (B) CRY2 minigene in untreated plants and BLM treated plants. Values processed with antibody (+α) are represented as the mean + SEM relative to 10% of Input. Experiments were repeated at least two times independently, with similar results. Promoter regions are depicted in Figure 32A. The retrotransposon TA3 was used as a negative control. Dotted line represents threshold enrichment. Unpaired t-test was performed to evaluate the statistical significance of differences between each condition and TA3. * P-value ≤ 0,05, ** P-value ≤ 0,01, *** P-value ≤ 0,001.

13. Altered *CRY2* expression affects cell death and leaf emergence after BLM treatment

We next investigated whether the observed phenotypes were transduced into cellular and physiological responses to DNA damage. One common cellular response is cell death after prolonged DNA damage. We used Trypan blue staining, which only penetrates death cells and thus discriminates between non-viable (blue) and viable (transparent) cells (Strober, 2001). Analyses of WT plants clearly indicated the cell death in leaves of BLM treated plants (Figure 34A). In *cry2-1* mutant leaves, BLM treatment also induced cell death but to a lesser extent than in WT plants (Figure 34B). The differences were slight but significant and reproducible (Figure 34B). The use of *parg1-2* mutant plants confirmed the efficacy of both the BLM treatment inducing cell death and the Trypan blue staining of death cells (Figure 34).

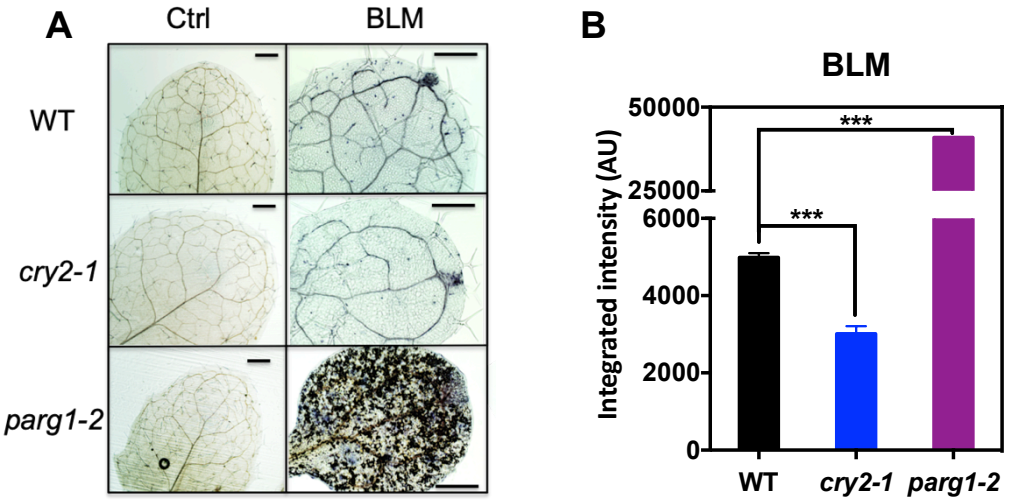

Figure 34. Cell death triggered by DSBs is decreased in *cry2-1* mutant. (A) Trypan blue staining of untreated WT, *cry2-1* and *parg1-2* plants and BLM treated plants (BLM) for 7 days under entraining conditions. (B) Integrated intensity is represented for WT, *cry2-1* and *parg1-2* BLM treated leaves. Similar results were obtained in at least two independent experiments. Scale bars represent 0.2mm. Unpaired t-test was performed to evaluate the statistical significance of differences between each condition. *** P-value ≤ 0,001.

DSBs promote cell cycle arrest that leads to transient or stable developmental defects (Yoshiyama et al., 2014). We therefore monitored leaf emergence every 2 days as an indirect way of measuring meristem activity. The emergence of the first pair of true leaves was scored as the percentage of the number of seedlings with true leaves versus total number of seedlings in the condition. Control non-treated plants showed no evident differences in leaf emergence in all genotypes examined (Figure 35B). Treatment with BLM led to a severe delayed emergence of true leaves compared to untreated plants (Figure 35A). However, the examined genotypes responded differently to BLM. Compared to WT, leaf emergence was accelerated in *cry2-1* mutant at 9, 11 and 13 days after germination (dag) (Figure 35B). Over-expression of *CRY2* showed a slight but reproducible delayed of true leaf emergence particularly evident at later stages (11-13 dag) (Figure 35A). Leaf emergence of the *parg1-2* mutant was severely affected after BLM treatment (Figure 35B). Taken together, our results suggest a key role of CRY2 regulating leaf emergence in response to DSBs.

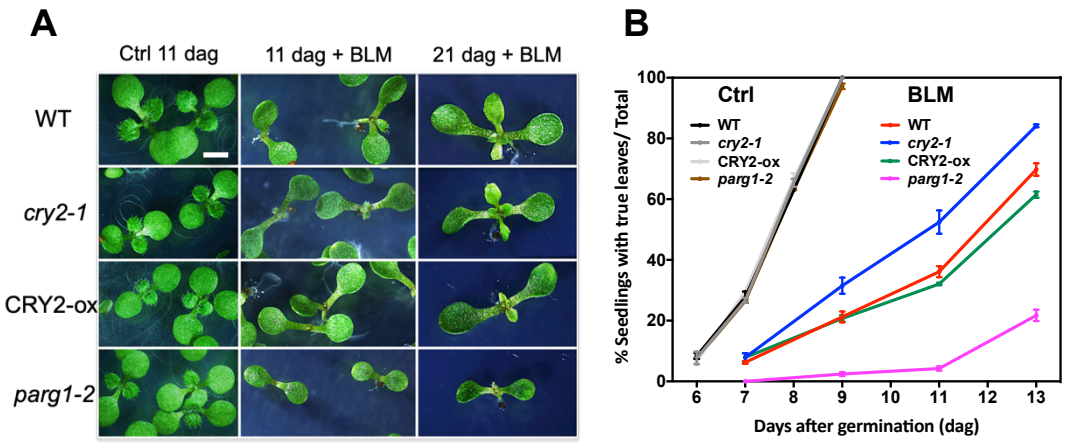

Figure 35. *CRY2* expression correlates with true leave emergence in response to DSB. (A) Pictures of WT, *cry2-1,* CRY2-ox and *parg1-2* non-treated plants and BLM treated plants after 11 and 21 days after germination (dag). (B) True leaf emergence is represented as the mean + SEM of at least two biological replicates. Scale bar represents 0.5 mm.

DISCUSSION

Discussion

The DNA damage needs to be properly repaired to ensure genome integrity and stability (Manova & Gruszka, 2015). Although genome instability is the basis of adaptation and evolution (Spampinato, 2017, Puchta, 2005), organisms have evolved efficient and specific repair mechanisms to avoid DNA defects that can lead to genetic diseases and ultimately compromise development and growth (Manova & Gruszka, 2015). The different mechanisms involved in the detection and repair of the DNA entail high energy-demand and numerous metabolic changes that require a tight synchronization in space and time with the cellular processes (West et al., 2004). In this Doctoral Thesis, we have studied the role of the circadian clock regulating the timing of the DDR response to DNA DSBs in Arabidopsis. Our studies have shown that plant cells display a circadianly regulated response to DNA DSBs. We also found that the cryptochrome CRY2 plays an essential role mediating this regulation.

DSBs are particularly harmful for the cells and need to be repaired in order to avoid chromosome rearrangements that can lead to cell cycle arrest and cell death (Waterworth et al., 2011). In mammals, DSBs are commonly associated to cancer development due to the chromosomal instabilities and mutagenic effects that compromise the cell cycle (Aplan, 2006). The comet assays are very valuable techniques to measure the extent of DSBs (Santos et al., 2015). Several studies have reported the efficacy of the method in plants exposed to a wide range of genotoxic stresses. For instance, using comet assays, Moreno-Romero et al (2012) found that DSBs are rapidly repaired in plants lacking a functional CASEIN KINASE 2 (CK2) activity (Moreno-Romero et al., 2012). Our comet assays revealed that DSBs after bleomycin treatment are higher during the day than at night, which opens the possibility that the repair mechanisms might be preferentially enhanced at night. The enhanced response might be related to the protection against DNA damage during DNA replication. The cell cycle checkpoints guarantee proper genome integrity to the next cells by enhancing DNA repair right before the S-phase (DNA replication) and M-phase (cell division) (Kaufmann & Paules, 1996). During replication of the DNA, nucleosomes and other interacting proteins are removed from the DNA and thus exposing and making

the DNA more vulnerable to DNA damage. In this context, studies in several eukaryotic organisms support the "escape from light" hypothesis (Pittendrigh, 1993), which proposes that the DNA replication during the S-phase occurs predominantly at night when the risk of DNA damage by solar radiation or other DNA stresses is lower. In Arabidopsis, the timing of the S-phase is also regulated by the circadian clock in a mechanism that relies on the repression of the licensing factor *CDC6* by TOC1 (Fung-Uceda et al., 2018). In mammals, the circadian clock is able to couple the DDR with the cell cycle in order to coordinate proper cell cycle checkpoints upon DNA damage (Sancar et al., 2010). In unicellular photosynthetic organisms such as *Chlamydomonas reinhardtii,* UV-sensitive processes also occur at night when the UV levels are low or absent (Nikaido & Johnson, 2000). Thus, our results support the "escape from light" hypothesis suggesting that DNA damage by DSBs might be more efficiently repaired at night to reduce the possible DNA lesions during the S-phase of the cell cycle.

Our results showed that the circadian clock is important for proper regulation of the timing of expression and promoter activity of key DDR genes. We found rhythms upon BLM treatment under both LD and LL conditions. The amplitude of the response slightly dampened under LL. This effect might be due to the slight progressive uncoupling among individual oscillators from cells and tissues as previously reported (Yakir et al., 2011). The implication of the circadian clock in the control of biotic and abiotic stress responses to the most appropriate time-of-day has been extensively reported in plants (Dodd et al., 2015, Lu et al., 2005, Niwa et al., 2009). For example, defense genes involved in pathogen resistance are rhythmically regulated by CCA1 to anticipate pathogen infection (Wang et al., 2011). Moreover, drought responses are also coordinated by the circadian clock through direct regulation of ABA-related genes by TOC1 (Legnaioli et al., 2009). The circadian function regulating stress responses has been proposed to provide an efficient advantage and proper energy-management of the resources (Nohales & Kay, 2016).

The DNA damage recognition and recruitment of the DDR factors are quickly triggered in terms of seconds to minutes upon DSB formation (Polo & Jackson, 2011). Typically,

NHEJ factors are recruited within few seconds and dissociate from the DSBs after several hours, while HR factors display a slight delayed response compared to NHEJ (Polo & Jackson, 2011). In some instances, different metabolic and transcriptional responses are triggered depending on the duration of the stress (Fleta-Soriano & Munne-Bosch, 2016, Junker et al., 2017, Yang et al., 2014). Short-term stresses involve an initial alarm phase in which cells inhibit growth-related processes and trigger stress-response mechanisms to cope with the stress as soon as possible (Fleta-Soriano & Munne-Bosch, 2016). Upon prolonged or long-term stresses, the initial imprint of the stress acts as a memory response allowing the cells to modulate the activity of the defense responses to withstand the stress and repair the damage (Fleta-Soriano & Munne-Bosch, 2016). In our studies, we observed that DNA DSBs boosts a rapid response of the DDR promoter activity and mRNA expression right after BLM treatment while the circadian clock would rhythmically modulate the DDR activity after prolonged DSB damage. Consistent with this idea, our analyses using plants with a disrupted clock confirm that responses to DSBs rely on the proper functioning of the clock. The possible connection of the circadian clock with the DDR response was previously hinted in studies showing the role of TEJ regulating proper periodicity of the circadian oscillations in a light-dependent manner (Panda et al., 2002). In Arabidopsis, the phase in the promoter activity of key clock genes is quite similar to that of their respective mRNAs. However, we have observed a slight advanced phase in the promoter activities of some DDR genes in comparison with their mRNA expression. The phase change might be due to a delay of the transcriptional activity, mRNA processing and stability as reported in other studies (Liu & Tjian, 2018, Honkela et al., 2015).

The circadian responses rely on a robust and complex regulatory clock structure that perceives and responds to external and internal cues (Stelling et al., 2004, Fukuda et al., 2013). We found that the expression of a number of Arabidopsis circadian clock genes is not severely disrupted after BLM treatment, confirming the robustness of the circadian system upon stress. The resilience of the circadian system might allow to sustain proper rhythms of outputs that are essential for the stress response (Fukuda et al., 2013). The circadian clock is also a dynamic and flexible system that continuously

adapts to entraining factors (Nohales & Kay, 2016). This phenotypic plasticity can involve quick clock adjustments in phase, period and in the amplitude of the circadian oscillations to be in-tune with the responses (Webb et al., 2019). Our results suggest that the DSBs would promote changes in the expression and/or promoter activity of a subset of clock genes that might be important for the proper-gated DDR. Consistent with this idea, our studies showed that miss-expression of *CCA1* or *PRR7* leads to alterations in the expression and promoter activity of key DDR genes. We found that *PRR7* mRNA induction after BLM treatment was not recapitulated in our analyses of promoter activity. It is possible that our cloning of the *PRR7* promoter is lacking motifs not included within the 1080 bp upstream of the transcription start site (TSS) cloned in our construct. It is also possible that post-transcriptional mechanisms are involved in the regulation of *PRR7* mRNA (Honkela et al., 2015). Future studies are needed to fully elucidate the cellular and molecular mechanistic insights of CCA1 and PRR7 function on the DDR.

DSB repair involves a subset of controlled changes in the activity and cell location of many proteins through post-translational modifications (PTMs) that enable amplification of the DNA damage signal, recruitment of repair factors and efficient DNA repair (Pellegrino & Altmeyer, 2016). The tight coordination among the multiple PTMs strengthens and balances the DNA damage signaling and repair. Particularly, protein parylation plays an essential role in response to DSBs as a platform to recruit repair factors to the DNA lesion, but also in other biological processes including the cell cycle (Lamb et al., 2012). Consistently, we found that upon DSBs not only transcription but also protein parylation are controlled by the circadian clock in a time-dependent manner. It is possible that TEJ might be involved in the circadian regulation of protein parylation upon DNA damage as TEJ function is important sustaining proper circadian period by the clock (Panda et al., 2002).

Several components involved in the DDR response in plants are influenced by environmental factors including light changes (Boyko et al., 2005). In the case of mammals, the interplay between the DDR and the circadian clock is mediated by the

blue light photoreceptors cryptochromes (Sancar et al., 2010). Despite the structural and functional differences in plants compared to mammals, we found that the proper regulation of the DDR by the clock requires CRY2. Plant cryptochromes have lost the characteristic photorepair activity found in photolyases that enable repair DNA photoproducts generated by solar radiation (Manova & Gruszka, 2015). However, our data suggest that CRY2 directly or indirectly is involved in the DDR pathway. Indeed, over-expression of *CRY2* not only up-regulated the expression of DDR related genes but also the DSB accumulation. Conversely, *CRY2* mutant plants showed down-regulated DDR expression and decreased amount of DSBs. van Zanten et al (2010) indicated that CRY2 activity correlated with the relaxation state of the chromatin (van Zanten et al., 2010). Particularly, CRY2 promoted decompaction of the chromatin in a light-dependent manner. Changes in the chromatin compaction are essential particularly during DNA replication and cell division (Ma et al., 2015) but also in the DDR pathway (Stadler & Richly, 2017). In response to DSBs, PARP enzymes trigger chromatin decondensation events for protein recruitment and DNA repair (Vainonen et al., 2016). Several studies have shown that the dynamic changes in the compaction-relaxation of the chromatin might play an essential role in DNA protection to DNA damage, predominantly to DSBs (Takata et al., 2013, Yoshikawa et al., 2008). Decondensed chromatin is more prone to be damaged by chemical agents due to exposed DNA whereas a compacted chromatin is less susceptible to DNA damage and thus plays a protecting role by reducing up to 5-50 times the frequency of DSBs (Takata et al., 2013). In absence of a functional CRY2, DSBs would occur less frequently due to a more compacted chromatin. In contrast, over-expression of CRY2 would lead to a more relaxed chromatin exposing more DNA, and hence increasing the DSB damage despite the up-regulated DDR related genes. Gene expression analyses in the *parg1-4* mutant showed an up-regulation of DDR response genes (Zhang et al., 2015b). This up-regulation of DDR genes was not efficient in repairing the DNA as DSBs were increased in the mutant (Zhang et al., 2015b). This situation resembles that of *CRY2-ox* plants displaying increased expression of DDR response genes and increased DNA damage. Overall, we propose that in response to DSBs, proper function of CRY2 modulates the

DDR activity and sensitivity to DSBs by regulating the compaction-relaxation state of the chromatin.

The compaction state of the chromatin can be connected with different DNA secondary structures. The RNA transcription generates structural changes in the chromatin called DNA-RNA hybrids or R-loops, which are known to be associated with genomic instability (Halasz et al., 2017). In plants, R-loop formation is associated with active histone marks, transposable elements, non-coding RNAs and the transcription state determining transcription initiation and termination (Xu et al., 2017). We found that CRY2 is important for R-loop formation in response to DSBs correlating with the induction of the DDR genes. It is possible that CRY2 regulation of the compaction state of the chromatin might affect the formation of DNA-RNA hybrids in response to DSBs.

The implication of CRY2 of the DDR pathway seems to be direct as our ChIP assays have shown that CRY2 is recruited at the promoters of key factors of the DSB repair including *PARP2* and *TEJ*. The transcriptional regulation of crucial components of the DDR pathway would be sufficient to trigger the expression of other factors from the DDR pathway such as *RAD51*. In response to DSBs, CRY2 preferentially controls factors involved in the A-NHEJ pathway, which is predominantly active during the S-phase (Truong et al., 2013). These data correlate with previous transcriptional observations of gene expression and R-loop formation of key DDR genes. Although the A-NHEJ is a fast DSB repair mechanism, is prone to induce DNA deletions and thus genome instability (Manova & Gruszka, 2015). Responses to DSBs involve multiple and complex interplay of the different DNA repair mechanisms depending on the DSB complexity and frequency (Kakarougkas & Jeggo, 2014). In the G2-phase of mammalian cells, both NHEJ and HR contribute to DSB repair. NHEJ is the first choice to rapidly repair DSBs but is coupled with the HR to efficiently resect the DSBs (Kakarougkas & Jeggo, 2014). Accordingly, we hypothesize that the up-regulated A-NHEJ pathway by CRY2 might be part of a rapid response that could be complemented by the function of other components and DSB repair mechanisms to efficiently repair DSBs and preserve the genome stability.

Genome instability is a source of growth-related defects that can ultimately lead to programmed cell death (PCD) responses. PCD is a normal developmental event during plant growth including lateral root emergence, leaf senescence and the development of xylem (Beers, 1997). However, plant cells exposed to constant or severe stress conditions undergo PCD events to reduce the amount of cells with compromised genomes (Yoshiyama et al., 2014). This response is crucial in active cell populations as the stem cell niches located in the shoot and root apical meristems, due to their relevance in overall plant growth and development (Fulcher & Sablowski, 2009). We found that in response to constant DSB stress, CRY2 contributes to the PCD responses. We also found that the meristem activity, indirectly measured as the speed of leaf emergence, was affected in CRY2 miss-expressing plants. Efficient DSB repair is crucial to mitigate prolonged pausing of the cell cycle in order to repair the DNA before replication or mitosis (Waterworth et al., 2011). Mutations in DDR genes as *ULTRAVIOLET HYPERSENSITIVE 1 (UVH1)* promote delayed leaf emergence due to G2-phase cell cycle arrest in response to γ-rays (Preuss & Britt, 2003). Similarly, abnormal growth due to changes in the CRY2 activity suggest transient cell cycle arrest of meristematic cells in response to DSBs that would lead to altered true leaf emergence.

Altogether, our studies show that the circadian clock regulates the DDR response following DNA DSBs in *Arabidopsis thaliana*. Upon BLM treatment, the circadian clock up-regulates the DSB repair mechanisms at night and rhythmically controls the DDR response. Thus, proper function of the circadian clock is important for the induction and rhythmic expression of the DDR genes as well as for protein parylation in response to DSBs. We found that CRY2 plays an essential role regulating the induction of key DSB repair genes. We postulate that by modulating the R-loop formation in response to DSBs, CRY2 might regulate the DDR response. Consistently, changes in leaf emergence and programmed cell death require a proper function of CRY2 upon DNA DSB formation.

CONCLUSIONS

Conclusions

In this Doctoral Thesis, we have discovered a role for the circadian clock regulating the timing of the DNA Damage and Repair response in Arabidopsis. Our studies have shown that the circadian clock rhythmically regulates the promoter activity and mRNA expression of key DNA Damage and Repair genes upon bleomycin treatment. We also found that cryptochrome CRY2 is an important component in the regulation of this response. The specific conclusions of this Doctoral Thesis are described below:

1. **Following bleomycin treatment, double strand breaks (DSBs) accumulate at a higher rate during the day than at night.** The results suggest that the DNA Damage and Repair response might be enhanced at night**.**

2. **The promoter activity and mRNA expression of key DNA Damage and Repair genes after bleomycin treatment is rhythmically controlled by the circadian clock and show a circadian peak at night.** The results are consistent with the reduced double strand break accumulation during the night.

3. **Miss-expression of clock components alters the rhythmic promoter activity and mRNA expression of key DNA Damage and Repair genes after bleomycin treatment.** However, the expression of a subset of key clock components is not importantly altered by the treatment.

4. **Proper expression and activity of CRY2 is important in the control of the DNA Damage and Repair response to double strand breaks.** CRY2 regulates the accumulation of double strand breaks and the transcriptional changes of key DNA Damage and Response genes.

5. **CRY2 transcriptionally regulates the DNA Damage and Repair response through its direct binding to the promoters of *PARP2* and *TEJ* in response to bleomycin.**

6. **The DNA-RNA hybrid (R-loop) formation is regulated in response to double strand breaks and requires the proper function of CRY2.** The results are also consistent with the role of CRY2 regulating chromatin compaction.

7. **CRY2 is important for proper regulation of programmed cell death (PCD) and leaf emergence after bleomycin treatment.** The changes in DNA secondary structure, DNA double strand breaks and transcriptional regulation by CRY2 after bleomycin treatment correlate with changes in downstream cellular responses following double strand breaks.

RESUMEN EN CASTELLANO

Resumen en castellano

En la mayoría de los organismos estudiados, el reloj circadiano mantiene ritmos en fisiología, metabolismo y desarrollo en sintonía con los cambios medioambientales que suceden durante los ciclos diurnos y nocturnos. En plantas, el reloj circadiano regula la correcta periodicidad de muchos procesos cruciales como las respuestas a un gran número de estreses abióticos y bióticos. En esta Tesis Doctoral, hemos estudiado la conexión entre el reloj circadiano y la vía de respuesta al daño y reparación del DNA (*DNA Damage and Repair (DDR))* en respuesta al daño de doble cadena del DNA (*double strand breaks (DSBs)).* Los resultados obtenidos indican que el reloj circadiano rítmicamente regula las respuestas biológicas y moleculares frente a los DSBs. También identificamos al foto-receptor de luz azul CRYPTOCHROME 2 (CRY2) como regulador clave en la repuesta DDR. En respuesta a los DSBs inducidos por la droga bleomicina, nuestros *comet assays* realizados a diferentes momentos del ciclo diurno mostraron que los DSBs disminuyen por la noche en comparación con los DSBs durante el día. Además, la actividad de los promotores y expresión del mRNA de genes cruciales en la respuesta DDR mostraron oscilaciones rítmicas y robustas con un pico máximo en la noche. Los resultados sugieren que los mecanismos de reparación del DNA podrían estar favorecidos en la noche. La función circadiana no sólo controla transcripción si no también modificaciones post-traduccionales como la parilación de las proteínas. Nuestros estudios mostraron que la sobre-expresión y mutación de un número de genes del reloj circadiano modifica los ritmos de la respuesta DDR. Sin embargo, con algunas excepciones, la expresión de la mayoría de los genes clave del reloj no presenta importantes cambios en respuesta a los tratamientos con bleomicina. Nuestros estudios también mostraron que la desregulación del foto-receptor CRY2 altera el grado de formación de los DSBs y la expresión transcripcional de genes clave en la respuesta DDR como *POLY-(ADP-RIBOSE) POLYMERASE 2 (PARP2)* y *RAD ASSOCIATED WITH DIABETES 51 (RAD51)*. La regulación podría suceder mediante la interacción directa de CRY2, ya que ensayos de immunoprecipitación de la cromatina revelaron enriquecimiento de la proteína CRY2 en varios loci de genes importantes de la DDR, que incluyen *PARP2* y *POLY-(ADP-RIBOSE) GLYCOHYDROLASE 1 (PARG1 or TEJ)*. La correcta expresión y función de CRY2 es también importante en la formación de una clase particular de estructuras secundarias del DNA o híbridos de DNA-RNA conocidos como R-loops. Los resultados que conectan CRY2 con los híbridos de DNA-RNA en los genes de la respuesta DDR son relevantes, ya que los R-loops han sido previamente conectados con la localización y reparación de los DSBs. Mediante el uso de plantas con la función de CRY2 alterada también hallamos que la muerte celular programada y la aparición de hojas verdaderas en respuesta a los DSBs, requieren una correcta expresión y función de CRY2. Por lo tanto, nuestros estudios demuestran una regulación circadiana de la DDR en Arabidopsis. Esta regulación podría ser relevante para proteger el DNA en momentos en los que es más vulnerable como durante la replicación, que en varios organismos incluidas las plantas, sucede cuando anochece o durante la noche. Nuestros estudios también sugieren que la función de CRY2 en la respuesta DDR podría llevarse a cabo mediante cambios en la compactación de la cromatina y la formación de R-loops.

SUMMARY IN ENGLISH

Summary in english

In most organisms examined to date, the circadian clock sustains rhythms in physiology, metabolism and development in tune with the environmental changes that occur during the day and night cycle. In plants, the circadian clock controls the proper timing of many essential processes including among others plant responses to a number of abiotic and biotic stresses. In this Doctoral Thesis, we aimed to study the connection between the circadian clock and the DNA Damage and Repair (DDR) response triggered by DNA double strand breaks (DSBs). We found that the circadian clock rhythmically regulates molecular and biological responses to DSBs. We also identified the blue-light photoreceptor CRYPTOCHROME 2 (CRY2) as an important regulator of the DDR response. Upon DSB formation by the drug bleomycin, our comet assays performed at different times during the diurnal cycle showed that DSBs are decreased at night compared to DSBs during the day. In addition, the promoter activity and mRNA expression of key DDR genes followed robust rhythmic oscillations with a peak during the night. The results suggest that DNA repair mechanisms might be enhanced at night. The circadian function not only controls transcription but also post-translational modifications such as protein parylation. Our studies showed that over-expression and mutation of a number of circadian clock genes alter the rhythms of the DDR response. However, with some exceptions, the expression of most key clock genes is not importantly affected by bleomycin treatment. Our studies also showed that miss-expression of the photoreceptor CRY2 affects the degree of DSB formation and the transcriptional expression of key DDR response genes including the *POLY-(ADP-RIBOSE) POLYMERASE 2 (PARP2)* and *RAD ASSOCIATED WITH DIABETES 51 (RAD51)*. The regulation might occur through direct binding as chromatin immunoprecipitation assays revealed the enrichment of CRY2 protein at several key DDR loci including *PARP2* and *POLY-(ADP-RIBOSE) GLYCOHYDROLASE 1 (PARG1 or TEJ)*. Proper expression and function of CRY2 is also important for the formation of a particular class of DNA secondary structure or DNA-RNA hybrids known as R-loops. The results connecting CRY2 with DNA-RNA hybrids at the DDR response genes are relevant as R-loops have been previously connected with DSB localization and repairing. By using plants miss-expressing CRY2 we also found that programmed cell death and true leaf emergence in response to DSBs also require proper expression and activity of CRY2. Altogether, our results demonstrate an important role for the circadian clock regulating the timing of the DDR response in *Arabidopsis thaliana*. This regulation might be relevant for protecting the DNA at a very sensitive time such as during replication, which in several organisms including plants is timed to occur at dusk or during the night. Our studies also suggest that CRY2 function in the DDR response might occur through changes in chromatin compaction and R-loop formation.

MATERIALS AND METHODS

Materials and Methods

1. Plant material and growth conditions

The *Arabidopsis thaliana* lines used in this study (Table 1) were surface sterilized with 75% ethanol (v/v) with 0.1% (v/v) of Triton X-100 for 15 min. After several washes with sterile water for 5 min, seeds were stratified for 48 h at 4ºC in darkness and subsequently germinated in plates containing half-strength Murashige and Skoog (MS) agar medium without sucrose (½MS-). Seedlings were grown under entraining light:dark cycles (12 h light/ 12 h dark or 16 h light/ 8 h dark, 22ºC) in environmentally-controlled chambers (INKOA S. L. or Percival) with 60 µmol m^{-2} s^{-1} of cool white fluorescent light. Similarly for blue light experiments, seedlings were grown under entraining light:dark conditions with 50-60 µmol m^{-2} s^{-1} of blue LED light.

Table 1. *Arabidopsis thaliana* lines used in this study.

Line	Ecotype	Source
Col-0 (WT)	Col-0	This study
pBRCA1:LUC	Col-0	This study
pRAD51:LUC	Col-0	This study
pPRR7:LUC	Col-0	This study
pCCA1:LUC	Col-0	(Salome & McClung, 2005)
pTOC1:LUC	Col-0	(Perales & Mas, 2007)
pPRR9:LUC	Col-0	(Para et al., 2007)
CCA1-ox	Col-0	(Wang & Tobin, 1998)
PRR7-ox	Col-0	This study
prr7-11	Col-0	(Yamamoto et al., 2003)
prr579	Col-0	(Fukushima et al., 2009)
parg1-2	Col-0	(Zhang et al., 2015b)
CRY2-ox	Col-0	This study
cry2-1	Col-0	(Lin et al., 1998)
CRY2 minigene	Col-0	This study

2. Plasmid construction and plant transformation

Constructs containing the promoter sequences of the *BRCA1, RAD51* and *PRR7* genes were generated by PCR-mediated amplification followed by cloning of the PCR products in the pENTR/D-TOPO vector (Invitrogen). Subsequently, the promoters were transferred to the plant destination vector pGWB635 containing the *LUC* gene (No promoter, C-*LUC*) (Nakagawa et al., 2007a, Nakagawa et al., 2007b). Vectors containing the coding sequences of *PRR7* (Farre et al., 2005), *CRY2* and the genomic sequence of *CRY2* were cloned into the plant destination vector pGWB406 (35S promoter, N-sGFP), pGWB518 (35S promoter, N-4xMYC), and pGWB504 (No promoter, C-sGFP), respectively (Nakagawa et al., 2007a, Nakagawa et al., 2007b). The transgenic lines were generated by floral dipping transformation of the constructs using *Agrobacterium tumefaciens* (GV2260)-mediated transfer (Clough & Bent, 1998).

3. Bleomycin treatments

Genotoxic treatments were carried out with a water-diluted solution of bleomycin sulfate (Abcam 142977). For gene expression analyses, *in vivo* luminescence experiments and comet assays, 7-8 day-old seedlings were transferred individually to 96-well plates and acclimated for 2-3 days in the same growing conditions. At specific times, about 50-100 µl of 1 µM BLM solution was added directly to each well. For DRIP-qPCR, ChIP-qPCR and Western-blot analyses, ½ MS- plates containing 10-12 day-old Arabidopsis seedlings were subjected to 4-6 ml of 10 µM BLM. Control mock-treated samples were similarly processed but just adding water without BLM. For the physiological experiments, Arabidopsis seeds were sown directly on ½ MS- medium supplemented or not with 5 µM BLM.

4. Comet assays

Comet assays were performed as previously described (Moreno-Romero et al., 2012) with some modifications. About 5-6 of 10-12 day-old Arabidopsis seedlings were collected after 1 h and 6 h with 1 µM BLM at ZT7 and ZT19, and after 8h at ZT9. Seedlings were chopped with 200 µl cold 1x PBS + 20 mM EDTA under dim light to

avoid extra damage. Approximately 50-100 µl of the plant suspensions were pipetted out in a 1.5 ml tube and gently mixed with 200 µl of 37ºC preheated 1% low-melting-point agarose (LMA) (Trevigen). 50 µl were immediately loaded onto precoated 1% agarose microscope slides (Trevigen), carefully flatted with a coverslide and incubated for 5-10 min under cold and dark conditions. After removing the coverslides, samples were covered with pre-cold 1x high-salt buffer (2.5 M NaCl, 10 mM Tris-HCl pH 7, 100 mM EDTA, pH 7.5) for 1 h at 4ºC followed by an equilibration step with cold 1x TAE buffer (100 mM Tris-acetate, 10 mM EDTA, pH 8) for 15 min at 4ºC. Slides were then subjected to electrophoresis (1 V cm^{-1}) in the Comet Assay Electrophoresis system II® (Trevigen) with 1x TAE buffer at 4ºC. Samples were dehydratated with progressive incubation with 75%, 100% ethanol for 5 min each, and finally air-dried at 37ºC for 10 min. Slides were then stained with 100 µl of 1x SYBR Green (Invitrogen) diluted in 1x TE buffer and incubated in the darkness for 30 min at room temperature. After gently washes with sterile water the slides were air-dried. Comet pictures were captured using an epifluorescence vertical confocal microscope SP5 and DM6 (Leica), and images quantified with ImageJ. Approximately 40-50 comets were scored for condition from at least two biological replicates.

5. Gene expression analyses by RT-qPCR

Approximately 8-10 seedlings were collected and immediately frozen in liquid nitrogen at every 2 h over a 24-h diurnal cycle following 24 h BLM treatments (24 h time courses), and at ZT9 after 8 h, 4 h, 2 h, 1 h BLM treatments (short time courses). Total RNA was extracted using a Maxwell 16 LEV plant RNA kit following the manufacturer's recommendations (Promega). Single stranded cDNA was prepared with iScript™ Reverse Transcription Supermix for RT-qPCR (Bio-Rad) with 1 µg of RNA. cDNA was diluted 5 times with nuclease-free water (DEPC) followed by quantitative real-time gene expression analyses. qPCR was performed with 10% of diluted cDNA with Brilliant III Ultra-Fast SYBR Green qPCR Master Mix (Agilent) or iTag Universal SYBR Green Supermix (Bio-Rad) in a 96-well CFX96 Touch Real-Time PCR detection system (Bio-Rad). Three technical replicates were performed for each sample and gene tested. Sequences of the primers used for gene expression are listed in Table 2. Gene

expression data were normalized to *UB10 (UBIQUITIN 10)* and calculated by the comparative Ct method (Livak & Schmittgen, 2001). At least two biological replicates were performed per experiment.

6. Bioluminescence assays

Approximately 7-8 day-old seedlings grown under entraining light conditions were transferred to 96-well plates containing 160 µl of ½MS- supplemented with 40 µl D-luciferine solution consisting of 1.45 mM luciferine (Biotherma) in 2.6 mM 2-(*N*-morpholino)ethanesulfonic acid (MES) at pH 5.8. After 1 day, 6-10 seedlings were treated with 1 µM BLM at ZT3 and ZT15 for LD experiments, and at CT3 for LL experiments. *In vivo* luminescence was monitored every 2 h with 5 seconds of measurement per well in a microplate luminometer LB-960 (Berthold Technologies) using the Microwin 2000 software (Mikrotek Laborsysteme). Every biological replicate included 6-10 seedlings per condition and genotype. The experiments were repeated at least twice.

7. Western-blot analyses

Approximately 30-40 of 10-12 day-old Arabidopsis seedlings were subjected to 10 µM BLM treatments for 12 h and collected at ZT3 and ZT15 and immediately frozen in liquid nitrogen. Total protein was extracted in cold grinding buffer (50 mM Tris-HCl pH 8, 150 mM NaCl, 5 mM EDTA, 0.5% Triton X-100, 10% glycerol, 1x protease inhibitor cocktail (Sigma-Aldrich), and 50 µM MG-132). After centrifugation for 10min at max speed, the supernatant was recovered and protein concentration was quantified using standard curves with the Bradford method (Bradford, 1976). Approximately 30-40 µg of protein were mixed with 4x SDS loading buffer (200 mM Tris-HCl pH 6.8, 8% SDS, 0.4% bromophenol blue, 40% glycerol, and 10% β-mercaptoethanol), heated at 98ºC for 5min and then loaded into SDS-PAGE gels. Resulting gels were transferred to PVDF membranes and inmunoblotted overnight (O/N) with polyclonal anti-PAR antibody (1:1000) (4335-MC-100-AC, Trevigen). At least two biological replicates were performed per experiment.

8. DRIP-qPCR assay

DRIP-qPCR analyses were performed as described previously (Xu et al., 2017) with minor modifications. Briefly, nuclei extracts were isolated from frozen samples of 1-2 g of 10-12 day-old Arabidopsis seedlings in extraction buffer (0.4 M D-sucrose, 10 mM Tris pH 8, 1 mM EDTA, 5mM β-mercaptoethanol). Extracts were filtered through miracloth (EMD Millipore) and subsequently washed in washing buffer (0.25 M D-sucrose, 10 mM Tris pH 8, 1 mM EDTA, 10 mM $MgCl_2$, 1% Triton X-100, 5 mM β-mercaptoethanol) and centrifuged for 20 min at 1000 *g*. Purified nuclei were incubated with Proteinase K (0.1 mg/ml Proteinase K (Sigma Aldrich)) in lysis buffer (10 mM Tris pH 8, 1 mM EDTA, 0,5% SDS) with gentle shaking (300-400 rpm) for 5 h at 65ºC in order to remove all proteins. Genomic DNA (gDNA) was then extracted with phenol:chloroform extraction with the following modifications. Aqueous phases were precipitated by adding 1/10 volumes of 5M NaCl supplemented with 1 volume of Isopropanol and 1 µl of glycogen (20 mg/ml) for 45 min at room temperature. The pellets were precipitated and washed with cold 70% ethanol, air-dried under vacuum (SpeedVac®) and eluted in 10 mM Tris-HCl pH 8. Purified gDNA was sonicated for 10 min (30 s ON, 30 s OFF, low intensity) with a sonicator (Bioruptor, Diagnode). 5 µg of total fragmented DNA was incubated with 4 µl of S9.6 antibody (Ab01137-2, Kerafast; and MABE1095, EMD-Millipore) in 1x DRIP buffer (100 mM $NaPO_4$, 1,4 M NaCl, 0,5% Triton X-100) O/N at 4ºC in a rotator. The antibody-(DNA-RNA) hybrid complexes were incubated with 50 µl slurry protein G-Dynabeads beads (Invitrogen) for 4 h at 4ºC. Complexes were subjected to several washes with 1x DRIP buffer and eluted by incubating in 250 µl of elution buffer (50 mM Tris pH 8, 10 mM EDTA, 0.5% SDS, 0.1 mg/ml Proteinase K) for 1 h at 60ºC. DNA-RNA hybrids were next purified by phenol:chloroform extraction and eluted in 10 mM Tris-HCl pH 8. qPCR was performed with 1 µl of immunoprecipitated DNA-RNA hybrids and Brilliant III Ultra-Fast SYBR Green qPCR Master Mix (Agilent) or iTag Universal SYBR Green Supermix (Bio-Rad) in a 96-well CFX96 Touch Real-Time PCR detection system (Bio-Rad). Two technical replicates were performed for each region and gene. DRIP-qPCR values were normalized to 10% of Input values. Primers used for DRIP-qPCR are described in Table 2.

9. ChIP assays

ChIP assays were performed as previously described (Yamaguchi et al., 2014) with minor modifications. Briefly, approximately, 1 g of BLM treated and untreated 12 day-old Arabidopsis seedlings were collected and fixed in 30-50 ml of fixation buffer (1x PBS, 1% formaldehyde solution) under vacuum condition for 12-15 min. Subsequently, fixation buffer was replaced by 10 ml of 125 mM glycine solution and incubated under vacuum for 5 min. Fixed seedlings were washed several times with cold 1x PBS and frozen in liquid nitrogen. Following grinding, the powder was mixed with 50 ml of Extraction buffer (0.4 M D-sucrose, 10 mM Tris pH 8, 1 mM EDTA, 5 mM β-mercaptoethanol, 1 mM PMSF, 5 mg/mL leupeptin, 1 mg/mL aprotinin, 1 mg/mL E-64, 5 mg/mL antipain, 1 mg/mL pepstatin, 5 mg/mL chymostatin, and 50 mM MG-132) and filtered through miracloth (EMD Millipore). Nuclei were then washed several times in washing buffer (0.25M D-sucrose, 10 mM Tris pH 8, 1 mM EDTA, 10 mM $MgCl_2$, 1% Triton X-100, 5 mM β-mercaptoethanol) and centrifuged at 1000 *g* for 20 min at 4ºC. The pellet was resuspended in 1ml of lysis buffer (50 mM Tris pH 8, 10 mM EDTA, 1% SDS) and sonicated for 8 min (30 s ON, 30 s OFF, low intensity) with a sonicator (Bioruptor, Diagnode). Sonicated chromatin was spin at max speed for 5 min and supernatant was collected. 50 µl of slurry protein G-Dynabeads beads (Invitrogen) were conjugated with monoclonal anti-MYC antibody (M4439 Sigma-Aldrich) for 4 h at 4ºC. About 20-25 µg of sonicated chromatin was diluted in 700-800 µl cold ChIP dilution buffer (15 mM Tris pH 8, 150 mM NaCl, 1 mM EDTA, 1.1% Triton X-100, 0.01% SDS) and incubated with the beads-antibody complexes O/N in a rotator at 4ºC. The beads were sequentially washed for 5 min with different washing buffers: low-salt buffer (20 mM Tris-HCl, pH 8.0, 150 mM NaCl, 1% Triton X-100, 2 mM EDTA, 0.1% SDS), high-salt buffer (20 mM Tris-HCl, pH 8.0, 500 mM NaCl, 1% Triton X-100, 2 mM EDTA, 0.1% SDS), LiCl buffer (10 mM Tris-HCl, pH 8.0, 1 mM EDTA, 250 mM LiCl, 1% Nonidet P-40, 1% sodium deoxycholate), and TE buffer (10 mM Tris-HCl, pH 8.0, and 1 mM EDTA). Beads were resuspended in 300 µl lysis buffer and incubated for 1 h at 65°C. Recovered DNA-antibody complexes were reverse cross-linked for 15 min at 95ºC. DNA was purified using a Gel Extraction Kit (Qiagen) following the manufacturer's recommendation. qPCR analyses were performed as described for DRIP-qPCR assays.

Primers used for DRIP-qPCR are listed in Table 2.

10. Trypan blue staining

Trypan blue staining was performed as previously described (van Wees, 2008). Briefly, 7 day-old Arabidopsis seedlings grown in ½MS- and ½MS- supplemented with 5 µM BLM were placed in tubes containing Trypan blue solution (50 ml contain 10 ml lactic acid 85% (w/w), 10 ml phenol pH 7.5, 10 ml glycerol, 40 mg of trypan blue (Sigma-Aldrich), 10ml of distilled water). Samples were boiled for 5 min or until seedlings were fully stained. Under the flow hood, trypan blue trypan blue was discarded and then Chloral hydrate (Sigma-Aldrich) solution was added followed by incubation at 65ºC for 4 h. Chloral hydrate was discarded and stained seedlings were resuspended in 50% glycerol. Seedlings were imaged with an optical microscope (Zeiss Axiophot). Images were quantified with ImageJ. At least two biological replicates were performed per experiment.

11. Leaf emergence analyses

Arabidopsis seedlings grown in ½MS- and ½MS- supplemented with 5 µM BLM were monitored every two days after the germination with an optical magnifying microscope coupled with the digital camera DP71 (Olympus). Leaf emergence of the first true leaves was scored as the percentage of the number of seedlings with true leaves versus total number of seedlings in the condition. About 50 plants were scored from at least two independent biological replicates.

Table 2. List of primers used in this Doctoral thesis.

Name		Sequence (5' --> 3')	Experiment
UB10	Forward	AAATCTCGTCTCTGTTATGCTT	Gene expression
	Reverse	TTTTACATGAAACGAAACATTG	
PARP2	Forward	TGGCGAATTTCGTGGGATGA	Gene expression
	Reverse	TGGTTCCTGTTGTATCTAAGCCT	
TEJ	Forward	CTTTCCCATAAATGGACTGTTGG	Gene expression
	Reverse	GGTTTGTTGGTGGTAGCTAGAG	
RAD51	Forward	CGAGGAAGGATCTCTTGCAG	Gene expression
	Reverse	GCACTAGTGAACCCCAGAGG	

BRCA1	Forward	CCATGTATTTTGCAATGCGTG	Gene expression
	Reverse	TGTGGAGCACCTCGAATCTCT	
CCA1	Forward	TCGAAAGACGGGAAGTGGAACG	Gene expression
	Reverse	GTCGATCTTCATTGGCCATCTCAG	
TOC1	Forward	TCTTCGCAGAATCCCTGTGAT	Gene expression
	Reverse	GCTGCACCTAGCTTCAAGCA	
PRR5	Forward	AATGGTGGTGATGCCCAGAG	Gene expression
	Reverse	GCACTCCATCTGTACTGCGT	
PRR7	Forward	AAGTAGTGATGGGAGTGGCG	Gene expression
	Reverse	GAGATACCGCTCGTGGACTG	
PRR9	Forward	ACCAATGAGGGGATTGCTGG	Gene expression
	Reverse	TGCAGCTTCTCTCTGGCTTC	
LUX	Forward	CGCTACGTGGTGGATCTTCA	Gene expression
	Reverse	CGAATCCGATCCAGGACTGC	
promoter RAD51	Forward	CACCGGTTGGGCCCTATATGTTTTAGTTT	Clonning
	Reverse	CTCTCAATCAGAGCAGATTCGGGT	
promoter BRCA1	Forward	CACCCAAATTCTACGGACAATCTTCGTTA	Clonning
	Reverse	ATCTTCACTCAGAGAAAACGAAACG	
promoter PRR7	Forward	CACCGTCAGATATTACGATTTTTTAATTTCC	Clonning
	Reverse	CACACCAACTCTGCTTCGCT	
TEJ region 1	Forward	AAGTCTACGCTGTGGGTTCC	DRIP/ChIP-qPCR
	Reverse	TGACTGGAAAATAGAAGGTGTGTG	
TEJ region 2	Forward	TCGCGATTCTCCATTTTTCGAT	DRIP/ChIP-qPCR
	Reverse	GCAGCAGAATCTTGTCGCAG	
PARP2 region 1	Forward	TGCACGTCCTTGGAAAAGTG	DRIP/ChIP-qPCR
	Reverse	TGCTGGTTGTTTAACGAAAAGA	
PARP2 region 2	Forward	GTCTCATTCCCTTTCCGACGA	DRIP/ChIP-qPCR
	Reverse	GCTCGGCGAGTTTTAAACGG	
PARP2 region 3	Forward	ACAGGACCTCTATAGCCATTCA	DRIP/ChIP-qPCR
	Reverse	TCATGTCTCCCAAAGCAACCT	
RAD51 region 1	Forward	TCTGGTGACCCGAATCTGCT	DRIP/ChIP-qPCR
	Reverse	AAAGGTCCGTGCTGGGTTTC	
RAD51 region 2	Forward	TTGGAATTGTGGTGGTTCTCG	DRIP/ChIP-qPCR
	Reverse	GACCGCCGAGTGATACC	
MRE11 region 1	Forward	CTCTCCCCACCTCATATTCCA	DRIP/ChIP-qPCR
	Reverse	ACAGCGAATATGTATAGAGAAACGG	
MRE11 region 2	Forward	GACGATGAGAGCACTAAAGGC	DRIP/ChIP-qPCR
	Reverse	ACCACGTTTTGAAGTCCCAGA	
LIG4 region 1	Forward	GTTCTCGATCAAGCGACGGA	DRIP/ChIP-qPCR
	Reverse	CAGAAACGATCCAAATTCCGCA	
LIG4 region 2	Forward	TTTGAGCAGTTCTCCGGCAA	DRIP/ChIP-qPCR
	Reverse	ATACATCTGTGAACGCAGGC	
TA3	Forward	TAGGGTTCTTAGTTGATCTTGTATTGAGCTC	ChIP-qPCR
	Reverse	TTTGCTCTCAAACTCTCAATTGAAGTTT	

BIBLIOGRAPHY

Bibliography

Adams S, Manfield I, Stockley P, Carre IA, 2015. Revised Morning Loops of the Arabidopsis Circadian Clock Based on Analyses of Direct Regulatory Interactions. *PLoS One* **10**, e0143943.

Ahmad M, Jarillo JA, Klimczak LJ*, et al.*, 1997. An enzyme similar to animal type II photolyases mediates photoreactivation in Arabidopsis. *Plant Cell* **9**, 199-207.

Ahmad M, Jarillo JA, Smirnova O, Cashmore AR, 1998. The CRY1 blue light photoreceptor of Arabidopsis interacts with phytochrome A in vitro. *Mol Cell* **1**, 939-48.

Alabadi D, Oyama T, Yanovsky MJ, Harmon FG, Mas P, Kay SA, 2001. Reciprocal regulation between TOC1 and LHY/CCA1 within the Arabidopsis circadian clock. *Science* **293**, 880-3.

Alekseev S, Coin F, 2015. Orchestral maneuvers at the damaged sites in nucleotide excision repair. *Cell Mol Life Sci* **72**, 2177-86.

Amasino RM, Michaels SD, 2010. The timing of flowering. *Plant Physiol* **154**, 516-20.

Amiard S, Depeiges A, Allain E, White CI, Gallego ME, 2011. Arabidopsis ATM and ATR kinases prevent propagation of genome damage caused by telomere dysfunction. *Plant Cell* **23**, 4254-65.

Amiard S, Gallego ME, White CI, 2013. Signaling of double strand breaks and deprotected telomeres in Arabidopsis. *Front Plant Sci* **4**, 405.

Aplan PD, 2006. Causes of oncogenic chromosomal translocation. *Trends Genet* **22**, 46-55.

Aschoff J, 1979. Circadian rhythms: influences of internal and external factors on the period measured in constant conditions. *Z Tierpsychol* **49**, 225-49.

Asher G, Reinke H, Altmeyer M, Gutierrez-Arcelus M, Hottiger MO, Schibler U, 2010. Poly(ADP-ribose) polymerase 1 participates in the phase entrainment of circadian clocks to feeding. *Cell* **142**, 943-53.

Atamian HS, Harmer SL, 2016. Circadian regulation of hormone signaling and plant physiology. *Plant Mol Biol* **91**, 691-702.

Balestrazzi A, Confalonieri M, Macovei A, Dona M, Carbonera D, 2011. Genotoxic stress and DNA repair in plants: emerging functions and tools for improving crop productivity. *Plant Cell Rep* **30**, 287-95.

Bartolomei G, Leutert M, Manzo M, Baubec T, Hottiger MO, 2016. Analysis of Chromatin ADP-Ribosylation at the Genome-wide Level and at Specific Loci by ADPr-ChAP. *Mol Cell* **61**, 474-85.

Bauer D, Viczian A, Kircher S*, et al.*, 2004. Constitutive photomorphogenesis 1 and multiple photoreceptors control degradation of phytochrome interacting factor 3, a transcription factor required for light signaling in Arabidopsis. *Plant Cell* **16**, 1433-45.

Beemster GT, De Veylder L, Vercruysse S*, et al.*, 2005. Genome-wide analysis of gene expression profiles associated with cell cycle transitions in growing organs of Arabidopsis. *Plant Physiol* **138**, 734-43.

Beers EP, 1997. Programmed cell death during plant growth and development. *Cell Death Differ* **4**, 649-61.

Belbin FE, Noordally ZB, Wetherill SJ, Atkins KA, Franklin KA, Dodd AN, 2017. Integration of light and circadian signals that regulate chloroplast transcription by a nuclear-encoded sigma factor. *New Phytol* **213**, 727-38.

Bendix C, Marshall Carine m, Harmon Frank g, 2015. Circadian Clock Genes Universally Control Key Agricultural Traits. *Molecular Plant* **8**, 1135-52.

Bodenstein C, Heiland I, Schuster S, 2012. Temperature compensation and entrainment in circadian rhythms. *Phys Biol* **9**, 036011.

Bouly JP, Giovani B, Djamei A*, et al.*, 2003. Novel ATP-binding and autophosphorylation activity associated with Arabidopsis and human cryptochrome-1. *Eur J Biochem* **270**, 2921-8.

Bouly JP, Schleicher E, Dionisio-Sese M*, et al.*, 2007. Cryptochrome blue light photoreceptors are activated through interconversion of flavin redox states. *J Biol Chem* **282**, 9383-91.

Boyko A, Filkowski J, Hudson D, Kovalchuk I, 2006. Homologous recombination in plants is organ specific. *Mutat Res* **595**, 145-55.

Boyko A, Filkowski J, Kovalchuk I, 2005. Homologous recombination in plants is temperature and day-length dependent. *Mutat Res* **572**, 73-83.

Bradbury JM, Jackson SP, 2003. ATM and ATR. *Curr Biol* **13**, R468.

Bradford MM, 1976. A rapid and sensitive method for the quantitation of microgram quantities of protein utilizing the principle of protein-dye binding. *Anal Biochem* **72**, 248-54.

Briggs AG, Bent AF, 2011. Poly(ADP-ribosyl)ation in plants. *Trends Plant Sci* **16**, 372-80.

Broekaert WF, Delaure SL, De Bolle MF, Cammue BP, 2006. The role of ethylene in host-pathogen interactions. *Annu Rev Phytopathol* **44**, 393-416.

Broekgaarden C, Caarls L, Vos IA, Pieterse CM, Van Wees SC, 2015. Ethylene: Traffic Controller on Hormonal Crossroads to Defense. *Plant Physiol* **169**, 2371-9.

Brown Steven a, Kowalska E, Dallmann R, 2012. (Re)inventing the Circadian Feedback Loop. *Developmental Cell* **22**, 477-87.

Busheva M, Garab G, Liker E, Toth Z, Szell M, Nagy F, 1991. Diurnal Fluctuations in the Content and Functional Properties of the Light Harvesting Chlorophyll a/b Complex in Thylakoid Membranes : Correlation with the Diurnal Rhythm of the mRNA Level. *Plant Physiol* **95**, 997-1003.

Caruso LB, Martin KA, Lauretti E*, et al.*, 2018. Poly(ADP-ribose) Polymerase 1, PARP1, modifies EZH2 and inhibits EZH2 histone methyltransferase activity after DNA damage. *Oncotarget* **9**, 10585-605.

Chan YW, West S, 2015. GEN1 promotes Holliday junction resolution by a coordinated nick and counter-nick mechanism. *Nucleic Acids Res* **43**, 10882-92.

Charbonnel C, Allain E, Gallego ME, White CI, 2011. Kinetic analysis of DNA double-strand break repair pathways in Arabidopsis. *DNA Repair (Amst)* **10**, 611-9.

Chen IP, Haehnel U, Altschmied L, Schubert I, Puchta H, 2003. The transcriptional response of Arabidopsis to genotoxic stress - a high-density colony array study (HDCA). *Plant J* **35**, 771-86.

Chen P, Umeda M, 2015. DNA double-strand breaks induce the expression of flavin-containing monooxygenase and reduce root meristem size in Arabidopsis thaliana. *Genes Cells* **20**, 636-46.

Clough SJ, Bent AF, 1998. Floral dip: a simplified method for Agrobacterium-mediated transformation of Arabidopsis thaliana. *Plant J* **16**, 735-43.

Covington MF, Maloof JN, Straume M, Kay SA, Harmer SL, 2008. Global transcriptome analysis reveals circadian regulation of key pathways in plant growth and development. *Genome Biol* **9**, R130.

Delacote F, Lopez BS, 2008. Importance of the cell cycle phase for the choice of the appropriate DSB repair pathway, for genome stability maintenance: the trans-S double-strand break repair model. *Cell Cycle* **7**, 33-8.

Devlin PF, Kay SA, 2000. Cryptochromes are required for phytochrome signaling to the circadian clock but not for rhythmicity. *Plant Cell* **12**, 2499-510.

Ding Z, Millar AJ, Davis AM, Davis SJ, 2007. TIME FOR COFFEE encodes a nuclear regulator in the Arabidopsis thaliana circadian clock. *Plant Cell* **19**, 1522-36.

Dodd AN, Belbin FE, Frank A, Webb AA, 2015. Interactions between circadian clocks and photosynthesis for the temporal and spatial coordination of metabolism. *Front Plant Sci* **6**, 245.

Dodd AN, Gardner MJ, Hotta CT*, et al.*, 2007. The Arabidopsis circadian clock incorporates a cADPR-based feedback loop. *Science* **318**, 1789-92.

Dodd AN, Salathia N, Hall A*, et al.*, 2005. Plant circadian clocks increase photosynthesis, growth, survival, and competitive advantage. *Science* **309**, 630-3.

Doherty CJ, Kay SA, 2010. Circadian control of global gene expression patterns. *Annu Rev Genet* **44**, 419-44.

Dong MA, Farre EM, Thomashow MF, 2011. Circadian clock-associated 1 and late elongated hypocotyl regulate expression of the C-repeat binding factor (CBF) pathway in Arabidopsis. *Proc Natl Acad Sci U S A* **108**, 7241-6.

Dubowy C, Sehgal A, 2017. Circadian Rhythms and Sleep in Drosophila melanogaster. *Genetics* **205**, 1373-97.

Ellison CT, Vandenbussche F, Van Der Straeten D, Harmer SL, 2011. XAP5 CIRCADIAN TIMEKEEPER regulates ethylene responses in aerial tissues of Arabidopsis. *Plant Physiol* **155**, 988-99.

Endo M, Araki T, Nagatani A, 2016. Tissue-specific regulation of flowering by photoreceptors. *Cell Mol Life Sci* **73**, 829-39.

Endo M, Shimizu H, Nohales MA, Araki T, Kay SA, 2014. Tissue-specific clocks in Arabidopsis show asymmetric coupling. *Nature* **515**, 419-22.

Endo M, Tanigawa Y, Murakami T, Araki T, Nagatani A, 2013. PHYTOCHROME-DEPENDENT LATE-FLOWERING accelerates flowering through physical interactions with phytochrome B and CONSTANS. *Proc Natl Acad Sci U S A* **110**, 18017-22.

Ezer D, Jung JH, Lan H*, et al.*, 2017. The evening complex coordinates environmental and endogenous signals in Arabidopsis. *Nat Plants* **3**, 17087.

Facella P, Lopez L, Chiappetta A, Bitonti MB, Giuliano G, Perrotta G, 2006. CRY-DASH gene expression is under the control of the circadian clock machinery in tomato. *FEBS Lett* **580**, 4618-24.

Farinas B, Mas P, 2011. Functional implication of the MYB transcription factor RVE8/LCL5 in the circadian control of histone acetylation. *Plant J* **66**, 318-29.

Farre EM, Harmer SL, Harmon FG, Yanovsky MJ, Kay SA, 2005. Overlapping and distinct roles of PRR7 and PRR9 in the Arabidopsis circadian clock. *Curr Biol* **15**, 47-54.

Farre EM, Weise SE, 2012. The interactions between the circadian clock and primary metabolism. *Curr Opin Plant Biol* **15**, 293-300.

Filichkin SA, Mockler TC, 2012. Unproductive alternative splicing and nonsense mRNAs: a widespread phenomenon among plant circadian clock genes. *Biol Direct* **7**, 20.

Fleta-Soriano E, Munne-Bosch S, 2016. Stress Memory and the Inevitable Effects of Drought: A Physiological Perspective. *Front Plant Sci* **7**, 143.

Fraser DP, Hayes S, Franklin KA, 2016. Photoreceptor crosstalk in shade avoidance. *Curr Opin Plant Biol* **33**, 1-7.

Friesner JD, Liu B, Culligan K, Britt AB, 2005. Ionizing radiation-dependent gamma-H2AX focus formation requires ataxia telangiectasia mutated and ataxia telangiectasia mutated and Rad3-related. *Mol Biol Cell* **16**, 2566-76.

Fukuda H, Murase H, Tokuda IT, 2013. Controlling circadian rhythms by dark-pulse perturbations in Arabidopsis thaliana. *Sci Rep* **3**, 1533.

Fukushima A, Kusano M, Nakamichi N*, et al.*, 2009. Impact of clock-associated Arabidopsis pseudo-response regulators in metabolic coordination. *Proc Natl Acad Sci U S A* **106**, 7251-6.

Fulcher N, Sablowski R, 2009. Hypersensitivity to DNA damage in plant stem cell niches. *Proc Natl Acad Sci U S A* **106**, 20984-8.

Fung-Uceda J, Lee K, Seo PJ, Polyn S, De Veylder L, Mas P, 2018. The Circadian Clock Sets the Time of DNA Replication Licensing to Regulate Growth in Arabidopsis. *Dev Cell* **45**, 101-13 e4.

Gendron JM, Pruneda-Paz JL, Doherty CJ, Gross AM, Kang SE, Kay SA, 2012. Arabidopsis circadian clock protein, TOC1, is a DNA-binding transcription factor. *Proc Natl Acad Sci U S A* **109**, 3167-72.

Gerhart-Hines Z, Lazar MA, 2015. Circadian metabolism in the light of evolution. *Endocr Rev* **36**, 289-304.

Gil KE, Kim WY, Lee HJ*, et al.*, 2017. ZEITLUPE Contributes to a Thermoresponsive Protein Quality Control System in Arabidopsis. *Plant Cell* **29**, 2882-94.

Glei M, Schneider T, Schlormann W, 2016. Comet assay: an essential tool in toxicological research. *Arch Toxicol* **90**, 2315-36.

Golubov A, Yao Y, Maheshwari P*, et al.*, 2010. Microsatellite instability in Arabidopsis increases with plant development. *Plant Physiol* **154**, 1415-27.

Goodspeed D, Chehab EW, Min-Venditti A, Braam J, Covington MF, 2012. Arabidopsis synchronizes jasmonate-mediated defense with insect circadian behavior. *Proc Natl Acad Sci U S A* **109**, 4674-7.

Gould PD, Locke JC, Larue C*, et al.*, 2006. The molecular basis of temperature compensation in the Arabidopsis circadian clock. *Plant Cell* **18**, 1177-87.

Grabarz A, Barascu A, Guirouilh-Barbat J, Lopez BS, 2012. Initiation of DNA double strand break repair: signaling and single-stranded resection dictate the choice between homologous recombination, non-homologous end-joining and alternative end-joining. *Am J Cancer Res* **2**, 249-68.

Graeff M, Straub D, Eguen T*, et al.*, 2016. MicroProtein-Mediated Recruitment of CONSTANS into a TOPLESS Trimeric Complex Represses Flowering in Arabidopsis. *PLoS Genet* **12**, e1005959.

Gray JA, Shalit-Kaneh A, Chu DN, Hsu PY, Harmer SL, 2017. The REVEILLE Clock Genes Inhibit Growth of Juvenile and Adult Plants by Control of Cell Size. *Plant Physiol* **173**, 2308-22.

Grundy J, Stoker C, Carre IA, 2015. Circadian regulation of abiotic stress tolerance in plants. *Front Plant Sci* **6**, 648.

Hajdu A, Adam E, Sheerin DJ*, et al.*, 2015. High-level expression and phosphorylation of phytochrome B modulates flowering time in Arabidopsis. *Plant J* **83**, 794-805.

Halasz L, Karanyi Z, Boros-Olah B*, et al.*, 2017. RNA-DNA hybrid (R-loop) immunoprecipitation mapping: an analytical workflow to evaluate inherent biases. *Genome Res* **27**, 1063-73.

Harmer SL, Hogenesch JB, Straume M*, et al.*, 2000. Orchestrated transcription of key pathways in Arabidopsis by the circadian clock. *Science* **290**, 2110-3.

Hartung F, Suer S, Bergmann T, Puchta H, 2006. The role of AtMUS81 in DNA repair and its genetic interaction with the helicase AtRecQ4A. *Nucleic Acids Res* **34**, 4438-48.

Hassidim M, Dakhiya Y, Turjeman A*, et al.*, 2017. CIRCADIAN CLOCK ASSOCIATED1 (CCA1) and the Circadian Control of Stomatal Aperture. *Plant Physiol* **175**, 1864-77.

Hastings MH, Maywood ES, Brancaccio M, 2019. The Mammalian Circadian Timing System and the Suprachiasmatic Nucleus as Its Pacemaker. *Biology (Basel)* **8**.

Haydon MJ, Roman A, Arshad W, 2015. Nutrient homeostasis within the plant circadian network. *Front Plant Sci* **6**, 299.

Helfer A, Nusinow DA, Chow BY, Gehrke AR, Bulyk ML, Kay SA, 2011. LUX ARRHYTHMO encodes a nighttime repressor of circadian gene expression in the Arabidopsis core clock. *Curr Biol* **21**, 126-33.

Honkela A, Peltonen J, Topa H*, et al.*, 2015. Genome-wide modeling of transcription kinetics reveals patterns of RNA production delays. *Proc Natl Acad Sci U S A* **112**, 13115-20.

Honma S, 2018. The mammalian circadian system: a hierarchical multi-oscillator structure for generating circadian rhythm. *The Journal of Physiological Sciences* **68**, 207-19.

Hovhannisyan GG, 2010. Fluorescence in situ hybridization in combination with the comet assay and micronucleus test in genetic toxicology. *Mol Cytogenet* **3**, 17.

Hsu PY, Devisetty UK, Harmer SL, 2013. Accurate timekeeping is controlled by a cycling activator in Arabidopsis. *Elife* **2**, e00473.

Huang W, Perez-Garcia P, Pokhilko A*, et al.*, 2012. Mapping the core of the Arabidopsis circadian clock defines the network structure of the oscillator. *Science* **336**, 75-9.

Inoue K, Araki T, Endo M, 2017. Integration of Input Signals into the Gene Network in the Plant Circadian Clock. *Plant and Cell Physiology* **58**, 977-82.

Inoue K, Araki T, Endo M, 2018. Oscillator networks with tissue-specific circadian clocks in plants. *Semin Cell Dev Biol* **83**, 78-85.

Ito S, Nakamichi N, Nakamura Y*, et al.*, 2007. Genetic linkages between circadian clock-associated components and phytochrome-dependent red light signal transduction in Arabidopsis thaliana. *Plant Cell Physiol* **48**, 971-83.

Ito S, Niwa Y, Nakamichi N, Kawamura H, Yamashino T, Mizuno T, 2008. Insight into missing genetic links between two evening-expressed pseudo-response regulator genes TOC1 and PRR5 in the circadian clock-controlled circuitry in Arabidopsis thaliana. *Plant Cell Physiol* **49**, 201-13.

J. DM, ed, 1729. *Observation botanique*.

Jung JH, Domijan M, Klose C*, et al.*, 2016. Phytochromes function as thermosensors in Arabidopsis. *Science* **354**, 886-9.

Junker LV, Kleiber A, Jansen K*, et al.*, 2017. Variation in short-term and long-term responses of photosynthesis and isoprenoid-mediated photoprotection to soil water availability in four Douglas-fir provenances. *Sci Rep* **7**, 40145.

Kaiser G, Kleiner O, Beisswenger C, Batschauer A, 2009. Increased DNA repair in Arabidopsis plants overexpressing CPD photolyase. *Planta* **230**, 505-15.

Kakarougkas A, Jeggo PA, 2014. DNA DSB repair pathway choice: an orchestrated handover mechanism. *Br J Radiol* **87**, 20130685.

Karapetyan S, Dong X, 2018. Redox and the circadian clock in plant immunity: A balancing act. *Free Radic Biol Med* **119**, 56-61.

Kaufmann WK, Paules RS, 1996. DNA damage and cell cycle checkpoints. *FASEB J* **10**, 238-47.

Kavakli IH, Baris I, Tardu M*, et al.*, 2017. The Photolyase/Cryptochrome Family of Proteins as DNA Repair Enzymes and Transcriptional Repressors. *Photochem Photobiol* **93**, 93-103.

Kazan K, Manners JM, 2013. MYC2: the master in action. *Mol Plant* **6**, 686-703.

Kiba T, Henriques R, Sakakibara H, Chua NH, 2007. Targeted degradation of PSEUDO-RESPONSE REGULATOR5 by an SCFZTL complex regulates clock function and photomorphogenesis in Arabidopsis thaliana. *Plant Cell* **19**, 2516-30.

Kim H, Kim HJ, Vu QT*, et al.*, 2018. Circadian control of ORE1 by PRR9 positively regulates leaf senescence in Arabidopsis. *Proc Natl Acad Sci U S A* **115**, 8448-53.

Kinner A, Wu W, Staudt C, Iliakis G, 2008. Gamma-H2AX in recognition and signaling of DNA double-strand breaks in the context of chromatin. *Nucleic Acids Res* **36**, 5678-94.

Kolmos E, Chow BY, Pruneda-Paz JL, Kay SA, 2014. HsfB2b-mediated repression of PRR7 directs abiotic stress responses of the circadian clock. *Proc Natl Acad Sci U S A* **111**, 16172-7.

Kumar V, Sharma A, 2018. Common features of circadian timekeeping in diverse organisms. *Current Opinion in Physiology* **5**, 58-67.

Kurup S, Jones HD, Holdsworth MJ, 2000. Interactions of the developmental regulator ABI3 with proteins identified from developing Arabidopsis seeds. *Plant J* **21**, 143-55.

Lai AG, Doherty CJ, Mueller-Roeber B, Kay SA, Schippers JH, Dijkwel PP, 2012. CIRCADIAN CLOCK-ASSOCIATED 1 regulates ROS homeostasis and oxidative stress responses. *Proc Natl Acad Sci U S A* **109**, 17129-34.

Lamb RS, Citarelli M, Teotia S, 2012. Functions of the poly(ADP-ribose) polymerase superfamily in plants. *Cell Mol Life Sci* **69**, 175-89.

Lario LD, Ramirez-Parra E, Gutierrez C, Casati P, Spampinato CP, 2011. Regulation of plant MSH2 and MSH6 genes in the UV-B-induced DNA damage response. *J Exp Bot* **62**, 2925-37.

Lario LD, Ramirez-Parra E, Gutierrez C, Spampinato CP, Casati P, 2013. ANTI-SILENCING FUNCTION1 proteins are involved in ultraviolet-induced DNA damage repair and are cell cycle regulated by E2F transcription factors in Arabidopsis. *Plant Physiol* **162**, 1164-77.

Latrasse D, Benhamed M, Bergounioux C, Raynaud C, Delarue M, 2016. Plant programmed cell death from a chromatin point of view. *J Exp Bot* **67**, 5887-900.

Lee HG, Mas P, Seo PJ, 2016. MYB96 shapes the circadian gating of ABA signaling in Arabidopsis. *Sci Rep* **6**, 17754.

Legnaioli T, Cuevas J, Mas P, 2009. TOC1 functions as a molecular switch connecting the circadian clock with plant responses to drought. *EMBO J* **28**, 3745-57.

Legris M, Klose C, Burgie ES*, et al.*, 2016. Phytochrome B integrates light and temperature signals in Arabidopsis. *Science* **354**, 897-900.

Li G, Siddiqui H, Teng Y*, et al.*, 2011. Coordinated transcriptional regulation underlying the circadian clock in Arabidopsis. *Nat Cell Biol* **13**, 616-22.

Li W, Chen C, Markmann-Mulisch U*, et al.*, 2004. The Arabidopsis AtRAD51 gene is dispensable for vegetative development but required for meiosis. *Proc Natl Acad Sci U S A* **101**, 10596-601.

Lin C, Yang H, Guo H, Mockler T, Chen J, Cashmore AR, 1998. Enhancement of blue-light sensitivity of Arabidopsis seedlings by a blue light receptor cryptochrome 2. *Proc Natl Acad Sci U S A* **95**, 2686-90.

Liu B, Yang Z, Gomez A, Liu B, Lin C, Oka Y, 2016. Signaling mechanisms of plant cryptochromes in Arabidopsis thaliana. *J Plant Res* **129**, 137-48.

Liu H, Yu X, Li K*, et al.*, 2008. Photoexcited CRY2 interacts with CIB1 to regulate transcription and floral initiation in Arabidopsis. *Science* **322**, 1535-9.

Liu XL, Covington MF, Fankhauser C, Chory J, Wagner DR, 2001. ELF3 encodes a circadian clock-regulated nuclear protein that functions in an Arabidopsis PHYB signal transduction pathway. *Plant Cell* **13**, 1293-304.

Liu Z, Tjian R, 2018. Visualizing transcription factor dynamics in living cells. *J Cell Biol* **217**, 1181-91.

Livak KJ, Schmittgen TD, 2001. Analysis of relative gene expression data using real-time quantitative PCR and the 2(-Delta Delta C(T)) Method. *Methods* **25**, 402-8.

Lobrich M, Shibata A, Beucher A*, et al.*, 2010. gammaH2AX foci analysis for monitoring DNA double-strand break repair: strengths, limitations and optimization. *Cell Cycle* **9**, 662-9.

Lu SX, Webb CJ, Knowles SM, Kim SH, Wang Z, Tobin EM, 2012. CCA1 and ELF3 Interact in the control of hypocotyl length and flowering time in Arabidopsis. *Plant Physiol* **158**, 1079-88.

Lu Y, Gehan JP, Sharkey TD, 2005. Daylength and circadian effects on starch degradation and maltose metabolism. *Plant Physiol* **138**, 2280-91.

Ma Y, Gil S, Grasser KD, Mas P, 2018. Targeted Recruitment of the Basal Transcriptional Machinery by LNK Clock Components Controls the Circadian Rhythms of Nascent RNAs in Arabidopsis. *Plant Cell* **30**, 907-24.

Ma Y, Kanakousaki K, Buttitta L, 2015. How the cell cycle impacts chromatin architecture and influences cell fate. *Front Genet* **6**, 19.

Mannuss A, Trapp O, Puchta H, 2012. Gene regulation in response to DNA damage. *Biochim Biophys Acta* **1819**, 154-65.

Manova V, Gruszka D, 2015. DNA damage and repair in plants - from models to crops. *Front Plant Sci* **6**, 885.

Mao J, Zhang YC, Sang Y, Li QH, Yang HQ, 2005. From The Cover: A role for Arabidopsis cryptochromes and COP1 in the regulation of stomatal opening. *Proceedings of the National Academy of Sciences* **102**, 12270-5.

Martin G, Rovira A, Veciana N*, et al.*, 2018. Circadian Waves of Transcriptional Repression Shape PIF-Regulated Photoperiod-Responsive Growth in Arabidopsis. *Curr Biol* **28**, 311-8 e5.

Mas P, Devlin PF, Panda S, Kay SA, 2000. Functional interaction of phytochrome B and cryptochrome 2. *Nature* **408**, 207-11.

Mas P, Kim WY, Somers DE, Kay SA, 2003. Targeted degradation of TOC1 by ZTL modulates circadian function in Arabidopsis thaliana. *Nature* **426**, 567-70.

Mawphlang OIL, Kharshiing EV, 2017. Photoreceptor Mediated Plant Growth Responses: Implications for Photoreceptor Engineering toward Improved Performance in Crops. *Front Plant Sci* **8**, 1181.

Mcclung CR, Hsu M, Painter JE, Gagne JM, Karlsberg SD, Salome PA, 2000. Integrated temporal regulation of the photorespiratory pathway. Circadian regulation of two Arabidopsis genes encoding serine hydroxymethyltransferase. *Plant Physiol* **123**, 381-92.

Mcwatters HG, Bastow RM, Hall A, Millar AJ, 2000. The ELF3 zeitnehmer regulates light signalling to the circadian clock. *Nature* **408**, 716-20.

Mcwatters HG, Devlin PF, 2011. Timing in plants--a rhythmic arrangement. *FEBS Lett* **585**, 1474-84.

Mcwatters HG, Kolmos E, Hall A*, et al.*, 2007. ELF4 is required for oscillatory properties of the circadian clock. *Plant Physiol* **144**, 391-401.

Mei Q, Dvornyk V, 2015. Evolutionary History of the Photolyase/Cryptochrome Superfamily in Eukaryotes. *PLoS One* **10**, e0135940.

Millar AJ, Short SR, Chua NH, Kay SA, 1992. A novel circadian phenotype based on firefly luciferase expression in transgenic plants. *Plant Cell* **4**, 1075-87.

Mladenov E, Iliakis G, 2011. Induction and repair of DNA double strand breaks: the increasing spectrum of non-homologous end joining pathways. *Mutat Res* **711**, 61-72.

Mohawk JA, Green CB, Takahashi JS, 2012. Central and peripheral circadian clocks in mammals. *Annu Rev Neurosci* **35**, 445-62.

Moreno-Romero J, Armengot L, Mar Marques-Bueno M, Britt A, Carmen Martinez M, 2012. CK2-defective Arabidopsis plants exhibit enhanced double-strand break repair rates and reduced survival after exposure to ionizing radiation. *Plant J* **71**, 627-38.

Nagel DH, Doherty CJ, Pruneda-Paz JL, Schmitz RJ, Ecker JR, Kay SA, 2015. Genome-wide identification of CCA1 targets uncovers an expanded clock network in Arabidopsis. *Proc Natl Acad Sci U S A* **112**, E4802-10.

Nakagawa T, Kurose T, Hino T*, et al.*, 2007a. Development of series of gateway binary vectors, pGWBs, for realizing efficient construction of fusion genes for plant transformation. *J Biosci Bioeng* **104**, 34-41.

Nakagawa T, Suzuki T, Murata S*, et al.*, 2007b. Improved Gateway binary vectors: high-performance vectors for creation of fusion constructs in transgenic analysis of plants. *Biosci Biotechnol Biochem* **71**, 2095-100.

Nakajima S, Sugiyama M, Iwai S*, et al.*, 1998. Cloning and characterization of a gene (UVR3) required for photorepair of 6-4 photoproducts in Arabidopsis thaliana. *Nucleic Acids Res* **26**, 638-44.

Nakamichi N, Kiba T, Henriques R, Mizuno T, Chua NH, Sakakibara H, 2010. PSEUDO-RESPONSE REGULATORS 9, 7, and 5 are transcriptional repressors in the Arabidopsis circadian clock. *Plant Cell* **22**, 594-605.

Nakamichi N, Kita M, Ito S, Yamashino T, Mizuno T, 2005. PSEUDO-RESPONSE REGULATORS, PRR9, PRR7 and PRR5, together play essential roles close to the circadian clock of Arabidopsis thaliana. *Plant Cell Physiol* **46**, 686-98.

Nikaido SS, Johnson CH, 2000. Daily and circadian variation in survival from ultraviolet radiation in Chlamydomonas reinhardtii. *Photochem Photobiol* **71**, 758-65.

Niwa Y, Ito S, Nakamichi N*, et al.*, 2007. Genetic linkages of the circadian clock-associated genes, TOC1, CCA1 and LHY, in the photoperiodic control of flowering time in Arabidopsis thaliana. *Plant Cell Physiol* **48**, 925-37.

Niwa Y, Yamashino T, Mizuno T, 2009. The circadian clock regulates the photoperiodic response of hypocotyl elongation through a coincidence mechanism in Arabidopsis thaliana. *Plant Cell Physiol* **50**, 838-54.

Nohales MA, Kay SA, 2016. Molecular mechanisms at the core of the plant circadian oscillator. *Nat Struct Mol Biol* **23**, 1061-9.

Noordally ZB, Ishii K, Atkins KA*, et al.*, 2013. Circadian control of chloroplast transcription by a nuclear-encoded timing signal. *Science* **339**, 1316-9.

Nowsheen S, Yang ES, 2012. The intersection between DNA damage response and cell death pathways. *Exp Oncol* **34**, 243-54.

Nusinow DA, Helfer A, Hamilton EE*, et al.*, 2011. The ELF4-ELF3-LUX complex links the circadian clock to diurnal control of hypocotyl growth. *Nature* **475**, 398-402.

Oakenfull RJ, Davis SJ, 2017. Shining a light on the Arabidopsis circadian clock. *Plant Cell Environ* **40**, 2571-85.

Ohle C, Tesorero R, Schermann G, Dobrev N, Sinning I, Fischer T, 2016. Transient RNA-DNA Hybrids Are Required for Efficient Double-Strand Break Repair. *Cell* **167**, 1001-13 e7.

Olive PL, Banath JP, 2006. The comet assay: a method to measure DNA damage in individual cells. *Nat Protoc* **1**, 23-9.

Olive PL, Durand RE, 2005. Heterogeneity in DNA damage using the comet assay. *Cytometry A* **66**, 1-8.

Osakabe K, Osakabe Y, Toki S, 2010. Site-directed mutagenesis in Arabidopsis using custom-designed zinc finger nucleases. *Proc Natl Acad Sci U S A* **107**, 12034-9.

Osman K, Higgins JD, Sanchez-Moran E, Armstrong SJ, Franklin FC, 2011. Pathways to meiotic recombination in Arabidopsis thaliana. *New Phytol* **190**, 523-44.

Ozgur S, Sancar A, 2006. Analysis of autophosphorylating kinase activities of Arabidopsis and human cryptochromes. *Biochemistry* **45**, 13369-74.

Ozkan-Dagliyan I, Chiou YY, Ye R, Hassan BH, Ozturk N, Sancar A, 2013. Formation of Arabidopsis Cryptochrome 2 photobodies in mammalian nuclei: application as an optogenetic DNA damage checkpoint switch. *J Biol Chem* **288**, 23244-51.

Oztas O, Selby CP, Sancar A, Adebali O, 2018. Genome-wide excision repair in Arabidopsis is coupled to transcription and reflects circadian gene expression patterns. *Nat Commun* **9**, 1503.

Panda S, Poirier GG, Kay SA, 2002. tej defines a role for poly(ADP-ribosyl)ation in establishing period length of the arabidopsis circadian oscillator. *Dev Cell* **3**, 51-61.

Para A, Farre EM, Imaizumi T, Pruneda-Paz JL, Harmon FG, Kay SA, 2007. PRR3 Is a vascular regulator of TOC1 stability in the Arabidopsis circadian clock. *Plant Cell* **19**, 3462-73.

Park E, Kim Y, Choi G, 2018. Phytochrome B Requires PIF Degradation and Sequestration to Induce Light Responses across a Wide Range of Light Conditions. *Plant Cell* **30**, 1277-92.

Park MJ, Kwon YJ, Gil KE, Park CM, 2016. LATE ELONGATED HYPOCOTYL regulates photoperiodic flowering via the circadian clock in Arabidopsis. *BMC Plant Biol* **16**, 114.

Paull TT, Rogakou EP, Yamazaki V, Kirchgessner CU, Gellert M, Bonner WM, 2000. A critical role for histone H2AX in recruitment of repair factors to nuclear foci after DNA damage. *Curr Biol* **10**, 886-95.

Pedmale UV, Huang SC, Zander M*, et al.*, 2016. Cryptochromes Interact Directly with PIFs to Control Plant Growth in Limiting Blue Light. *Cell* **164**, 233-45.

Pellegrino S, Altmeyer M, 2016. Interplay between Ubiquitin, SUMO, and Poly(ADP-Ribose) in the Cellular Response to Genotoxic Stress. *Front Genet* **7**, 63.

Perales M, Mas P, 2007. A functional link between rhythmic changes in chromatin structure and the Arabidopsis biological clock. *Plant Cell* **19**, 2111-23.

Perez-Garcia P, Ma Y, Yanovsky MJ, Mas P, 2015. Time-dependent sequestration of RVE8 by LNK proteins shapes the diurnal oscillation of anthocyanin biosynthesis. *Proc Natl Acad Sci U S A* **112**, 5249-53.

Pittendrigh CS, 1993. Temporal organization: reflections of a Darwinian clock-watcher. *Annu Rev Physiol* **55**, 16-54.

Polo SE, Jackson SP, 2011. Dynamics of DNA damage response proteins at DNA breaks: a focus on protein modifications. *Genes Dev* **25**, 409-33.

Portoles S, Mas P, 2010. The functional interplay between protein kinase CK2 and CCA1 transcriptional activity is essential for clock temperature compensation in Arabidopsis. *PLoS Genet* **6**, e1001201.

Preuss SB, Britt AB, 2003. A DNA-damage-induced cell cycle checkpoint in Arabidopsis. *Genetics* **164**, 323-34.

Priest HD, Filichkin SA, Mockler TC, 2009. Cis-regulatory elements in plant cell signaling. *Curr Opin Plant Biol* **12**, 643-9.

Puchta H, 2005. The repair of double-strand breaks in plants: mechanisms and consequences for genome evolution. *J Exp Bot* **56**, 1-14.

Puchta H, Fauser F, 2014. Synthetic nucleases for genome engineering in plants: prospects for a bright future. *Plant J* **78**, 727-41.

Quint M, Delker C, Franklin KA, Wigge PA, Halliday KJ, Van Zanten M, 2016. Molecular and genetic control of plant thermomorphogenesis. *Nat Plants* **2**, 15190.

Rauf M, Arif M, Dortay H*, et al.*, 2013. ORE1 balances leaf senescence against maintenance by antagonizing G2-like-mediated transcription. *EMBO Rep* **14**, 382-8.

Rawat R, Takahashi N, Hsu PY*, et al.*, 2011. REVEILLE8 and PSEUDO-REPONSE REGULATOR5 form a negative feedback loop within the Arabidopsis circadian clock. *PLoS Genet* **7**, e1001350.

Rissel D, Losch J, Peiter E, 2014. The nuclear protein Poly(ADP-ribose) polymerase 3 (AtPARP3) is required for seed storability in Arabidopsis thaliana. *Plant Biol (Stuttg)* **16**, 1058-64.

Roldan-Arjona T, Ariza RR, 2009. Repair and tolerance of oxidative DNA damage in plants. *Mutat Res* **681**, 169-79.

Roy S, 2014. Maintenance of genome stability in plants: repairing DNA double strand breaks and chromatin structure stability. *Front Plant Sci* **5**, 487.

Rugnone ML, Faigon Soverna A, Sanchez SE*, et al.*, 2013. LNK genes integrate light and clock signaling networks at the core of the Arabidopsis oscillator. *Proc Natl Acad Sci U S A* **110**, 12120-5.

Sakuraba Y, Jeong J, Kang MY, Kim J, Paek NC, Choi G, 2014. Phytochrome-interacting transcription factors PIF4 and PIF5 induce leaf senescence in Arabidopsis. *Nat Commun* **5**, 4636.

Salome PA, Mcclung CR, 2005. PSEUDO-RESPONSE REGULATOR 7 and 9 are partially redundant genes essential for the temperature responsiveness of the Arabidopsis circadian clock. *Plant Cell* **17**, 791-803.

Salome PA, Weigel D, Mcclung CR, 2010. The role of the Arabidopsis morning loop components CCA1, LHY, PRR7, and PRR9 in temperature compensation. *Plant Cell* **22**, 3650-61.

Sancar A, Lindsey-Boltz LA, Kang TH, Reardon JT, Lee JH, Ozturk N, 2010. Circadian clock control of the cellular response to DNA damage. *FEBS Lett* **584**, 2618-25.

Sanchez SE, Kay SA, 2016. The Plant Circadian Clock: From a Simple Timekeeper to a Complex Developmental Manager. *Cold Spring Harb Perspect Biol* **8**.

Santos CL, Pourrut B, Ferreira De Oliveira JM, 2015. The use of comet assay in plant toxicology: recent advances. *Front Genet* **6**, 216.

Schaffer R, Ramsay N, Samach A*, et al.*, 1998. The late elongated hypocotyl mutation of Arabidopsis disrupts circadian rhythms and the photoperiodic control of flowering. *Cell* **93**, 1219-29.

Selby CP, Sancar A, 2006. A cryptochrome/photolyase class of enzymes with single-stranded DNA-specific photolyase activity. *Proc Natl Acad Sci U S A* **103**, 17696-700.

Shalit-Kaneh A, Kumimoto RW, Filkov V, Harmer SL, 2018. Multiple feedback loops of the Arabidopsis circadian clock provide rhythmic robustness across environmental conditions. *Proc Natl Acad Sci U S A* **115**, 7147-52.

Sheerin DJ, Menon C, Zur Oven-Krockhaus S*, et al.*, 2015. Light-activated phytochrome A and B interact with members of the SPA family to promote photomorphogenesis in Arabidopsis by reorganizing the COP1/SPA complex. *Plant Cell* **27**, 189-201.

Shim JS, Kubota A, Imaizumi T, 2017. Circadian Clock and Photoperiodic Flowering in Arabidopsis: CONSTANS Is a Hub for Signal Integration. *Plant Physiol* **173**, 5-15.

Shin J, Heidrich K, Sanchez-Villarreal A, Parker JE, Davis SJ, 2012. TIME FOR COFFEE represses accumulation of the MYC2 transcription factor to provide time-of-day regulation of jasmonate signaling in Arabidopsis. *Plant Cell* **24**, 2470-82.

Siebert R, Puchta H, 2002. Efficient repair of genomic double-strand breaks by homologous recombination between directly repeated sequences in the plant genome. *Plant Cell* **14**, 1121-31.

Singh M, Mas P, 2018. A Functional Connection between the Circadian Clock and Hormonal Timing in Arabidopsis. *Genes (Basel)* **9**.

Singh SK, Roy S, Choudhury SR, Sengupta DN, 2010. DNA repair and recombination in higher plants: insights from comparative genomics of Arabidopsis and rice. *BMC Genomics* **11**, 443.

Skourti-Stathaki K, Proudfoot NJ, 2014. A double-edged sword: R loops as threats to genome integrity and powerful regulators of gene expression. *Genes Dev* **28**, 1384-96.

Song J, Keppler BD, Wise RR, Bent AF, 2015. PARP2 Is the Predominant Poly(ADP-Ribose) Polymerase in Arabidopsis DNA Damage and Immune Responses. *PLoS Genet* **11**, e1005200.

Song Q, Ando A, Xu D*, et al.*, 2018a. Diurnal down-regulation of ethylene biosynthesis mediates biomass heterosis. *Proceedings of the National Academy of Sciences* **115**, 5606-11.

Song Y, Jiang Y, Kuai B, Li L, 2018b. CIRCADIAN CLOCK-ASSOCIATED 1 Inhibits Leaf Senescence in Arabidopsis. *Front Plant Sci* **9**, 280.

Song YH, Estrada DA, Johnson RS*, et al.*, 2014. Distinct roles of FKF1, Gigantea, and Zeitlupe proteins in the regulation of Constans stability in Arabidopsis photoperiodic flowering. *Proc Natl Acad Sci U S A* **111**, 17672-7.

Song YH, Smith RW, To BJ, Millar AJ, Imaizumi T, 2012. FKF1 conveys timing information for CONSTANS stabilization in photoperiodic flowering. *Science* **336**, 1045-9.

Soy J, Leivar P, Gonzalez-Schain N*, et al.*, 2016. Molecular convergence of clock and photosensory pathways through PIF3-TOC1 interaction and co-occupancy of target promoters. *Proc Natl Acad Sci U S A* **113**, 4870-5.

Spampinato CP, 2017. Protecting DNA from errors and damage: an overview of DNA repair mechanisms in plants compared to mammals. *Cell Mol Life Sci* **74**, 1693-709.

Spampinato CP, Gomez RL, Galles C, Lario LD, 2009. From bacteria to plants: a compendium of mismatch repair assays. *Mutat Res* **682**, 110-28.

Stadler J, Richly H, 2017. Regulation of DNA Repair Mechanisms: How the Chromatin Environment Regulates the DNA Damage Response. *Int J Mol Sci* **18**.

Stelling J, Gilles ED, Doyle FJ, 3rd, 2004. Robustness properties of circadian clock architectures. *Proc Natl Acad Sci U S A* **101**, 13210-5.

Strasser B, Sanchez-Lamas M, Yanovsky MJ, Casal JJ, Cerdan PD, 2010. Arabidopsis thaliana life without phytochromes. *Proc Natl Acad Sci U S A* **107**, 4776-81.

Strober W, 2001. Trypan blue exclusion test of cell viability. *Curr Protoc Immunol* **Appendix 3**, Appendix 3B.

Suarez-Lopez P, Wheatley K, Robson F, Onouchi H, Valverde F, Coupland G, 2001. CONSTANS mediates between the circadian clock and the control of flowering in Arabidopsis. *Nature* **410**, 1116-20.

Takahashi JS, 2017. Transcriptional architecture of the mammalian circadian clock. *Nat Rev Genet* **18**, 164-79.

Takahashi N, Hirata Y, Aihara K, Mas P, 2015. A Hierarchical Multi-oscillator Network Orchestrates the Arabidopsis Circadian System. *Cell* **163**, 148-59.

Takata H, Hanafusa T, Mori T*, et al.*, 2013. Chromatin compaction protects genomic DNA from radiation damage. *PLoS One* **8**, e75622.

Takeuchi T, Newton L, Burkhardt A, Mason S, Farre EM, 2014. Light and the circadian clock mediate time-specific changes in sensitivity to UV-B stress under light/dark cycles. *J Exp Bot* **65**, 6003-12.

Tilbrook K, Arongaus AB, Binkert M, Heijde M, Yin R, Ulm R, 2013. The UVR8 UV-B Photoreceptor: Perception, Signaling and Response. *Arabidopsis Book* **11**, e0164.

Tornaletti S, Hanawalt PC, 1999. Effect of DNA lesions on transcription elongation. *Biochimie* **81**, 139-46.

Tornaletti S, Reines D, Hanawalt PC, 1999. Structural characterization of RNA polymerase II complexes arrested by a cyclobutane pyrimidine dimer in the transcribed strand of template DNA. *J Biol Chem* **274**, 24124-30.

Toth R, Kevei E, Hall A, Millar AJ, Nagy F, Kozma-Bognar L, 2001. Circadian clock-regulated expression of phytochrome and cryptochrome genes in Arabidopsis. *Plant Physiol* **127**, 1607-16.

Truong LN, Li Y, Shi LZ*, et al.*, 2013. Microhomology-mediated End Joining and Homologous Recombination share the initial end resection step to repair DNA double-strand breaks in mammalian cells. *Proc Natl Acad Sci U S A* **110**, 7720-5.

Uanschou C, Siwiec T, Pedrosa-Harand A*, et al.*, 2007. A novel plant gene essential for meiosis is related to the human CtIP and the yeast COM1/SAE2 gene. *EMBO J* **26**, 5061-70.

Vainonen JP, Shapiguzov A, Vaattovaara A, Kangasjarvi J, 2016. Plant PARPs, PARGs and PARP-like Proteins. *Curr Protein Pept Sci* **17**, 713-23.

Van Wees S, 2008. Phenotypic analysis of Arabidopsis mutants: trypan blue stain for fungi, oomycetes, and dead plant cells. *CSH Protoc* **2008**, pdb prot4982.

Van Zanten M, Tessadori F, Mcloughlin F*, et al.*, 2010. Photoreceptors CRYTOCHROME2 and phytochrome B control chromatin compaction in Arabidopsis. *Plant Physiol* **154**, 1686-96.

Wang W, Barnaby JY, Tada Y*, et al.*, 2011. Timing of plant immune responses by a central circadian regulator. *Nature* **470**, 110-4.

Wang ZY, Tobin EM, 1998. Constitutive expression of the CIRCADIAN CLOCK ASSOCIATED 1 (CCA1) gene disrupts circadian rhythms and suppresses its own expression. *Cell* **93**, 1207-17.

Waterworth WM, Bray CM, West CE, 2015. The importance of safeguarding genome integrity in germination and seed longevity. *J Exp Bot* **66**, 3549-58.

Waterworth WM, Drury GE, Bray CM, West CE, 2011. Repairing breaks in the plant genome: the importance of keeping it together. *New Phytol* **192**, 805-22.

Webb AaR, Seki M, Satake A, Caldana C, 2019. Continuous dynamic adjustment of the plant circadian oscillator. *Nat Commun* **10**, 550.

Weidler G, Zur Oven-Krockhaus S, Heunemann M*, et al.*, 2012. Degradation of Arabidopsis CRY2 is regulated by SPA proteins and phytochrome A. *Plant Cell* **24**, 2610-23.

West CE, Waterworth WM, Sunderland PA, Bray CM, 2004. Arabidopsis DNA double-strand break repair pathways. *Biochem Soc Trans* **32**, 964-6.

Xie Q, Wang P, Liu X*, et al.*, 2014. LNK1 and LNK2 are transcriptional coactivators in the Arabidopsis circadian oscillator. *Plant Cell* **26**, 2843-57.

Xu W, Xu H, Li K*, et al.*, 2017. The R-loop is a common chromatin feature of the Arabidopsis genome. *Nat Plants* **3**, 704-14.

Yakir E, Hassidim M, Melamed-Book N, Hilman D, Kron I, Green RM, 2011. Cell autonomous and cell-type specific circadian rhythms in Arabidopsis. *Plant J* **68**, 520-31.

Yamaguchi N, Winter CM, Wu MF, Kwon CS, William DA, Wagner D, 2014. PROTOCOLS: Chromatin Immunoprecipitation from Arabidopsis Tissues. *Arabidopsis Book* **12**, e0170.

Yamamoto Y, Sato E, Shimizu T*, et al.*, 2003. Comparative genetic studies on the APRR5 and APRR7 genes belonging to the APRR1/TOC1 quintet implicated in circadian rhythm, control of flowering time, and early photomorphogenesis. *Plant Cell Physiol* **44**, 1119-30.

Yang C, Liu J, Dong X, Cai Z, Tian W, Wang X, 2014. Short-term and continuing stresses differentially interplay with multiple hormones to regulate plant survival and growth. *Mol Plant* **7**, 841-55.

Yang L, Mo W, Yu X*, et al.*, 2018. Reconstituting Arabidopsis CRY2 Signaling Pathway in Mammalian Cells Reveals Regulation of Transcription by Direct Binding of CRY2 to DNA. *Cell Rep* **24**, 585-93 e4.

Yang Z, Liu B, Su J, Liao J, Lin C, Oka Y, 2017. Cryptochromes Orchestrate Transcription Regulation of Diverse Blue Light Responses in Plants. *Photochem Photobiol* **93**, 112-27.

Yang Z, Tang L, Li M*, et al.*, 2010. Monitoring homologous recombination in rice (Oryza sativa L.). *Mutat Res* **691**, 55-63.

Yeom M, Kim H, Lim J*, et al.*, 2014. How do phytochromes transmit the light quality information to the circadian clock in Arabidopsis? *Mol Plant* **7**, 1701-4.

Yoshii T, Hermann-Luibl C, Helfrich-Forster C, 2016. Circadian light-input pathways in Drosophila. *Commun Integr Biol* **9**, e1102805.

Yoshikawa Y, Mori T, Magome N, Hibino K, Yoshikawa K, 2008. DNA compaction plays a key role in radioprotection against double-strand breaks as revealed by single-molecule observation. *Chemical Physics Letters* **456**, 80-3.

Yoshiyama K, Conklin PA, Huefner ND, Britt AB, 2009. Suppressor of gamma response 1 (SOG1) encodes a putative transcription factor governing multiple responses to DNA damage. *Proc Natl Acad Sci U S A* **106**, 12843-8.

Yoshiyama KO, 2016. SOG1: a master regulator of the DNA damage response in plants. *Genes Genet Syst* **90**, 209-16.

Yoshiyama KO, Kimura S, Maki H, Britt AB, Umeda M, 2014. The role of SOG1, a plant-specific transcriptional regulator, in the DNA damage response. *Plant Signal Behav* **9**, e28889.

Yoshiyama KO, Kobayashi J, Ogita N*, et al.*, 2013. ATM-mediated phosphorylation of SOG1 is essential for the DNA damage response in Arabidopsis. *EMBO Rep* **14**, 817-22.

Yu JW, Rubio V, Lee NY*, et al.*, 2008. COP1 and ELF3 control circadian function and photoperiodic flowering by regulating GI stability. *Mol Cell* **32**, 617-30.

Yu X, Sayegh R, Maymon M*, et al.*, 2009. Formation of nuclear bodies of Arabidopsis CRY2 in response to blue light is associated with its blue light-dependent degradation. *Plant Cell* **21**, 118-30.

Zhang B, Wang L, Zeng L, Zhang C, Ma H, 2015a. Arabidopsis TOE proteins convey a photoperiodic signal to antagonize CONSTANS and regulate flowering time. *Genes Dev* **29**, 975-87.

Zhang H, Gu Z, Wu Q*, et al.*, 2015b. Arabidopsis PARG1 is the key factor promoting cell survival among the enzymes regulating post-translational poly(ADP-ribosyl)ation. *Sci Rep* **5**, 15892.

Zheng XY, Zhou M, Yoo H*, et al.*, 2015. Spatial and temporal regulation of biosynthesis of the plant immune signal salicylic acid. *Proc Natl Acad Sci U S A* **112**, 9166-73.

Zhou M, Wang W, Karapetyan S*, et al.*, 2015. Redox rhythm reinforces the circadian clock to gate immune response. *Nature* **523**, 472-6.

Zhu L, Zee PC, 2012. Circadian rhythm sleep disorders. *Neurol Clin* **30**, 1167-91.

Zhu Y, Liu L, Shen L, Yu H, 2016. NaKR1 regulates long-distance movement of FLOWERING LOCUS T in Arabidopsis. *Nat Plants* **2**, 16075.

ANNEXES

Annexes

Targeted Recruitment of the Basal Transcriptional Machinery by LNK Clock Components Controls the Circadian Rhythms of Nascent RNAs in Arabidopsis

Yuan Ma,[a] Sergio Gil,[a] Klaus D. Grasser,[b] and Paloma Mas[a,c,1]

[a] Centre for Research in Agricultural Genomics, CSIC-IRTA-UAB-UB, Campus UAB, Bellaterra, 08193 Barcelona, Spain
[b] Department of Cell Biology and Plant Biochemistry, Biochemistry Center, University of Regensburg, D-93053 Regensburg, Germany
[c] Consejo Superior de Investigaciones Científicas, 08028 Barcelona, Spain

ORCID IDs: 0000-0001-8975-1975 (Y.M.); 0000-0002-7080-5520 (K.D.G.); 0000-0002-3780-8041 (P.M.)

The rhythms of steady-state mRNA expression pervade nearly all circadian systems. However, the mechanisms behind the rhythmic transcriptional synthesis and its correlation with circadian expression remain fully unexplored, particularly in plants. Here, we discovered a multifunctional protein complex that orchestrates the rhythms of transcriptional activity in *Arabidopsis thaliana*. The expression of the circadian oscillator genes *TIMING OF CAB EXPRESSION1/PSEUDO-RESPONSE REGULATOR1* and *PSEUDO-RESPONSE REGULATOR5* initially relies on the modular function of the clock-related factor REVEILLE8: its MYB domain provides the DNA binding specificity, while its LCL domain recruits the clock components, NIGHT LIGHT-INDUCIBLE AND CLOCK-REGULATED proteins (LNKs), to target promoters. LNKs, in turn, specifically interact with RNA Polymerase II and the transcript elongation FACT complex to rhythmically co-occupy the target loci. The functional interaction of these components is central for chromatin status, transcript initiation, and elongation as well as for proper rhythms in nascent RNAs. Thus, our findings explain how genome readout of environmental information ultimately results in rhythmic changes of gene expression.

INTRODUCTION

Organisms have developed a complex mechanism that can anticipate the predictable changes in the surrounding environment to adjust their physiology and development in a timely manner (Zhang and Kay, 2010). This mechanism, known as the circadian clock, provides a remarkable adaptive advantage, allowing for the synchronization of internal biology with the external environment. In *Arabidopsis thaliana*, the clock machinery is quite sophisticated and involves reciprocal regulation among clock components that ultimately leads to biological rhythms that oscillate in resonance with the environment (Greenham and McClung, 2015). The organization of the circadian system in plants is hierarchical, with specific circadian coupling or communication among clock cells at the plant shoot apex that is important for clock synchronization in roots (Takahashi et al., 2015). The coupling of cells at the vasculature also plays a role in synchronizing neighboring mesophyll cells (Endo et al., 2014). Differences in coupling and/or circadian function in different parts of the plant were also reported in various studies (Thain et al., 2002; James et al., 2008; Yakir et al., 2011; Wenden et al., 2012; Bordage et al., 2016).

Transcriptional regulation is one of the many layers underlying the circadian function in plants. Therefore, it is not surprising to find, at the core of the plant clock, a high number of transcription factors including, among others, the MYB domain proteins (Carré and Kim, 2002). Single MYB domain transcription factors such as CCA1 (CIRCADIAN CLOCK ASSOCIATED1) and LHY (LATE ELONGATED HYPOCOTYL) operate very close to the Arabidopsis circadian oscillator and belong to a family of 11 members that share close sequence similarity within the MYB-like domain. Five of these single MYB factors (REVEILLE/LHY-CCA1-LIKE [RVE/LCL] proteins) were assigned to a family subgroup based on the presence of the so-called LCL domain (; Farinas and Mas, 2011), which is absent in other members of the single MYB family. Analyses of Arabidopsis plants misexpressing the RVEs have provided some clues about their role in circadian clock function. For instance, plants misexpressing RVE8/LCL5 display changes in phase, period, and amplitude of key oscillator genes (Farinas and Mas, 2011; Rawat et al., 2011; Hsu et al., 2013). Furthermore, the activation of the dusk-expressed gene *TOC1/PRR1* (*TIMING OF CAB EXPRESSION1/PSEUDO-RESPONSE REGULATOR1*) by RVE8 is antagonized by CCA1 and involves changes in the pattern of Histone 3 acetylation at the *TOC1* promoter (Farinas and Mas, 2011). Activation of *TOC1* and *PRR5* (another member of the TOC1/PRR1 family) occurs through direct binding of RVE8 to their promoters and requires interaction with two members of the NIGHT LIGHT-INDUCIBLE AND CLOCK-REGULATED (LNK) protein family, which together with RVEs form a transcriptional coactivator complex (Xie et al., 2014; Xing et al., 2015). In addition to altered gene expression, plants misexpressing RVE8 and/or LNKs show a variety of phenotypes affecting anthocyanin accumulation, plant growth, and photoperiodic regulation of flowering time (Farinas and Mas, 2011; Rawat et al., 2011; Pérez-García et al., 2015; Gray et al., 2017). Overall, LNKs connect circadian gene expression, growth, and development with

[1] Address correspondence to paloma.mas@cragenomica.es.
The author responsible for distribution of materials integral to the findings presented in this article in accordance with the policy described in the Instructions for Authors (www.plantcell.org) is: Paloma Mas (paloma.mas@cragenomica.es).
www.plantcell.org/cgi/doi/10.1105/tpc.18.00052

IN A NUTSHELL

Background: Circadian clocks are internal time-keeping mechanisms that help organisms adapt to the environmental changes that occur during the day and night cycle. In *Arabidopsis thaliana*, the circadian clock consists of multiple transcriptional regulatory feedback loops. The clock-associated components RVE8 and LNK were previously shown to interact directly to regulate rhythmic anthocyanin biosynthesis. Together, they also act as transcriptional activator and coactivator of the key core clock genes *PRR5* and *TOC1*.

Question: How are the circadian rhythms in *PRR5* and *TOC1* transcription generated, and what roles are played by RVE8 and LNKs?

Findings: Our studies identified a multifunctional protein complex in which each component exerts specific functions that contribute to the regulation of *PRR5* and *TOC1* transcription. The MYB domain of RVE8 provides the DNA binding specificity, while its LCL domain is responsible for the interaction with LNKs. LNKs in turn recruit RNA Polymerase II and the transcription elongation factor SSRP1 (STRUCTURE-SPECIFIC RECOGNITION PROTEIN1) to facilitate the initiation and elongation of clock transcripts. Mutation or inactivation of the protein complex components affects the expression of *PRR5* and *TOC1* nascent RNAs, delays the mRNA steady-state rising phase, and reduces the amplitude. We found that the rhythms in nascent RNA synthesis controlled by the protein complex determine the steady-state mRNA circadian oscillation.

Next steps: It has been reported that LNKs function as transcriptional repressors, so it would be interesting to investigate the molecular mechanisms underlying their repressing function and how they might act as both corepressors and coactivators.

seasonal changes in daylength and temperature (Rugnone et al., 2013; Mizuno et al., 2014; Xie et al., 2014).

Genome readout of environmental information ultimately results in controlled changes in gene expression exerted at its basis by the transcriptional machinery. Transcription of coding genes requires different phases, including initiation, elongation, and termination, followed by maturation and decay. Transcription initiation relies on the formation of the preinitiation complex (PIC), which includes the RNA Polymerase II (RNA Pol II) and a number of transcription factors and chromatin-related complexes that modulate RNA Pol II activity (Lee et al., 1999; Näär et al., 2001). Following PIC formation, the highly conserved heptapeptide repeats within the RNA Pol II C-terminal domain (CTD) (Allison et al., 1988; Nawrath et al., 1990) are susceptible of phosphorylation at specific residues, which facilitate the recruitment of particular protein complexes and the progression of initiation or elongation, depending on the position of the phosphorylated residue (Buratowski, 2009; Hajheidari et al., 2013). For instance, phosphorylation of Serine 5 (S5P) within the RNA Pol II CTD allows RNA Pol II to escape the PIC and initiate transcription (Komarnitsky et al., 2000). Thus, S5P is found at the promoters and 5′ ends of genes and is usually considered to be a marker of transcription initiation and early elongation. During the transition from initiation to elongation, decreased accumulation of S5P coincides with a progressive increase in Serine 2 phosphorylation (S2P) (Margaritis and Holstege, 2008), which aids in the recruitment of factors required for elongation (Hajheidari et al., 2013) followed by subsequent mRNA polyadenylation and termination at the 3′ ends of genes (McCracken et al., 1997; Birse et al., 1998).

Transcript elongation is also modulated by a number of transcript elongation factors, which associate with RNA Pol II and act as histone chaperones, modifying histones or RNA Pol II activity (Jonkers and Lis, 2015). In Arabidopsis, the histone chaperone FACT (FACILITATES CHROMATIN TRANSCRIPTION) complex is composed of SSRP1 (STRUCTURE-SPECIFIC RECOGNITION PROTEIN1) and SPT16 (SUPPRESSOR OF TY16) (Van Lijsebettens and Grasser, 2014). The FACT complex localizes throughout genomic regions of actively transcribed genes, and its binding correlates with gene transcription (Duroux et al., 2004). Notably, the FACT complex rhythmically binds to the promoter of *TOC1*, with a waveform paralleling *TOC1* mRNA oscillation (Perales and Más, 2007). Knockdown plants with decreased expression of *SSRP1* and *SPT16* show alterations in vegetative and reproductive development, while null *ssrp1* mutant plants are lethal (Lolas et al., 2010). Furthermore, together with other transcript elongation factors, the FACT complex copurifies with elongating RNA Pol II (Antosz et al., 2017), which suggests that the Arabidopsis FACT complex assists transcript elongation with a similar function to that described in yeast (Xin et al., 2009) and humans (Orphanides et al., 1998).

Here, we uncover the mechanisms controlling the dusk-phased rhythms in nascent RNAs and steady-state mature mRNAs in Arabidopsis. We provide evidence that LNKs act as molecular switches that recruit the transcriptional machinery for transcript initiation and elongation in a timely manner. Consistently, LNK function is essential for sustaining the rhythms in nascent RNAs. Binding to the circadian target gene promoters relies on the sequence-dependent specificity provided by the MYB domain of RVE8, while direct interaction of the LCL domain with LNKs conveys LNKs to the target promoters. Together, our study uncovers the role of clock components in regulating circadian transcription by directly recruiting the transcriptional machinery.

RESULTS

The MYB Domain of RVE8 Provides the DNA Binding Specificity to the *TOC1* and *PRR5* Promoters

To investigate the modular nature of RVE8 and the contribution of RVE8 domains to the overall function of the full-length protein

(RVE8-FL), we cloned a truncated version of RVE8 lacking the C-terminal LCL domain (Figure 1A). The construct, named ΔLCL, also contains GFP as a tag and is expressed under the control of the cauliflower mosaic virus 35S promoter. We produced Arabidopsis plants expressing the *TOC1* promoter fused to luciferase (*TOC1pro:LUC*) (Perales and Más, 2007) and examined promoter activity in wild-type and ΔLCL-overexpressing (ΔLCL-ox) lines under constant light (LL) conditions. Although the degree of overexpression was not very high (Supplemental Figure 1A), *TOC1pro:LUC* rhythms showed a delayed phase, a long period, and a slightly decreased amplitude in ΔLCL-ox compared with the wild type (Figures 1B and 1C). The decreased amplitude was also evident when rhythms were examined under light/dark cycles (12 h of light/12 h of dark [LD]) (Figures 1D and 1E; Supplemental Figure 1B). The circadian phenotypes of *TOC1pro:LUC* in ΔLCL-ox resembled those of *rve8* mutants (Supplemental Figures 1C and 1D), suggesting that ΔLCL-ox might interfere with RVE8 function. The similarities of ΔLCL-ox and *rve8* pervade other RVE8 targets, as *PRR5* expression also showed reduced amplitude under both LL (Figure 1F) and LD (Figure 1G) cycles, as assayed by RT-qPCR. Consistent with previous reports, our results revealed that, under constant red light conditions, RVE8-FL-ox showed significantly shorter hypocotyls while *rve8* mutant seedlings displayed longer hypocotyls compared with the wild type. The hypocotyls of ΔLCL-ox were also longer than those of the wild type (Supplemental Figure 1E).

Effector domains can modulate the transcriptional activity of DNA binding domains. As RVE8 regulates *TOC1* and *PRR5* expression through direct binding to their promoters, we examined the DNA binding capabilities of ΔLCL protein. Chromatin immunoprecipitation (ChIP) assays showed an evident enrichment of ΔLCL at both the *TOC1* and *PRR5* promoters (Figures 1H and 1I), suggesting that the MYB domain in ΔLCL retains the ability to bind to the target promoters despite the lack of the LCL domain. However, the observation that ΔLCL binding is not accompanied by the transcriptional activation of *TOC1* and *PRR5* suggests that ΔLCL might be competing with the endogenous RVE8 for promoter binding. Plants overexpressing ΔLCL in the *rve8* mutant background (ΔLCL-ox *rve8*) showed a clearly delayed phase of *TOC1pro:LUC* activity, along with a long period and decreased amplitude (Supplemental Figure 1F). Altogether, our results suggest that binding might be necessary but not sufficient for activation; thus, the LCL domain might play a prevalent role in the activating function of RVE8.

We also used confocal microscopy to compare RVE8-FL and ΔLCL distribution. Analysis of subcellular localization in hypocotyls and roots (Supplemental Figures 1G and 1I) revealed that RVE8-FL preferentially localized to the nucleus, although cytoplasmic strands with a reticulated pattern were also observed under confocal microscope settings of high gain. ΔLCL protein was also localized to the nucleus, with no evident sign of cytoplasmic strands under any gain conditions (Supplemental Figures 1H and 1J). The difference might be due to the absence of LCL or the reduced degree of overexpression in ΔLCL-ox. The nuclear localization of ΔLCL is consistent with the predicted bipartite nuclear localization signal (positions 103 to 125) (Supplemental Figure 1K) and with ΔLCL binding to nuclear DNA.

Overexpression of LCL-ox Exerts a Dominant-Negative Function in the Regulation of *TOC1* and *PRR5* Expression

The LCL domain amino acid sequence is highly conserved among a wide range of plant lineages (Supplemental Figures 2 and 3). Our results suggest that this domain might play an important role in RVE8 activity. To explore its function, we transformed the LCL domain fused to GFP under the control of the 35S promoter (Figure 2A) into *TOC1pro:LUC* plants to generate LCL-overexpressing lines (LCL-ox) (Supplemental Figure 4A). Bioluminescence analyses showed that the rhythmic oscillation of *TOC1pro:LUC* was clearly affected in LCL-ox plants, with a delayed phase and severely reduced amplitude under both LL and LD conditions (Figures 2B to 2E; Supplemental Figures 4C and 4D). The phenotypes were more severe than the ones observed in *rve8* mutants or in ΔLCL-ox plants (Figures 1B to 1E; Supplemental Figures 1B to 1D). *PRR5* expression was also severely disrupted in LCL-ox plants under LL and LD conditions (Figures 2F and 2G). Consistent with the severity of the gene expression phenotypes, LCL-ox hypocotyls were significantly longer than those of the wild type, ΔLCL-ox, and the *rve8* mutant, indicating that overexpression of LCL interferes with RVE8 function and results in enhanced plant hyposensitivity to red light (Figure 2H). Similarly, a clear delayed flowering time phenotype was observed in LCL-ox (Supplemental Figures 4E and 4F). Overexpression of LCL in the *rve8* mutant background (LCL-ox *rve8*) resulted in severe circadian phenotypes following the same trend to that of LCL-ox in the wild-type background (Supplemental Figures 4H and 4I). LCL-ox *rve8* hypocotyls were also significantly longer than those of the wild type (Supplemental Figure 4J). These results, together with the finding that LCL-ox phenotypes were more severe than those observed in *rve8*, suggest a possible dominant-negative role not only for RVE8 function but also for other members of the RVE family.

Our ChIP results showed the lack of enrichment of LCL on the *TOC1* and *PRR5* promoters in LCL-ox plants, which suggests that the LCL-ox dominant-negative function is not due to competition with the endogenous RVE8 for promoter binding. Analyses of the subcellular localization of LCL showed both nuclear and cytoplasmic accumulation (Supplemental Figure 4G). Altogether, our results show that the nucleus-localized LCL domain is not able to bind to the target gene promoters, but the circadian expression of these target genes is severely reduced in LCL-ox plants.

The RVE-LNK Tandem Regulates Both RNA Pol II and H3K4me3 Occupancy

To get further insights into the mechanisms of LCL function in the control of circadian gene expression, we performed a yeast two-hybrid screening with the LCL domain as bait. High-confidence-score (predicted biological score) analyses identified the members of the LNK protein family as proteins that interact with the LCL domain (Figure 3A). In vitro pull-down assays with *Escherichia coli* expressing the LCL domain fused to GST and LNK1 protein fused to MBP (Maltose Binding Protein) revealed a faint but reproducible coimmunoprecipitation (co-IP) of LNK1 with the LCL domain but not with GST-ΔLCL or with beads containing MBP-GFP (Figure

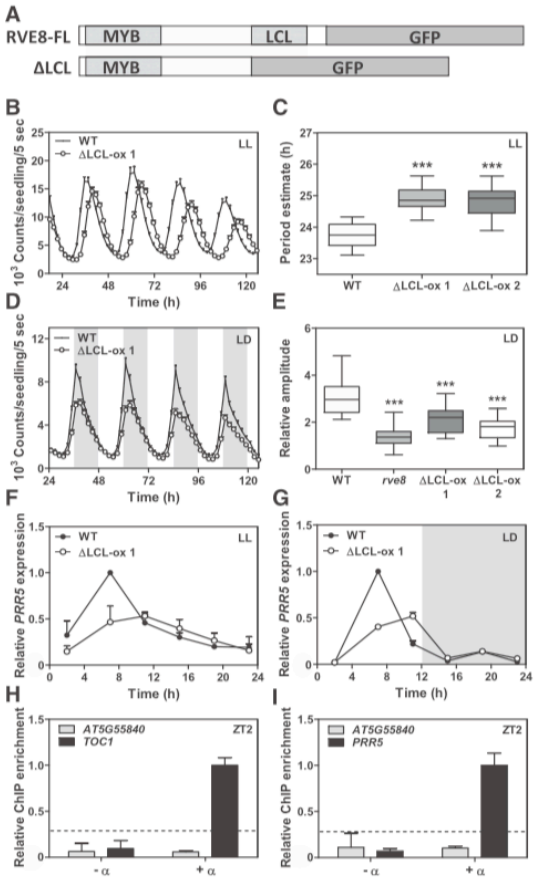

Figure 1. Overexpression of ΔLCL Alters *TOC1* and *PRR5* Circadian Gene Expression through the Binding of ΔLCL to Their Promoters.

(A) Schematic diagram depicting the full-length RVE8 protein (RVE8-FL) fused to GFP and a truncated version lacking the LCL domain (ΔLCL).
(B) Analysis of rhythmic oscillations of *TOC1pro:LUC* by in vivo luminescence assays in the wild type and ΔLCL-ox (line 1) under LL conditions.
(C) Period estimates of the circadian waveforms in the wild type and two different ΔLCL-ox lines (1 and 2) assayed as in **(B)** (***P < 0.001).
(D) Analysis of rhythmic oscillations of *TOC1pro:LUC* by in vivo luminescence assays in wild-type and ΔLCL-ox plants under LD cycles.
(E) Amplitude estimates of circadian waveforms in the wild type, *rve8* mutant, and two ΔLCL-ox lines assayed as in **(D)** (***P < 0.001).
(F) and **(G)** Time-course analysis by RT-qPCR assays of *PRR5* expression in wild-type and ΔLCL-ox plants grown under LL conditions for 2 d after synchronization under LD **(F)** or under LD cycles **(G)**. Data are represented as means + SE relative to *IPP2* (*ISOPENTENYL PYROPHOSPHATE:DIMETHYL-ALLYL PYROPHOSPHATE ISOMERASE*) expression and relative to the highest value.
(H) and **(I)** ChIP analyses with ΔLCL-ox plants assayed at ZT2 to examine binding to the *TOC1* **(H)** and *PRR5* **(I)** promoters. The promoter of the *AT5G55840* gene (*PPR*) was used as a negative control. Samples processed without (−α) and with (+α) antibody during the ChIP procedure are shown. ChIP enrichment is represented as means + SE relative to input and the highest value. Graphs include data from two biological replicates (samples from different starting material).
White and gray areas in **(D)** and **(G)** represent light and dark periods, respectively.

3B; Supplemental Figure 5A). An interaction was also observed for MBP-LNK3 with GST-LCL (Figure 3C; Supplemental Figure 5B). In vivo co-IP assays in plants using two different lines overexpressing both the LCL domain and LNK1 (LNK1-ox LCL-ox) revealed that the LCL domain effectively coimmunoprecipitated with LNK1 (Figures 3D and 3E). Co-IP was also observed in LNK3-ox LCL-ox plants (Figures 3F and 3G), which indicates the in vivo interaction of the LCL domain with LNK proteins.

As the rising phase of *TOC1* and *PRR5* expression is severely delayed in LCL-ox and in *lnk1 lnk2* double mutant plants, we hypothesized that the recruitment of the transcriptional machinery might be affected in these plants. Therefore, we assayed the distribution profiles of total RNA Pol II in wild-type and *lnk1 lnk2* plants. ChIP assays followed by qPCR showed that the accumulation of total RNA Pol II was reduced in *lnk1 lnk2* plants at the 5′ end, middle, and 3′ end regions of the *PRR5* and *TOC1* loci (Figures 4A to 4D; Supplemental Figures 5E and 5F). As RVE8 and RVE4 interact with LNKs (Xie et al., 2014), we also examined the enrichment of total RNA Pol II in *rve4 rve6 rve8* triple mutant plants. Our results showed a decreased enrichment of RNA Pol II in *rve4 rve6 rve8* compared with the wild type (Supplemental Figures 5C and 5D), suggesting that RNA Pol II binding at the *TOC1* and *PRR5* loci is altered in the absence of functional RVEs or LNKs. Analyses of the two main CTD-phosphorylated isoforms characteristic of transcription initiation (S5P) and elongation (S2P) showed that the enrichment of both was clearly reduced in *PRR5* and *TOC1*, most strikingly at Zeitgeber Time 7 (ZT7) and ZT11 (ZT0 is defined as the time of lights on) (Figures 4E to 4H), which coincide with their peak of expression and the time of RVE8 interaction with LNKs (Xie et al., 2014; Pérez-García et al., 2015). While, in wild-type plants, the RNA Pol II phosphorylated profiles clearly oscillated closely following the rhythms of gene expression, the oscillation was abolished in *lnk1 lnk2* plants (Figures 4E to 4H). These results suggest that LNK1 and LNK2 might be important for the circadian accumulation of RNA Pol II S5P and S2P at the *PRR5* and *TOC1* loci.

Different chromatin marks correlate with the occupancy of the transcriptional machinery. As this occupancy is altered in *lnk1 lnk2* plants, we asked whether chromatin marks were also affected. To this end, we examined the accumulation of trimethylated lysine 4 of Histone 3 (H3K4me3), a mark generally associated with transcriptionally active genes (Shukla et al., 2009). H3K4me3 accumulation is also important for a precise circadian oscillation and proper amplitude of clock gene expression (Malapeira et al., 2012). Our ChIP data showed that H3K4me3 accumulation was clearly reduced in *lnk1 lnk2* plants, primarily at ZT7 and ZT11, while no appreciable differences were observed at ZT3 (Figures 4I and 4J). Altogether, our results suggest that alteration of chromatin status as well as transcriptional initiation and elongation correlate with the altered waveforms of circadian gene expression in *lnk1 lnk2* plants.

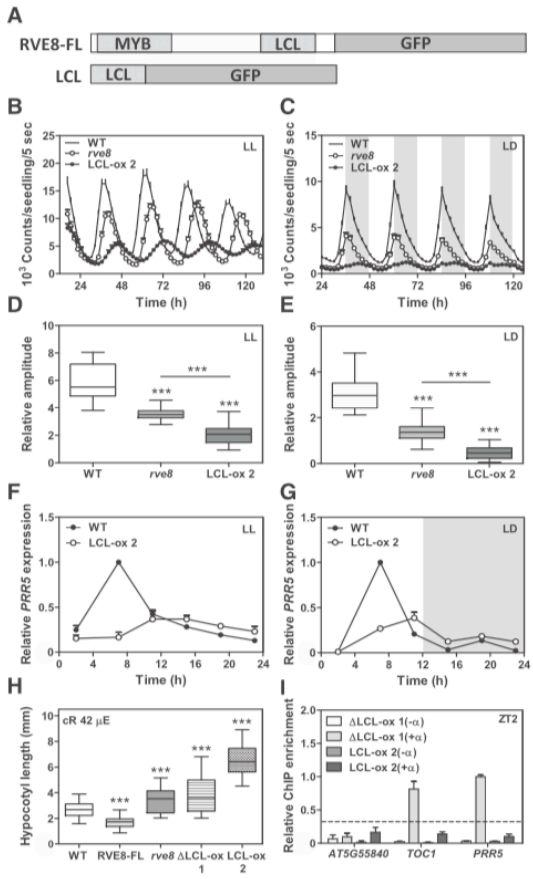

Figure 2. Alteration of Circadian Gene Expression and Hypocotyl Elongation in LCL-ox Plants.

(A) Schematic diagram depicting RVE8-FL fused to GFP and a truncated version consisting of the LCL domain.

(B) Analysis of rhythmic oscillations of *TOC1pro:LUC* by in vivo luminescence assays in the wild type, *rve8* mutant, and LCL-ox (line 2) grown under LL conditions following synchronization under LD cycles.

(C) Analysis of rhythmic oscillations of *TOC1pro:LUC* by in vivo luminescence assays in wild-type, *rve8* mutant, and LCL-ox plants under LD cycles.

(D) and **(E)** Amplitude estimates of circadian waveforms in wild-type, *rve8* mutant, and LCL-ox plants assayed as in **(B)** and **(C)**, respectively (***P < 0.001).

(F) and **(G)** Time-course analysis by RT-qPCR assays of *PRR5* expression in wild-type and LCL-ox plants grown under LL cycles **(F)** or under LD conditions **(G)**. Data are represented as means + SE of two biological replicates (samples from different starting material) relative to *IPP2* expression and the highest value.

(H) Hypocotyl length of the wild type, RVE8-FL-ox, *rve8*, ΔLCL-ox, and LCL-ox lines grown under constant red light (42 µmol·quanta·m^{-2}·s^{-1} [µE]). Data are means ± SE of two biological replicates (samples from different starting material) (***P < 0.001).

(I) ChIP analyses of ΔLCL-ox and LCL-ox plants assayed at ZT2 to examine the binding of ΔLCL and LCL, respectively, to the *TOC1* and *PRR5* promoters. The promoter of the *AT5G55840* gene (*PPR*) was used as a negative control. Samples processed without (−α) and with (+α) antibody during the ChIP procedure are shown. ChIP abundance is represented as means + SE of two biological replicates (samples from different starting material) and relative to the highest value.

White and gray areas in **(C)** and **(G)** represent light and dark periods, respectively.

LNKs Directly Interact with RNA Pol II and the FACT Complex

The severely reduced clock gene expression and reduced accumulation of RNA Pol II at the clock gene loci in *lnk1 lnk2* plants suggest a possible role for LNKs in recruiting the transcriptional machinery. To explore this possibility, we first checked the direct interaction of LNKs with RNA Pol II by in vitro pull-down studies using the CTD fused to GST and LNK1 fused to MBP. Our results showed efficient immunoprecipitation of GST-CTD (Supplemental Figure 6A) and reproducible MBP-LNK1 copurification with GST-CTD, whereas no interaction was observed with GST alone used as a negative control (Supplemental Figure 6B). The interaction was then assayed with protein extracts from LNK1-ox plants incubated with an anti-MYC antibody to immunoprecipitate LNK1. The immunoprecipitated protein complexes were then analyzed for total RNA Pol II. The antibody recognized phosphorylated and nonphosphorylated isoforms (Figure 5A, upper panel). Although we observed slightly higher accumulation of the nonphosphorylated protein (Figure 5A, upper panel), the phosphorylated isoforms were effectively immunoprecipitated with LNK1 (Figure 5B, upper panel). These results were confirmed in co-IP studies with specific antibodies recognizing CTD S5P and CTD S2P. Although a weak signal background was observed in wild-type plants and both antibodies had some cross-reactivity with nonphosphorylated isoforms, our results showed that S5P and S2P reproducibly coimmunoprecipitated with LNK1 (Figure 5B, middle and lower panels). Thus, LNK1 functions as a transcriptional coactivator that directly interacts with RNA Pol II. The interaction with S5P and S2P RNA Pol II isoforms also suggests that LNK1 might engage in the regulation of transcript initiation and elongation.

Our previous studies have shown that not only chromatin marks but also the binding of the histone chaperone complex FACT rhythmically oscillates at the *TOC1* promoter (Perales and Más, 2007). Furthermore, FACT forms part of a transcription elongation complex containing RNA Pol II (Antosz et al., 2017). To examine whether LNKs are also part of this complex, we performed in vitro pull-down studies of LNKs and SSRP1, a component of the FACT complex. Our results showed that both MBP-LNK1 (Figure 5C) and MBP-LNK3 (Figure 5D) coimmunoprecipitated with GST-SSRP1. To assay the interaction in vivo, protein extracts from plants overexpressing either LNK1 or LNK3 were immunoprecipitated with an anti-MYC antibody and analyzed with an anti-SSRP1 antibody (Duroux et al., 2004; Antosz et al., 2017). Although the amount of detected LNK1 protein was very low due to technical issues (Figure 5E), SSRP1 was still efficiently coimmunoprecipitated (Figure 5F). The use of LNK3-ox plants revealed that SSRP1 also interacted with LNK3 (Figures 5E and 5F). Altogether,

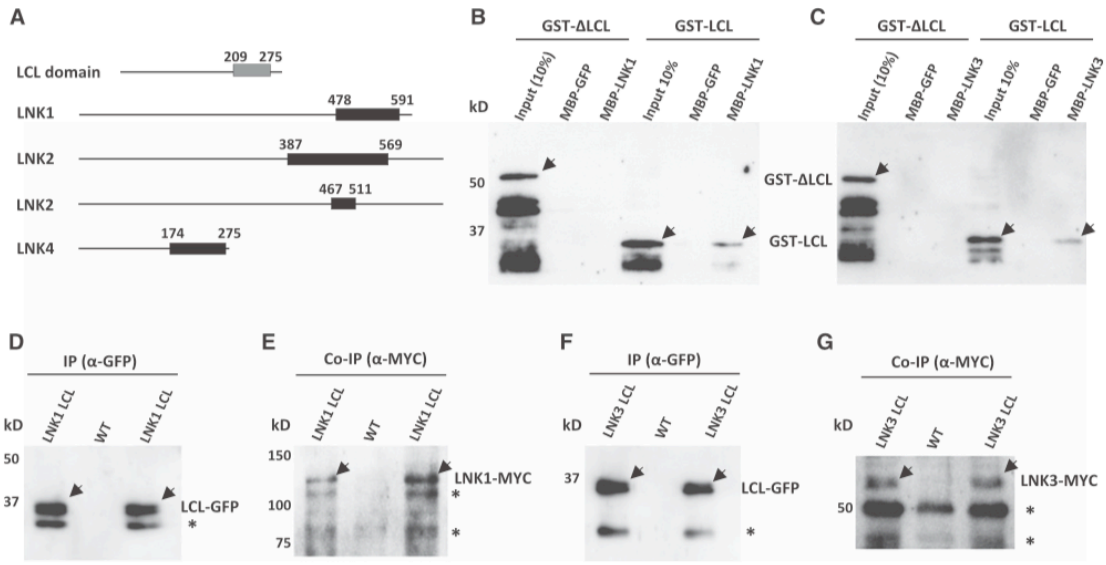

Figure 3. Direct Interaction of LNKs with the LCL Domain of RVE8.

(A) The coding sequence of the LCL domain (nucleotides 627 to 825, amino acids 209 to 275; gray box) was used as a bait in a yeast-two hybrid screen with a random-primed cDNA library from Arabidopsis. Selected interaction domains (black boxes) from LNKs were obtained by identifying the domains shared by all prey fragments matching the reference protein.

(B) and **(C)** In vitro pull-down assays of ΔLCL and LCL with LNK1 **(B)** and LNK3 **(C)**. Protein complexes were purified using amylose resin to detect GST fusion proteins (GST-ΔLCL and GST-LCL).

(D) to **(G)** Immunoblot analysis of two different double overexpressing LNK1-MYC-ox LCL-YFP-ox lines (**[D]** and **[E]**) and LNK3-MYC-ox LCL-YFP-ox (**[F]** and **[G]**). Protein extracts were immunoprecipitated (IP) with anti-GFP antibody (**[D]** and **[F]**) following detection with anti-MYC antibody (co-IP) (**[E]** and **[G]**). Wild-type protein extracts were similarly processed. Plants were grown under LD cycles for 10 d and processed at ZT7. Arrows indicate the specific detected proteins, while asterisks indicate unspecific or degraded protein products.

these results indicate that LNKs, RNA Pol II, and SSRP1 form part of the same protein complex.

If LNKs interact with RNA Pol II and the FACT complex, functional LNKs should localize to the *PRR5* and *TOC1* loci. Indeed, ChIP assays using LNK1-ox plants showed significant enrichment of LNK1 binding to *PRR5* and *TOC1* (Supplemental Figures 6C and 6D) compared with unrelated loci or with samples similarly processed but excluding incubation with the antibody (-α) (Supplemental Figures 6C and 6D). Although the size of sonicated chromatin required for efficient ChIP assays precludes obtaining a very precise spatial resolution, qPCR amplification at the 5′, middle, or 3′ region of *PRR5* and *TOC1* loci confirmed a significant enrichment at the 5′ ends of the genes, although above background amplification was also observed in the middle and 3′ ends of the genes (Supplemental Figures 6C and 6D). Notably, when the same distribution analyses were performed for RVE8, we found enrichment only at the 5′ end of the *PRR5* and *TOC1* genes (Supplemental Figures 6E and 6F). These results suggest that RVE8 recruits LNKs to the *PRR5* and *TOC1* promoters but that LNKs, together with RNA Pol II and the FACT complex, travel along the *PRR5* and *TOC1* loci. These results are also consistent with a role for LNKs in the regulation of *PRR5* and *TOC1* transcript initiation and elongation.

LNKs and the FACT Complex Co-Bind to *PRR5* and *TOC1* Loci and Regulate Their Circadian Transcription

Our results suggest that LNKs might aid in recruiting the transcriptional machinery to the target genes *PRR5* and *TOC1*. To investigate this hypothesis, we examined the occupancy of SSRP1 at the *PRR5* and *TOC1* loci via ChIP assays. In wild-type plants, SSRP1 was detected at *PRR5* and *TOC1*, whereas reduced accumulation was observed at the transcriptionally inactive retrotransposon TA3 (Figure 6A). In *lnk1 lnk2* plants, we found reduced SSRP1 occupancy close to background levels (Figure 6A), which suggests that LNKs might be important for proper SSRP1 association to the *PRR5* and *TOC1* loci. These results are consistent with the reduced S2P occupancy in *lnk1 lnk2* plants, which was specific for *PRR5* and *TOC1* loci but not for *ACT7* (*ACTIN7*) (Supplemental Figure 7A).

If LNKs form part of the same protein complex as FACT and RNA Pol II, then the lack of a functional FACT complex should affect RNA Pol II, which transits from the PIC to the initiation phase. This would lead to the failure of RNA Pol II to engage in the elongation phase, since an efficient passage through nucleosomal structures cannot be supported by a compromised FACT complex. Thus, we assayed the occupancy of RNA Pol II CTD-phosphorylated isoforms in *ssrp1* mutant plants. As SSRP1 is critical for viability

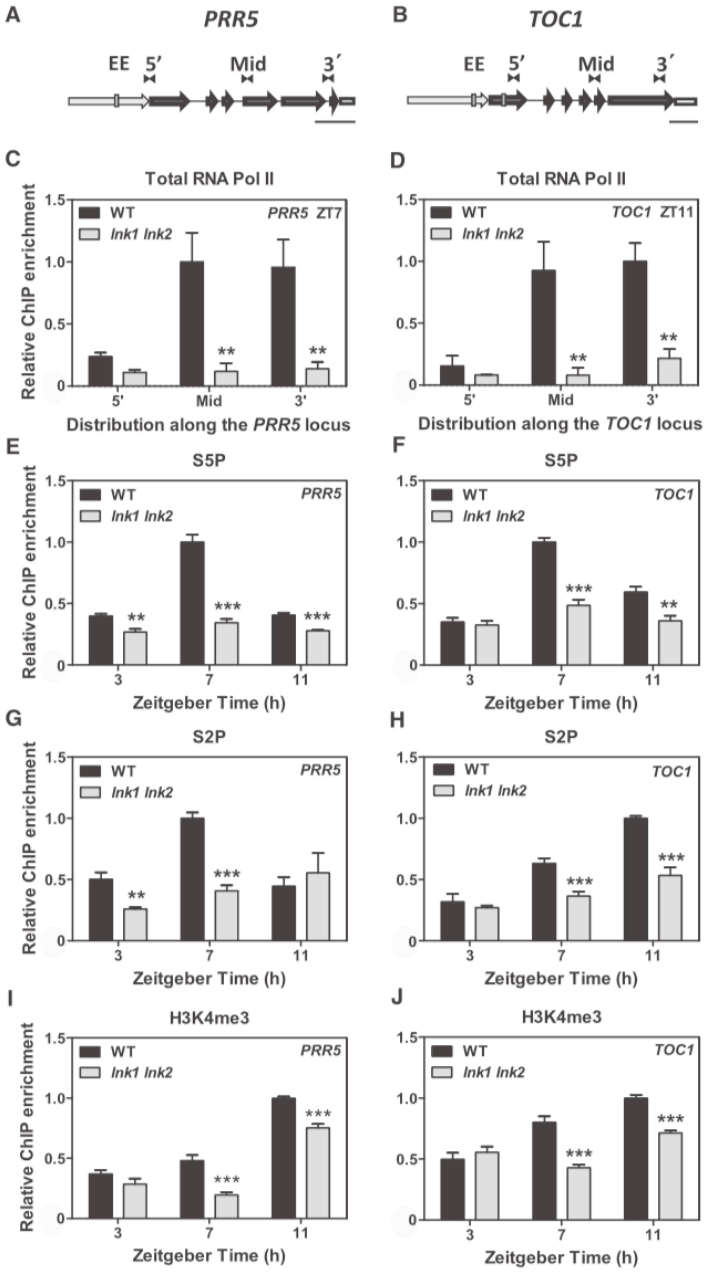

Figure 4. RNA Pol II and H3K4me3 Deposition at the *PRR5* and *TOC1* Loci Are Altered in *lnk1 lnk2* Double Mutant Plants.

(A) and **(B)** Diagrams depicting *PRR5* **(A)** and *TOC1* **(B)** loci. Double arrowheads indicate the primer positions for amplification of the 5′ end, middle (Mid), and 3′ end regions of each locus. Gray boxes represent evening element (EE) positions. Bars = 500 bp.

(Duroux et al., 2004), we used *ssrp1-2* mutant plants with a 50% reduction in *SSRP1* transcript accumulation (Lolas et al., 2010). We found that the accumulation of both phosphorylated isoforms was reduced at the *PRR5* and *TOC1* loci (Figures 6B and 6C; Supplemental Figures 7B and 7C). When we compared S2P occupancy in wild-type, *lnk1 lnk2*, and *ssrp1-2* plants, we found a similar marked reduction in S2P accumulation in *lnk1 lnk2* and *ssrp1-2* at *PRR5* and *TOC1* but not at *ACT7* (Supplemental Figure 7D). The reduction in RNA Pol II accumulation in *ssrp1-2* mutant plants was accompanied by a delayed rising phase and a marked decrease in *PRR5* expression at ZT7 (Figure 6D). Although *ssrp1-2* plants are only knockdown mutants, the circadian phenotypes of gene expression closely resembled those observed in ΔLCL-ox and LCL-ox (Figures 6E and 6F). Consistently, RNA Pol II S5P and S2P accumulation was also significantly reduced in ΔLCL-ox and LCL-ox plants (Supplemental Figures 7E and 7F). These results, together with the direct protein-protein interaction data, support the idea that LNKs and the FACT complex contribute together to the regulation of *PRR5* and *TOC1* circadian transcription.

To further support the functional relevance of LNKs and the FACT complex, we performed sequential ChIP assays to identify the possible co-binding of LNK1 and the FACT complex at the clock loci. Control analyses of double anti-MYC immunoprecipitation rounds in LNK1-ox plants revealed the enrichment of LNK1 at the *TOC1* promoter and verified the reliability of the double round of immunoprecipitation (Figure 6G). Immunoprecipitation with the anti-MYC antibody to pull down LNK1 followed by a second round of immunoprecipitation with the anti-SSRP1 antibody revealed that both proteins form part of the same complex, which binds to the middle and 3′ end regions of the *TOC1* locus (Figure 6H).

The interaction of LNKs with the elongating S2P CTD RNA Pol II and with SSRP1, together with its distribution along the target genes, suggests a role for LNKs in both transcript initiation and elongation. If that is the case, the pharmacological inhibition of transcript initiation and elongation should resemble the *lnk1 lnk2* phenotypes. To examine this possibility, we performed bioluminescence analyses with plants treated with kinase inhibitors such as flavopiridol (Flap) and seliciclib (Selic), which inhibit the CTD phosphorylation of S5 and S2, respectively (Ding et al., 2011). Our results showed a dose-dependent decreased amplitude and delayed phase of *TOC1pro:LUC* activity (Figures 7A to 7C; Supplemental Figures 8A to 8C), which indeed resembled the phenotypes of *lnk1 lnk2* plants. These results are consistent with the decreased binding of RNA Pol II (S5P and S2P) and SSRP1 to the *PRR5* and *TOC1* loci in plants treated with the inhibitors (Supplemental Figures 8G to 8I). We also reasoned that if the recruitment of the machinery responsible for clock transcript initiation and elongation is affected in *lnk1 lnk2* plants, then the effect of these inhibitors should be diminished in *lnk1 lnk2* compared with wild-type plants. Indeed, RT-qPCR analyses showed a delayed phase and evident reduction of *PRR5* and *TOC1* amplitude in inhibitor-treated wild-type plants (Figure 7D; Supplemental Figure 8D), while only a minor effect was observed in *lnk1 lnk2* plants (Figures 7E and 7F) and in the *rve4 rve6 rve8* triple mutant (Supplemental Figures 8E and 8F). Therefore, treatment of *lnk1 lnk2* plants with inhibitors had only a minor impact, as S5P and S2P accumulation is already affected in these plants. In agreement with our conclusions, the interaction of LNKs with SSRP1 was reduced following treatment with Selic, while SSRP1, LNK1, and LNK3 protein accumulation was not significantly affected by the treatment (Supplemental Figures 8J to 8M). Taken together, our results indicate that the function of LNKs is important for transcript initiation and the elongation of *PRR5* and *TOC1*.

The Rhythms of *PRR5* and *TOC1* Nascent RNAs Are Affected in *lnk1 lnk2* Plants

Our results suggest that LNKs affect *PRR5* and *TOC1* transcription, but their effects on gene expression were analyzed using steady-state mRNA. Therefore, we examined actual changes in transcript synthesis by analyzing nascent RNAs in wild-type and *lnk1 lnk2* plants. To this end, we isolated nuclei from plants sampled at ZT3, ZT7, and ZT11 and performed nuclear run-on transcription by bromouridine immunocapture, followed by the detection of labeled nascent transcripts by RT-qPCR. The primers used for nascent RNA detection (nr1, nr3, and nr5) spanned exon-intron boundaries (to exclude the amplification of possible mature spliced mRNA) along the 5′ end, gene body, and 3′ end of the genes (Supplemental Figure 9). In wild-type plants, *PRR5* and *TOC1* nascent RNAs exhibited a 5′ to 3′ gradient at each time point (Figures 7G to 7L). In addition, the peak accumulation of nascent RNAs correlated with the peak of steady-state mRNAs (i.e., ZT7 for *PRR5* and ZT11 for *TOC1*) (Figures 7G to 7L; Supplemental Figures 9C and 9D). The use of primers spanning two exons (ex-ex) rendered very low amplification, indicating the lack of mature mRNA contamination (Figures 7H and 7L). In *lnk1 lnk2* plants, nascent RNA accumulation was significantly low at all time points examined (Figures 7G to 7L; Supplemental Figures 9C and 9D). Reduced

Figure 4. (continued).

(C) and **(D)** ChIP-qPCR analyses of total RNA Pol II enrichment at the 5′ end, middle, and 3′ end regions of *PRR5* **(C)** and *TOC1* **(D)** in wild-type and *lnk1 lnk2* plants assayed at ZT7 and ZT11, respectively.

(E) and **(F)** ChIP-qPCR analyses of CTD S5P enrichment at the 5′ terminus in *PRR5* **(E)** and *TOC1* **(F)** in wild-type and *lnk1 lnk2* plants assayed at ZT3, ZT7, and ZT11.

(G) and **(H)** ChIP-qPCR analyses of CTD S2P enrichment at the middle regions in *PRR5* **(G)** and *TOC1* **(H)** in wild-type and *lnk1 lnk2* plants assayed at ZT3, ZT7, and ZT11.

(I) and **(J)** ChIP-qPCR enrichment of H3K4me3 in *PRR5* **(I)** and *TOC1* **(J)** in wild-type and *lnk1 lnk2* plants assayed at ZT3, ZT7, and ZT11 at the 5′ terminus. Data are represented as means + SE and relative to *ACTIN7* (*ACT7*) and the highest value. Graphs include data from two biological replicates (samples from different starting material). $^{**}P < 0.01$ and $^{***}P < 0.001$.

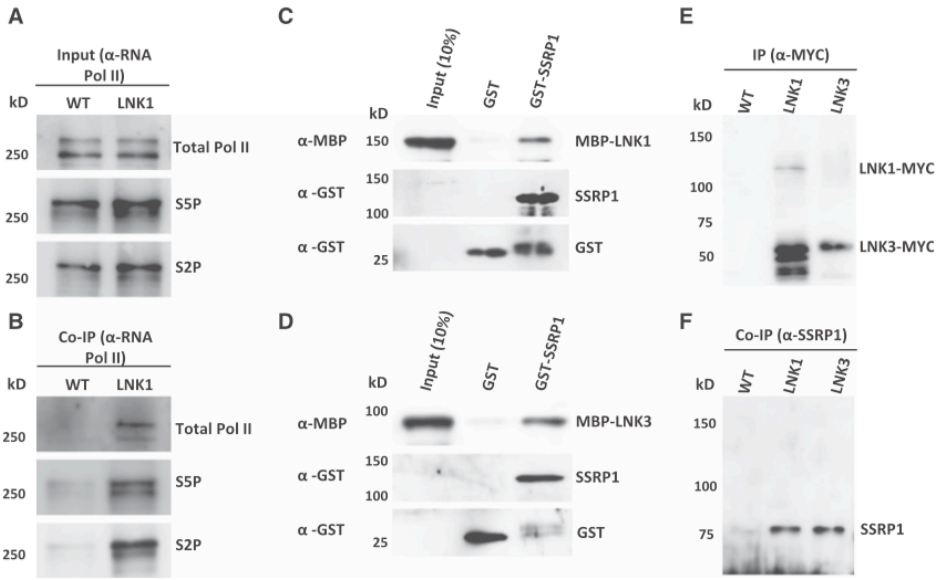

Figure 5. Direct Interaction of LNKs with the RNA Pol II and the Component of the FACT Complex SSRP1.

(A) and **(B)** Input of total RNA Pol II and the phosphorylated isoforms S5P and S2P **(A)** and co-IP with anti-MYC antibody following detection with anti-total RNA Pol II, S5P, and S2P antibodies **(B)** in wild-type and LNK1-ox plants.
(C) and **(D)** In vitro pull-down assays of SSRP1 with LNK1 **(C)** and LNK3 **(D)**. Protein complexes were purified using Glutathione Sepharose resin to detect MBP-fused proteins (MBP-LNK1 and MBP-LNK3).
(E) and **(F)** Co-IP assays by protein gel blot analysis of LNK1-MYC-ox and LNK3-MYC-ox.Plant protein extracts were immunoprecipitated with anti-MYC antibody following detection with anti-MYC antibody (IP) and anti-SSRP1 antibody (co-IP).
Plants were grown under LD cycles for 10 d and processed at ZT7.

nascent RNA accumulation in *lnk1 lnk2* plants was observed at the 5′ ends and at the gene bodies, suggesting that both transcript initiation and elongation were affected (changes in elongation would result in differences in the gene body but not at the 5′ terminus). The effect was specific to *PRR5* and *TOC1*, as nascent RNAs of a control gene such as *UBQ5* (UBIQUITIN5) showed similar accumulation patterns in wild-type and *lnk1 lnk2* plants (Figures 7H, 7I, 7K, and 7L). Together, these results indicate that, not only are the steady-state levels of *PRR5* and *TOC1* mRNA rhythmically expressed, but their nascent RNAs are as well. Our results also demonstrate that LNKs are important for the accumulation of these nascent RNAs.

Altogether, our results identify a multifunctional protein complex in which each component exerts specific functions in a timely manner that ultimately contribute to the temporal control of transcriptional synthesis of the clock genes *PRR5* and *TOC1* (Supplemental Figure 9E). The MYB domain of RVE8 provides DNA binding specificity, while its LCL domain is responsible for the interaction with LNKs. LNKs, in turn, recruit RNA Pol II and SSRP1 to facilitate the initiation and elongation of clock transcripts. The functions of all these components are essential, as mutation or inactivation of these activities affects nascent RNAs, delays the mRNA steady-state rising phase, and reduces the amplitude of the clock genes *PRR5* and *TOC1*.

DISCUSSION

Most transcription factors are modular, with DNA binding and effector domains that are responsible for the regulation of transcriptional activity (Du et al., 2009). Here, we functionally mapped the different RVE8 domains and found that the MYB domain is sufficient for DNA binding to target genes, while the LCL domain is responsible for the interaction with LNKs. The MYB family represents a large class of proteins that generally function as transcription factors (Dubos et al., 2010). Most of these proteins contain several imperfect repeats of a highly conserved MYB domain at their N termini. A particular subclass of MYB proteins has been separately grouped based on the presence of a single or partial MYB repeat. Based on structural properties, it is likely that the single MYB domain binds DNA in a different way from proteins containing several MYB repeats (Jin and Martin, 1999). Some members of the single MYB protein family have been characterized in several plant species and were shown to be involved in the regulation of secondary metabolism, cellular and organ morphogenesis, as well as circadian rhythms (Carré and Kim, 2002).

Unlike the highly conserved MYB domain at the N terminus, the C-terminal end is usually variable and is responsible for modulating the transcriptional activity of the protein. The LCL domain is

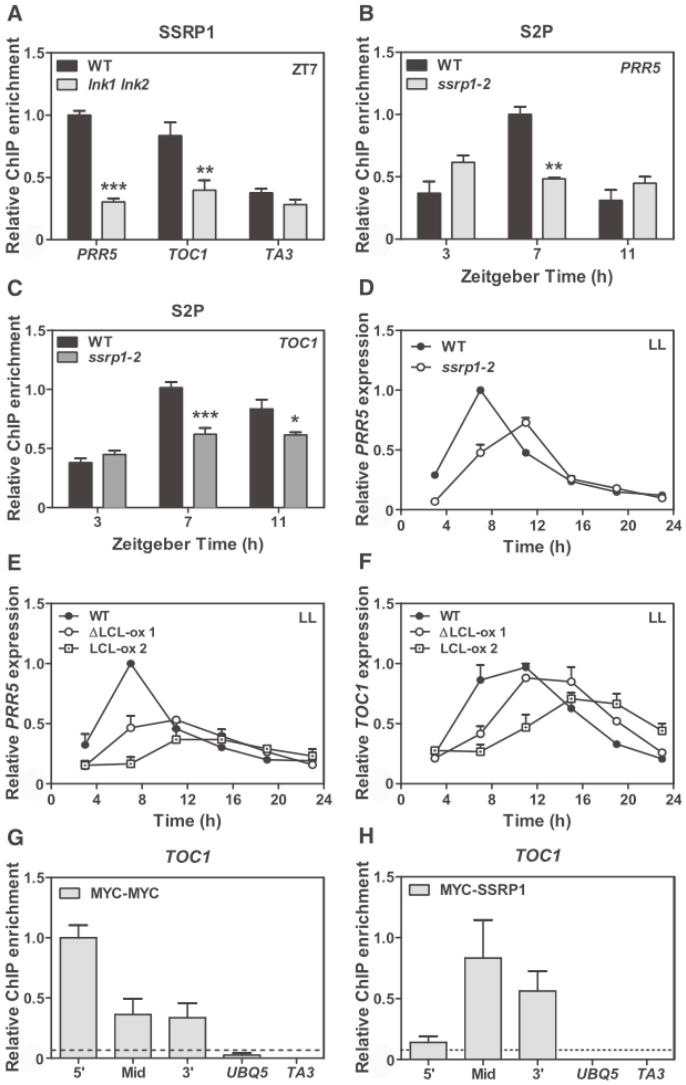

Figure 6. The Coordinated Function of SSRP1 and LNKs Is Important for RNA Pol II Recruitment and Circadian Gene Expression of Core Clock Genes.

(A) SSRP1 occupancy at the *PRR5*, *TOC1*, and *TA3* loci by ChIP assays in wild-type and *lnk1 lnk2* plants.
(B) and **(C)** Time-course analyses of CTD S2P profiles in *PRR5* **(B)** and *TOC1* **(C)** in the wild type and *ssrp1-2* at ZT3, ZT7, and ZT11.
(D) to **(F)** Time-course analysis by RT-qPCR of *PRR5* expression (**[D]** and **[E]**) and *TOC1* **(F)** in wild-type and *ssrp1-2* plants **(D)** and in wild-type, ΔLCL-ox, and LCL-ox plants (**[E]** and **[F]**) under LL conditions for 2 d after synchronization under LD. Data are represented as means + SE relative to *IPP2* expression and to the highest value.
(G) and **(H)** ChIP enrichment after a double round of immunoprecipitation with anti-MYC and anti-MYC antibodies **(G)** and with anti-MYC and anti-SSRP1 antibodies **(H)** to detect colocalization of LNK1 and SSRP1 at the *TOC1* gene body. ChIP enrichment is represented as means + SE relative to the input and to the highest value. *UBIQUITIN5* (*UBQ5*) and *TA3* were used as negative controls.
Data are represented as means + SE of two biological replicates (samples from different starting material). *P < 0.05, **P < 0.01, and ***P < 0.001.

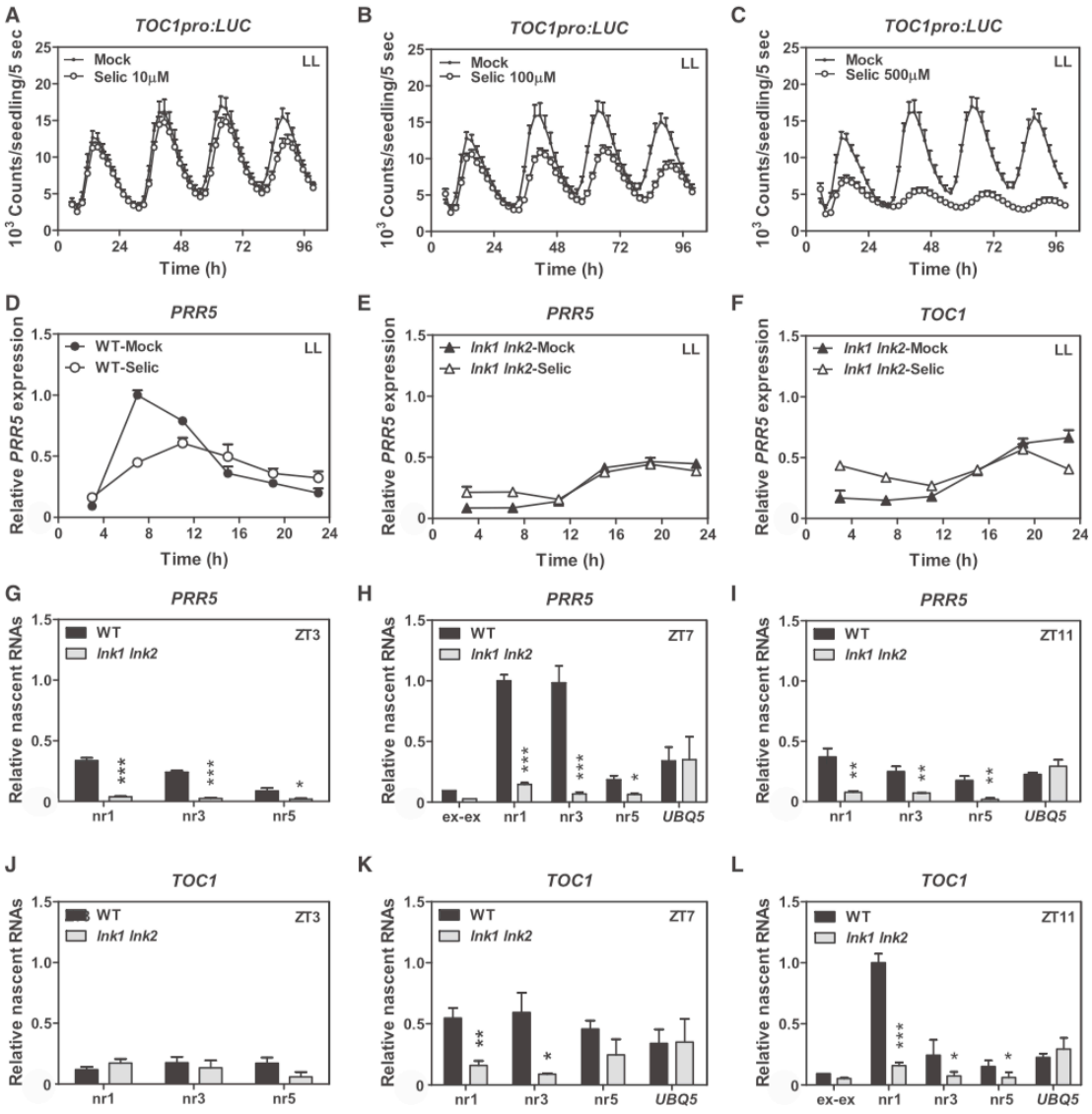

Figure 7. Role of LNKs in the Regulation of *PRR5* and *TOC1* Transcript Synthesis.

(A) to **(C)** Analysis of rhythmic oscillations of *TOC1pro:LUC* by in vivo luminescence assays in wild-type plants grown under LL conditions following synchronization under LD cycles treated with the indicated concentrations of seliciclib (Selic). Data are represented as means + SE of two biological replicates (samples from different starting material).

(D) to **(F)** Time-course analysis by RT-qPCR of *PRR5* (**[D]** and **[E]**) and *TOC1* **(F)** expression in wild-type **(D)** and *lnk1 lnk2* (**[E]** and **[F]**) plants in the absence or presence of Selic. Analyses were performed under LL conditions for 2 d after synchronization under LD. Data are represented as means + SE relative to *18S rRNA* expression and to the highest value.

(G) to **(L)** *PRR5* (**[G]** to **[I]**) and *TOC1* (**[J]** to **[L]**) nascent RNA accumulation at ZT3 (**[G]** and **[J]**), ZT7 (**[H]** and **[K]**), and ZT11 (**[I]** and **[L]**) using different sets of exon-intron primers along the loci (nr, nascent RNA primers). Nascent RNAs of *UBQ5* were also analyzed as a control (**[H]**, **[I]**, **[K]**, and **[L]**). Data are represented as means + SE relative to *ACT7* and to the highest value.

Graphs include data from two biological replicates (samples from different starting material). *P < 0.05, **P < 0.01, and ***P < 0.001.

exclusively found in the five members of the RVE/LCL subclass and is responsible for the interaction with LNKs. The binding and cooperative action of MYB proteins with other transcription factors are important for the control of numerous processes, including flavonoid biosynthesis, drought responses, epidermal differentiation, and patterning in root hairs and trichomes (Du et al., 2009). We found that the interaction of the RVE8 LCL domain with LNKs is central for controlling the circadian expression of core clock components such as *PRR5* and *TOC1*. Previous studies have already shown that RVEs and LNKs are cotranscriptional activators of circadian gene expression (Xie et al., 2014) but display an antagonistic function in the control of anthocyanin gene expression (Pérez-García et al., 2015).

Our understanding of the components and mechanisms of transcription in plants has been lagging behind that of animal systems. Global nuclear run-on sequencing and RNA sequencing have recently shown that, in plants, nascent transcripts correlate with steady-state transcript accumulation (Hetzel et al., 2016). This study also revealed the lack of divergent transcription or promoter-proximal pausing in plants, which are commonly found in other species (Preker et al., 2008; Jonkers and Lis, 2015). These results suggest that initiation is an important regulatory step in transcription in plants (Hetzel et al., 2016). Studies performed with a biochemically inactive variant of the SET-related protein ARABIDOPSIS HOMOLOG OF TRITHORAX1 (ATX1) revealed that promoter-proximal pausing can indeed be observed in plants (Ding et al., 2012). Further support of this notion was provided by another study showing cooperativity between SQUAMOSA PROMOTER BINDING PROTEIN-LIKE15 and SUPPRESSOR OF OVEREXPRESSION OF CONSTANS1 for the activation of *FRUITFULL* (Hyun et al., 2016).

Studies performed in *Drosophila melanogaster* (Rodriguez et al., 2013) and mouse (Menet et al., 2012) have shown that posttranscriptional regulation plays a crucial role in the regulation of circadian mRNA expression. Our results show that the expression of *PRR5* and *TOC1* nascent RNAs is rhythmic and follows the same oscillatory trend as steady-state mature mRNA. The rhythms were disrupted and the amount of nascent RNAs significantly reduced in *lnk1 lnk2* plants, which suggest that LNKs are important for proper rhythmic accumulation of *PRR5* and *TOC1* nascent RNAs. Our results show that LNKs bind to the 5′ regions of the *PRR5* and *TOC1* loci. LNKs interact with RNA Pol II S5P, and proper accumulation of RNA Pol II S5P also requires functional LNKs. Together with the repressed and delayed transcription of *PRR5* and *TOC1* in *lnk1 lnk2* plants, respectively, we conclude that LNKs are important for transcriptional initiation of *PRR5* and *TOC1*. LNKs aid in the recruitment of the transcriptional machinery to circadian targets. Target specificity is provided by the sequence-dependent binding of RVE8 to the *PRR5* and *TOC1* loci. The subsequent recruitment of RNA Pol II thus ensures proper circadian timing for the transcriptional machinery.

Our results also suggest that transcriptional elongation is modulated by RVE8 and LNKs. Two distinctive processes delineate transcriptional elongation: processivity (nucleotide additions per initiation event) and the elongation rate (nucleotide additions/min) (Mason and Struhl, 2005). Both a reduced and slow elongation rate of RNAP II might lead to premature dissociation along the chromatin template (Mason and Struhl, 2005). Our results show that LNKs interact with RNA Pol II S2P and with the elongation factor SSRP1 such that the observed reduced occupancy in the *lnk1 lnk2* double mutant might be due to their improper recruitment, leading to altered *PRR5* and *TOC1* gene expression. Thus, LNKs are important for both transcriptional initiation and elongation, a notion that is also supported by our nascent RNA results. The role of RVE8-LNKs in both transcriptional initiation and elongation might be useful for proper coordination between these two events, favoring transcription efficiency in concert with the production of chromatin marks at the appropriate circadian time. A tight coordination between transcriptional initiation and elongation was shown to be required for the precise regulation of *FLOWERING LOCUS C* expression (Wu et al., 2016), which is also controlled by FACT (Lolas et al., 2010). Our results point to the interesting possibility that LNKs might be important for ensuring a continuous flow from initiation to elongation, avoiding early termination. In the *lnk1 lnk2* double mutant, the initiation and transition to elongation are severely affected, and this explains the severity of the gene expression phenotypes.

Local chromatin organization influences transcription (Smolle and Workman, 2013). H3K4me3 is usually associated with transcriptionally active genes (Gardner et al., 2011). Our results show that H3K4me3 at the *PRR5* and *TOC1* loci is reduced in *lnk1 lnk2* double mutant plants. In yeast (*Saccharomyces cerevisiae*), RNA Pol II activity is required to recruit SET1/COMPASS (Ng et al., 2003), the catalytic subunit of the histone methyl transferase complex that methylates H3K4 (Briggs et al., 2001). In contrast, the sequential order is reversed in mammalian cells, as the presence of H3K4me3 appears to facilitate transcription initiation (Vermeulen et al., 2007). In plants, ATX1 forms a complex with TATA Binding Protein and RNA Pol II to control the formation of the PIC (Ding et al., 2011). Notably, the rhythmic accumulation of H3K4me3 at the promoters of core clock genes parallels the oscillation of clock gene expression. This chromatin signature has been shown to be important for blocking inhibitor binding to clock promoters, thus ensuring proper timing of repression (Malapeira et al., 2012). Our results showing that a chromatin mark is affected in *lnk1 lnk2* double mutant plants is also consistent with previous findings showing that another activating mark, H3 acetylation, is also affected in RVE8-ox and *rve8* mutant plants (Farinas and Mas, 2011). Therefore, the RVE8-LNKs interaction is central for the recruitment of the transcriptional machinery and enables a permissive chromatin environment, favoring clock gene activation and preventing advanced binding of clock repressors.

RNA Pol II transcription requires the coordination of different sets of proteins, including the basal transcription machinery and factors that bind to sequence-specific promoter elements. Here, we have demonstrated that LNKs relay the activating function of the transcription factor RVE8 to the transcriptional machinery. We propose that LNKs act as bridging proteins that function as an important scaffold for the regulation of circadian transcription of core clock genes expressed close to dusk.

METHODS

Plasmid Construction, Plant Material, and Growth Conditions

LNK1 and LNK3 plant overexpression vectors were generated by PCR-mediated amplification of the *LNK1* and *LNK3* coding sequences followed by cloning into the pENTR/D-TOPO vector (Invitrogen). The *LNK1* and *LNK3* coding sequences were subsequently cloned into the plant destination vector pGWB417/517 (Nakagawa et al., 2007a, 2007b) following the manufacturer's recommendations (Invitrogen). RVE8 and domain vectors were generated by cloning RVE8-FL, ΔLCL (nucleotides 1 to 624), and the LCL domain (nucleotides 625 to 885) first into the pENTR/D-TOPO vector and then into the plant destination vector pGWB505 (Nakagawa et al., 2007a, 2007b).

Bacterial expression vectors were generated by cloning the coding sequences of *LNK1*, *SSRP1*, *RNA PolII CTD*, *RVE8-FL*, *ΔLCL*, and *LCL* into the pENTR/D-TOPO vector. Each coding sequence was subsequently cloned into pDEST565 or pDEST_HIS_MBP (Nallamsetty et al., 2005) vectors using the LR reaction (Invitrogen). For MBP-LNK3, the coding sequence of *LNK3* was amplified by PCR and cloned into the pET_HIS_MBP vector (Bogomolovas et al., 2009) after digestion with *Nco*I and *Xho*I restriction enzymes (Roche) and ligation with T4 DNA ligase (Roche).

Arabidopsis thaliana plants were transformed using *Agrobacterium tumefaciens* (GV2260)-mediated DNA transfer (Clough and Bent, 1998). Seedlings were stratified at 4°C in the dark for 3 d on Murashige and Skoog (MS) agar medium supplemented with 3% sucrose. Plates were transferred to LD (12 h of light/12 h of dark) with 60 to 100 $\mu mol \cdot quanta \cdot m^{-2} \cdot s^{-1}$ cool white fluorescent light at 22°C. The *TOC1pro:LUC* (Perales and Más, 2007), *RVE8-FL-ox* (Farinas and Mas, 2011), *rve8* (SALK_016333C) (Farinas and Mas, 2011), *lnk1 lnk2* (SALK_024353, GK_484F07) (Rugnone et al., 2013), *rve4 rve6 rve8* (Hsu et al., 2013), and *ssrp1-2* (SALK_001283) (Lolas et al., 2010) lines were described elsewhere. Full-length RVE8-ox, ΔLCL-ox, and LCL-ox were transformed into the wild-type background as well as the *rve8* mutant background.

Protein Sequence Alignment and Phylogenetic Analyses

Multiple sequence alignment of the amino acid sequence of the LCL domain was performed using protein sequences from the EnsemblPlants database (http://plants.ensembl.org/index.html). The sequences were subjected to BLAST analysis against the LCL domain of Arabidopsis RVE8. Protein homologs with the closest sequence identity were aligned with ClustalW using the Bioedit program (Bioedit 7.2.5).

Phylogenetic analysis was performed using the maximum likelihood method based on a JTT matrix-based model (Jones et al., 1992). The tree with the highest log likelihood (−923.86) was selected. The initial tree for the heuristic search was obtained by applying Neighbor-Join and BioNJ algorithms to a matrix of pairwise distances estimated using the JTT model and then selecting the topology with superior log likelihood value. The number of bootstrap replicates was 1000. The tree was drawn to scale, with branch lengths measured in the number of substitutions per site (next to the branches). The analysis involved 45 amino acid sequences. All positions containing gaps and missing data were eliminated. There were 56 positions in the final data set. Evolutionary analyses were conducted in MEGA7 (Kumar et al., 2016).

Analyses of Hypocotyl Growth, Flowering Time, and Confocal Imaging

Seeds were stratified on plates with MS agar medium without sucrose for 4 d in the dark at 4°C. Seeds were then exposed to white light (80 $\mu mol \cdot quanta \cdot m^{-2} \cdot s^{-1}$) for 4 h and kept in the dark for 20 h following exposure to constant red light (42 $\mu mol \cdot quanta \cdot m^{-2} \cdot s^{-1}$) for 7 d. Approximately 20 to 25 seedlings were used for hypocotyl length measurements using ImageJ software (National Center for Biotechnology Information [NCBI]). For flowering time assays, seeds were synchronized for 4 d at 4°C and placed on soil. Plants were grown under long-day conditions (16 h of light/8 h of dark) with a light intensity of 80 to 100 $\mu mol \cdot quanta \cdot m^{-2} \cdot s^{-1}$ in walk-in chambers (INKOA). Bolting time and the number of rosette leaves of 10 to 15 plants were counted when the inflorescence stems reached 1 cm high. Two-tailed *t* tests were performed for statistical analyses (*$P < 0.05$, **$P < 0.01$, and ***$P < 0.001$). Two biological replicates were performed with plants grown at different times. Confocal analyses were performed with plants grown on MS agar medium supplemented with 3% sucrose under long-day cycles. Fluorescence signals from hypocotyl and root cells were imaged using an Olympus Fluoview FV1000 confocal microscope with a 515-nm argon laser (excitation, 488 nm; emission, 510 nm).

In Vivo Luminescence Assays

Seven-day-old plants synchronized under LD cycles (12 h of light/12 h of dark) at 22°C were transferred to 96-well plates and resynchronized for an additional 24 h under LD cycles before switching to LL conditions. In vivo luminescence assays were performed as described previously (Takahashi et al., 2015) with an LB960 luminometer (Berthold Technologies) using Microwin software (Mikrotek Laborsysteme). Periods, phases, and amplitudes were estimated using the Fast Fourier Transform-Non-Linear Least Squares suite using the BioDare online tool (www.biodare.ed.ac.uk) (Zielinski et al., 2014). Two-tailed *t* tests were performed for statistical analyses (*$P < 0.05$, **$P < 0.01$, and ***$P < 0.001$). For inhibitor analyses, different concentrations of Flap (1, 5, and 10 μM) and Selic (10, 100, and 500 μM) were vacuum-infiltrated for 5 to 8 min into 7-d-old seedlings before luminescence analyses. Two biological replicates were performed with seedlings grown at different times. Each biological replicate included 8 to 12 seedlings per condition and/or genotype.

Gene Expression Analyses by RT-qPCR

Seedlings were synchronized under LD cycles for 7 d and subsequently transferred to LL for 2 d. Samples were taken every 4 h over the third day under LL. RNA was purified using a Maxwell 16 LEV simplyRNA tissue kit following the manufacturer's recommendations (Promega). Purified RNA was treated with RNase-free Turbo DNase (Ambion), and single-stranded cDNA was synthesized using iScript Reverse Transcription Supermix for RT-qPCR (Bio-Rad) with 1 μg of RNA. qPCR was performed with iTag Universal SYBR Green Supermix (Bio-Rad) or Brilliant III Ultra-Fast SYBR Green qPCR Master Mix (Agilent) with a 96-well CFX96 Touch Real-Time PCR detection system (Bio-Rad). The expression data were normalized to *IPP2* (*ISOPENTENYL PYROPHOSPHATE: DIMETHYL-ALLYL PYROPHSPHATE ISOMERASE*) using the $2^{-\Delta\Delta CT}$ method (Livak and Schmittgen, 2001). For inhibitor analyses, Selic (500 μM) was vacuum-infiltrated for 5 to 8 min into 7-d-old seedlings, and samples were harvested the following day at different circadian times, as indicated. The expression data were normalized to *18S rRNA* using the $2^{-\Delta\Delta CT}$ method (Livak and Schmittgen, 2001). Two biological replicates were performed with seedlings grown and sampled at different times. Two to three technical replicates were performed within the same biological replicate. Primers used in this study are listed in Supplemental Table 1.

Yeast-Two Hybrid Screening

The coding sequence of the LCL domain (nucleotides 625 to 825) was PCR amplified and fused to the C-terminal end of LexA in the pB27 vector. The construct was used as a bait to screen a random-primed cDNA library of

Arabidopsis constructed into the pP6 vector (Hybrigenics Services). Using a mating approach with YHGX13 and L40ΔGal4 strains, ~64 million clones were screened and around 322 His+ colonies were selected on a medium lacking histidine, tryptophan, and leucine. The prey fragments of these positive clones were sequenced and used to search the GenBank database (NCBI) to identify potential interacting proteins with the LCL domain.

Protein Expression, Purification, and in Vitro Pull-Down

Transformed *Escherichia coli* cells (BL21, DE3) were grown until the OD_{600} values reached 0.6 to 0.8. Isopropyl β-D-1-thiogalactopyranoside-mediated induction of MBP-LNK3, GST-CTD, and GST-SSRP1 was performed at 28°C for 4 to 6 h. MBP-LNK1, GST-ΔLCL, and GST-LCL were induced at 17°C overnight. Bacteria were lysed by sonication for 2 to 3 min (30 s on, 30 s off, high intensity) using a sonicator (Bioruptor, Diagnode). Recombinant proteins were purified using gravity flow columns with amylose resin for MBP fusion proteins (New England Biolabs) and Glutathione Sepharose 4B for GST-tagged proteins (GE Healthcare). The purified recombinant proteins were concentrated using Amicon centrifugal filters (EMD Millipore).

For in vitro pull-down assays between ΔLCL, LCL, and LNKs, proteins were incubated in pull-down binding buffer (1× PBS, pH 7.4, 0.2% glycerol, 0.6% Triton X-100, and 1 mM β-mercaptoethanol) for 2 h at 4°C with end-over-end rotation. Amylose resin was then added and incubated for another 2 h at 4°C with end-over-end rotation. Beads were washed four to six times with pull-down washing buffer (1× PBS, pH 7.4, 0.6% Triton X-100, and 1 mM β-mercaptoethanol), and protein complexes were released by heating at 95°C for 5 min in 2× SDS loading buffer (100 mM Tris-HCl, pH 6.8, 4% SDS, 0.2% bromophenol blue, 20% glycerol, and 5% β-mercaptoethanol). Protein samples were analyzed by immunoblotting using an anti-MBP antibody (reference sc-809, Santa Cruz Biotechnology) (1:1000 dilution) or a monoclonal anti-GST antibody (reference 8-326; Thermo Fisher Scientific) (1:1000 dilution).

To test the interaction between LNKs and RNA Pol II CTD or SSRP1, proteins were processed as described above with minor modifications. Briefly, proteins were incubated in pull-down binding buffer (20 mM Tris-HCl, pH 7.9, 20% glycerol, 1 mM EDTA, 5 mM $MgCl_2$, 0.1% Nonidet P-40, 1 mM DTT, 0.2 mM PMSF, and 0.1 M NaCl) for 2 h at 4°C with end-over-end rotation. Glutathione Sepharose 4B was then added and incubated for another 2 h at 4°C with end-over-end rotation. Beads were washed four times with pull-down washing buffer (20 mM Tris-HCl, pH 7.9, 20% glycerol, 1 mM EDTA, 5 mM $MgCl_2$, 0.1% Nonidet P-40, 1 mM DTT, 0.2 mM PMSF, and 0.1 M NaCl), and protein complexes were released by heating at 95°C for 5 min in 2× SDS loading buffer (100 mM Tris-HCl, pH 6.8, 4% SDS, 0.2% bromophenol blue, 20% glycerol, and 5% β-mercaptoethanol). Protein samples were analyzed by immunoblotting with an anti-MBP antibody (reference sc-809, Santa Cruz Biotechnology) (1:1000 dilution) or with a monoclonal anti-GST antibody (reference 8-326, Thermo Fisher Scientific) (1:1000 dilution). Two biological replicates were performed per experiment and/or condition.

In Vivo Co-IP Assays in Plants

Analyses of LNKs and LCL interactions were performed with 10-d-old seedlings grown under LD cycles. At least two biological replicates with seedlings grown and sampled at different times were performed. Around 1 g of seedlings was ground in liquid nitrogen and resuspended in 1 mL of co-IP binding buffer (50 mM Tris-HCl, pH 7.5, 150 mM NaCl, 0.4% Nonidet P-40, 1 mM EDTA, 2 mM DTT, 5% glycerol, 1 mM PMSF, 5 μg/mL leupeptin, 1 μg/mL aprotinin, 5 μg/mL antipain, 1 μg/mL pepstatin, 5 μg/mL chymostatin, and 50 μM MG-132). Protein concentration was measured using standard curves with the Bradford method (Bradford, 1976). Supernatants containing equal amounts of total protein were incubated with 25 μL of GFP-trap magnetic beads (Chromotek) for 1 to 2 h at 4°C with end-over-end rotation. Beads were washed with co-IP washing buffer (50 mM Tris-HCl, pH 7.5, 150 mM NaCl, 1 mM EDTA, 2 mM DTT, 1 mM PMSF, 5 μg/mL leupeptin, 1 μg/mL aprotinin, 5 μg/mL antipain, 1 μg/mL pepstatin, 5 μg/mL chymostatin, and 50 μM MG-132). The protein complexes were released from the beads with 50 μL of 2× SDS loading buffer (100 mM Tris-HCl, pH 6.8, 4% SDS, 0.2% bromophenol blue, 20% glycerol, and 5% β-mercaptoethanol) and heating at 95°C for 5 min. The co-IP samples were then analyzed by immunoblot analyses using an anti-GFP antibody (reference A11122, Invitrogen) (1:2500 dilution) and an anti-Myc antibody (reference M4439, Sigma-Aldrich) (1:2500 dilution).

Analyses of the interaction of LNKs with RNA Pol II or SSRP1 were performed following the same protocol described above with slight modifications. Briefly, samples were resuspended in 1 mL of co-IP binding buffer (50 mM Tris-HCl, pH 7.5, 150 mM NaCl, 0.4% Nonidet P-40, 5 mM $MgSO_4$, 2 mM $CaCl_2$, 2 mM DTT, 5% glycerol, 1 mM PMSF, 30 μg/mL leupeptin, 30 μg/mL aprotinin, 30 μg/mL E-64, 7.5 μg/mL antipain, 3 μg/mL pepstatin, 7.5 μg/mL chymostatin, and 50 μM MG-132). Protein concentration was measured using standard curves with the Bradford method (Bradford, 1976). Supernatants containing equal amounts of total protein were treated with DNase I (Promega) or Benzonase (Novagen). Samples were then incubated with 25 μL of Myc-trap agarose beads (Chromotek) for 1 to 2 h at 4°C with end-over-end rotation. Beads were washed with co-IP binding buffer (50 mM Tris-HCl, pH 7.5, 150 mM NaCl, 0.4% Nonidet P-40, 5 mM $MgSO_4$, 2 mM $CaCl_2$, 2 mM DTT, 5% glycerol, 1 mM PMSF, 30 μg/mL leupeptin, 30 μg/mL aprotinin, 30 μg/mL E-64, 7.5 μg/mL antipain, 3 μg/mL pepstatin, 7.5 μg/mL chymostatin, and 50 μM MG-132). Protein complexes were released from the beads using 50 μL of 2× SDS loading buffer (100 mM Tris-HCl, pH 6.8, 4% SDS, 0.2% bromophenol blue, 20% glycerol, and 5% β-mercaptoethanol) and heating at 95°C for 5 min. The co-IP samples were analyzed by immunoblot analysis using a monoclonal anti-Myc antibody (reference M4439, Sigma-Aldrich) (1:2500 dilution), an anti-RNA Pol II CTD repeat YSPTSPS (phospho S2) antibody (reference ab5095, Abcam) (1:1000 dilution), an anti-RNA Pol II CTD repeat YSPTSPS (phospho S5) antibody (reference ab5131, Abcam) (1:1000 dilution), an anti-RNA Pol II antibody (reference at-300, Santa Cruz Biotechnology) (1:1000 dilution), and an anti-SSRP1 antibody (1:1000 dilution) (Duroux et al., 2004). For inhibitor analyses, Selic (300 μM) was vacuum-infiltrated for 8 min into 10-d-old seedlings at ZT3, and samples were harvested at ZT7 the following day. For Ponceau S staining, the membrane was incubated with Ponceau S solution (0.1% Ponceau S and 1% acetic acid) for 5 min with shaking and washed twice by water before imaging.

ChIP and Sequential ChIP Assays

Plants were grown under LD cycles for 10 to 14 d, and samples were collected under LD conditions or the third day under LL at the indicated time points. At least two biological replicates with seedlings grown and sampled at different times were performed. ChIP assays were essentially performed as described previously (Perales and Más, 2007) with some modifications. Briefly, 1 to 2 g of seedlings was fixed in fixation buffer (10 mM Tris-HCl, pH 8.0, 0.4 M sucrose, 1 mM EDTA, 1 mM PMSF, 0.25% Triton X-100, and 1% formaldehyde) for 10 to 15 min under a vacuum. The fixation was stopped by adding glycine to a final concentration of 0.125 M and vacuum for 10 min. Seedlings were washed twice with 50 mL of cold water, frozen in liquid nitrogen, and stored at −80°C. Samples were ground in liquid nitrogen to a fine powder and resuspended in extraction buffer I (10 mM Tris-HCl, pH 8.0, 0.4 M sucrose, 5 mM EDTA, 5 mM β-mercaptoethanol, 1 mM PMSF, 5 μg/mL leupeptin, 1 μg/mL aprotinin, 1 μg/mL E-64, 5 μg/mL antipain, 1 μg/mL pepstatin, 5 μg/mL chymostatin, and 50 μM MG-132). Following filtration with Miracloth (EMD Millipore), the cells were centrifuged at 1000*g* for 20 min and washed with extraction buffer II (10 mM Tris-HCl, pH 8.0, 0.25 M sucrose, 10 mM $MgCl_2$, 1% Triton X-100, 5 mM EDTA, 5 mM

β-mercaptoethanol, 1 mM PMSF, 5 μg/mL leupeptin, 1 μg/mL aprotinin, 1 μg/mL E-64, 5 μg/mL antipain, 1 μg/mL pepstatin, 5 μg/mL chymostatin, and 50 μM MG-132) to purify nuclei. The nuclei were then resuspended in 1 mL of nuclei lysis buffer (10 mM Tris-HCl, pH 8.0, 10 mM EDTA, 1% SDS, 1 mM PMSF, 5 μg/mL leupeptin, 1 μg/mL aprotinin, 1 μg/mL E-64, 5 μg/mL antipain, 1 μg/mL pepstatin, 5 μg/mL chymostatin, and 50 μM MG-132) and sonicated 4 min (30 s on, 30 s off, low intensity) with a sonicator (Bioruptor, Diagnode). Nuclear debris was removed by centrifugation at maximum speed. Approximately 20 to 25 μg of chromatin was then diluted with 1 mL of ChIP dilution buffer (15 mM Tris-HCl, pH 8.0, 167 mM NaCl, 1 mM EDTA, 1.1% Triton X-100, 1 mM PMSF, 5 μg/mL leupeptin, 1 μg/mL aprotinin, 5 μg/mL antipain, 1 μg/mL pepstatin, 5 μg/mL chymostatin, and 50 μM MG-132) and incubated with the corresponding antibody overnight at 4°C. Protein-DNA complexes were collected by incubation with 50 μL of equilibrated Protein G beads (Dynabeads, Invitrogen) for 2 to 3 h. The beads were sequentially washed with low-salt buffer (20 mM Tris-HCl, pH 8.0, 150 mM NaCl, 1% Triton X-100, 2 mM EDTA, 0.1% SDS, 1 mM PMSF, 5 μg/mL leupeptin, 1 μg/mL aprotinin, 1 μg/mL E-64, 5 μg/mL antipain, 1 μg/mL pepstatin, 5 μg/mL chymostatin, and 50 μM MG-132), high-salt buffer (20 mM Tris-HCl, pH 8.0, 500 mM NaCl, 1% Triton X-100, 2 mM EDTA, 0.1% SDS, 1 mM PMSF, 5 μg/mL leupeptin, 1 μg/mL aprotinin, 1 μg/mL E-64, 5 μg/mL antipain, 1 μg/mL pepstatin, 5 μg/mL chymostatin, and 50 μM MG-132), LiCl buffer (10 mM Tris-HCl, pH 8.0, 1 mM EDTA, 250 mM LiCl, 1% Nonidet P-40, 1% sodium deoxycholate, 1 mM PMSF, 5 μg/mL leupeptin, 1 μg/mL aprotinin, 1 μg/mL E-64, 5 μg/mL antipain, 1 μg/mL pepstatin, 5 μg/mL chymostatin, and 50 μM MG-132), and TE buffer (10 mM Tris-HCl, pH 8.0, and 1 mM EDTA). Protein-DNA complexes were released by incubation with 300 μL of ChIP elution buffer for 1 h at 65°C. Reverse cross-linking was performed by adding 0.2 M NaCl and incubating at 65°C overnight. DNA was purified using a Gel Extraction Kit (Qiagen) following the manufacturer's recommendation. qPCR was performed with iTag Universal SYBR Green Supermix (Bio-Rad) or Brilliant III Ultra-Fast SYBR Green qPCR Master Mix (Agilent) using a 96-well CFX96 Touch Real-Time PCR detection system (Bio-Rad). For inhibitor analyses, Flap (10 μM) or Selic (300 μM) was vacuum-infiltrated for 8 min into 12-d-old seedlings at ZT3, and samples were harvested at ZT7 the following day. To take into account differences in the immunoprecipitation efficiency in the different samples, *ACT7* was used as a positive control in ChIP assays of the basal transcriptional machinery. For ChIP analyses with LNKs or RVE8 domains, it is obviously not possible to use *ACT7* as a positive control. A two-tailed *t* test was performed for statistical analysis (*$P < 0.05$, **$P < 0.01$, and ***$P < 0.001$).

Sequential ChIP assays (Xie and Grotewold, 2008) were performed following the same ChIP procedure described above but including 2× washes with low-salt buffer (20 mM Tris-HCl, pH 8.0, 150 mM NaCl, 1% Triton X-100, 0.1% SDS, 2 mM EDTA, 1 mM PMSF, 5 μg/mL leupeptin, 1 μg/mL aprotinin, 1 μg/mL E-64, 5 μg/mL antipain, 1 μg/mL pepstatin, 5 μg/mL chymostatin, and 50 μM MG-132) and 2× washes with TE buffer (10 mM Tris-HCl, pH 8.0, and 1 mM EDTA) after the first round of immunoprecipitation with the anti-MYC antibody (reference M4439, Sigma-Aldrich) (1:500 dilution). Complexes were eluted with 15 mM DTT and incubated at 37°C for 30 min. Chromatin was then diluted in Sequential ChIP buffer (15 mM Tris-HCl, pH 8.0, 150 mM NaCl, 1 mM EDTA, 1 mM PMSF, 5 μg/mL leupeptin, 1 μg/mL aprotinin, 5 μg/mL antipain, 1 μg/mL pepstatin, 5 μg/mL chymostatin, and 50 μm MG132) and concentrated using Amicon centrifugal filters (EMD Millipore). Samples were then incubated overnight at 4°C either with an anti-Myc antibody (reference M4439, Sigma-Aldrich) (1:500 dilution) or with an anti-SSRP1 antibody (Duroux et al., 2004) (1:200 dilution). Complexes were washed, eluted, purified, and amplified as described above.

Nascent RNAs

Nascent RNA analyses were performed as described previously (Hetzel et al., 2016) with minor modifications. Briefly, seedlings were grown in MS medium supplemented with 3% sucrose for 5 d under LD cycles at 22°C. Plates were then moved to LL conditions, and ~20-g samples were collected at the indicated time points on the third day under LL. At least two biological replicates with seedlings grown and sampled at different times were performed. Samples were homogenized with an Ultra Turrax T-25 homogenizer in 100 mL of ice-cold grinding buffer (300 mM sucrose, 20 mM Tris, pH 8.0, 5 mM $MgCl_2$, 5 mM KCl, 0.2% [v/v] Triton X-100, 5 mM β-mercaptoethanol, and 35% [v/v] glycerol) at 4°C. Samples were then filtered through Miracloth (EMD Millipore) before being passed through a 60-μm cell strainer into 50-mL Falcon tubes. Tubes were centrifuged at 5000*g* for 10 min at 4°C. Pellets were then washed twice by homogenization with 30 mL of cold grinding buffer using a microstreaker. Pellets were resuspended in 2 mL of freezing buffer (50 mM Tris, pH 8.0, 5 mM $MgCl_2$, 20% [v/v] glycerol, and 5 mM β-mercaptoethanol), and nuclei were counted under a light microscope using a Neubauer chamber. Nuclei were then divided into aliquots in 1.5-mL tubes and frozen in liquid N_2. Nuclear run-on of ~5 to 6 × 10^6 nuclei was performed by adding 200 μL of 3× nuclear run-on reaction buffer (15 mM Tris-HCl, pH 8.0, 450 mM KCl, 7.5 mM $MgCl_2$, 1.5% [v/v] 20% sarkosyl, 1.5 mM DTT, 0.2 units/μL SUPERase-in [Fisher Scientific], 375 μM ATP, 375 μM GTP, 60 nM CTP, and 375 μM BrUTP [Sigma-Aldrich]). After 5 min of incubation at room temperature, run-on was stopped by adding 140 μL of DNase Mix (15 μL of 10× RQ1 DNase I buffer, 50 μL of nuclease-free deionized water, and 5 μL of RQ1 DNase [Promega]) for 15 min at room temperature, followed by the addition of 160 μL of STOP Mix (20 mM EDTA, 200 mM NaCl, 1% [v/v] SDS, and 0.3 mg/mL glycogen) plus 20 μL of 2.5 mg/mL proteinase K and incubation for 30 min at 37°C. Nuclei were centrifuged for 10 min at 1000*g* at 4°C, and RNA was extracted using a TRIzol-based protocol in which 250 μL of high-salt buffer (0.8 M sodium citrate [$NaH_2(C_3H_5O(COO)_3)$] and 1.2 M NaCl) and 1 μL of RNase-free glycogen were added for isopropanol precipitation. Prior to BrUTP precipitation, BrdU antibody beads (sc-32323 AC; Santa Cruz Biotechnology) were washed twice with ice-cold GRO binding buffer (0.25× saline-sodium-phosphate-EDTA buffer, 0.05% [v/v] Tween, 37.5 mM NaCl, and 1 mM EDTA). Approximately 50 μL of each RNA sample was diluted with 450 μL of cold GRO binding buffer and incubated with 40 μL of equilibrated BrdU antibody beads. The reaction was incubated under slow rotation for 1.5 h at 4°C. Beads were spun down for 20 min at 1000*g* at 4°C. Beads were then resuspended in 200 μL of cold grinding buffer and transferred to a Millipore MC column (UFC30HVNB EMD Millipore). After a spin down for 1 min at 1000*g*, beads were washed twice with 500 μL of cold grinding buffer for 5 min under fast rotation at 4°C. Columns were then moved to fresh 1.5-mL tubes, and RNA was eluted with 200 μL of TRIzol LS under gentle shaking for 5 min at room temperature. After a second TRIzol elution, 100 μL of nuclease-free deionized water was added to the column and eluted. RNA was extracted using a TRIzol-based protocol following the manufacturer's recommendations. cDNA synthesis was performed as described previously (Roberts et al., 2015). A High-Capacity cDNA Reverse Transcription Kit (Thermo Fisher Scientific) was used for reverse transcriptase-mediated PCR. RT-qPCR analyses were performed in a CFX96 Touch Real-Time PCR detection system using Brilliant III Ultra-Fast SYBR Green qPCR Master Mix (Agilent Technologies). The primers used for nascent RNA detection span exon-intron boundaries in order to exclude the amplification of mature mRNA, which was also verified by the use of primers amplifying exon-exon boundaries. Nascent RNA primers for *ACT7* and *UBQ5* were used as controls. The expression data were analyzed using the $2^{-\Delta\Delta CT}$ method (Livak and Schmittgen, 2001). The primers used are listed in Supplemental Table 1.

Accession Numbers

Sequence data in this study can be found in the Arabidopsis Genome Initiative under the following accession numbers: *RVE8* (AT3G09600), *LNK1* (AT5G64170), *LNK2* (AT3G54500), *LNK3* (AT3G12320), *LNK4*

(AT5G06980), *SSRP1* (AT3G28730), *SPT16* (AT4G10710), *RNA Pol II* (AT4G35800), *TOC1* (AT5G61380), *PRR5* (AT5G24470), *ACT7* (AT5G09810), *UBQ5* (AT3G62250), *PPR* (AT5G55840), *IPP2* (AT3G02780), and *TA3* (AT1G37110).

Supplemental Data

Supplemental Figure 1. Characterization of ΔLCL-ox.

Supplemental Figure 2. Multiple Sequence Alignment of the LCL Domain Amino Acid Sequence in Plants.

Supplemental Figure 3. Phylogenetic Analysis of the Closest Homologs to RVE8.

Supplemental Figure 4. Characterization of LCL-ox.

Supplemental Figure 5. Direct Interaction of LNKs with the LCL Domain of RVE8 and Total RNA Pol II Accumulation at the *PRR5* and *TOC1* Loci.

Supplemental Figure 6. In Vitro Interaction of LNK1 with RNA Pol II and Binding of LNK1 and RVE8 to the *PRR5* and *TOC1* Loci.

Supplemental Figure 7. LNKs and SSRP1 Are Important for RNA Pol II Recruitment at Core Clock Loci.

Supplemental Figure 8. Analyses of RNA Pol II S5P and S2P Inhibition.

Supplemental Figure 9. Role of LNKs in the Regulation of *PRR5* and *TOC1* Transcript Synthesis.

Supplemental Table 1. Primers Used in This Study.

ACKNOWLEDGMENTS

We thank Sascha H.C. Duttke (University of California, San Diego) and Jonathan Hetzel (Salk Institute, La Jolla) for insightful details about the nascent RNAs protocol. We thank G.A. Pizzio for insightful comments on the manuscript. We also thank Tsuyoshi Nakagawa (Shimane University) for providing the Gateway binary vectors and Stacey Harmer for the *rve4/6/8* mutant. The K.D.G. laboratory is funded by the European Commission Marie Curie Research Training Network (ChIP-ET) and by the German Research Foundation through Grant Gr1159/14-1. The P.M. laboratory is funded by the Spanish Ministry of Economy and Competitiveness, from the European Regional Development Fund, from the Generalitat de Catalunya (AGAUR), from the Global Research Network of the National Research Foundation of Korea, from the European Commission Marie Curie Research Training Network (ChIP-ET), and by the CERCA Programme/Generalitat de Catalunya. We acknowledge financial support from the Spanish Ministry of Economy and Competitiveness through the "Severo Ochoa Programme for Centres of Excellence in R&D" 2016-2019 (SEV-2015-0533). Y.M. was supported by a PhD fellowship from the China Scholarship Council and S.G. by a Formación de Personal Investigador fellowship (Ministerio de Economía y Competitividad).

AUTHOR CONTRIBUTIONS

Y.M. and S.G. performed the experiments. K.D.G. provided reagents and constructive comments on the manuscript. P.M. designed the experiments, analyzed the data, and wrote the manuscript. All authors read, revised, and approved the research article.

Received February 27, 2018; revised April 2, 2018; accepted April 2, 2018; published April 4, 2018.

REFERENCES

Allison, L.A., Wong, J.K., Fitzpatrick, V.D., Moyle, M., and Ingles, C.J. (1988). The C-terminal domain of the largest subunit of RNA polymerase II of *Saccharomyces cerevisiae*, *Drosophila melanogaster*, and mammals: a conserved structure with an essential function. Mol. Cell. Biol. **8:** 321–329.

Antosz, W., et al. (2017). The composition of the Arabidopsis RNA polymerase II transcript elongation complex reveals the interplay between elongation and mRNA processing factors. Plant Cell **29:** 854–870.

Birse, C.E., Minvielle-Sebastia, L., Lee, B.A., Keller, W., and Proudfoot, N.J. (1998). Coupling termination of transcription to messenger RNA maturation in yeast. Science **280:** 298–301.

Bogomolovas, J., Simon, B., Sattler, M., and Stier, G. (2009). Screening of fusion partners for high yield expression and purification of bioactive viscotoxins. Protein Expr. Purif. **64:** 16–23.

Bordage, S., Sullivan, S., Laird, J., Millar, A.J., and Nimmo, H.G. (2016). Organ specificity in the plant circadian system is explained by different light inputs to the shoot and root clocks. New Phytol. **212:** 136–149.

Bradford, M.M. (1976). A rapid and sensitive method for the quantitation of microgram quantities of protein utilizing the principle of protein-dye binding. Anal. Biochem. **72:** 248–254.

Briggs, S.D., Bryk, M., Strahl, B.D., Cheung, W.L., Davie, J.K., Dent, S.Y.R., Winston, F., and Allis, C.D. (2001). Histone H3 lysine 4 methylation is mediated by Set1 and required for cell growth and rDNA silencing in *Saccharomyces cerevisiae*. Genes Dev. **15:** 3286–3295.

Buratowski, S. (2009). Progression through the RNA polymerase II CTD cycle. Mol. Cell **36:** 541–546.

Carré, I.A., and Kim, J.-Y. (2002). MYB transcription factors in the Arabidopsis circadian clock. J. Exp. Bot. **53:** 1551–1557.

Clough, S.J., and Bent, A.F. (1998). Floral dip: a simplified method for Agrobacterium-mediated transformation of *Arabidopsis thaliana*. Plant J. **16:** 735–743.

Ding, Y., Avramova, Z., and Fromm, M. (2011). Two distinct roles of ARABIDOPSIS HOMOLOG OF TRITHORAX1 (ATX1) at promoters and within transcribed regions of ATX1-regulated genes. Plant Cell **23:** 350–363.

Ding, Y., Ndamukong, I., Xu, Z., Lapko, H., Fromm, M., and Avramova, Z. (2012). ATX1-generated H3K4me3 is required for efficient elongation of transcription, not initiation, at ATX1-regulated genes. PLoS Genet. **8:** e1003111.

Du, H., Zhang, L., Liu, L., Tang, X.F., Yang, W.J., Wu, Y.M., Huang, Y.B., and Tang, Y.X. (2009). Biochemical and molecular characterization of plant MYB transcription factor family. Biochemistry (Mosc.) **74:** 1–11.

Dubos, C., Stracke, R., Grotewold, E., Weisshaar, B., Martin, C., and Lepiniec, L. (2010). MYB transcription factors in Arabidopsis. Trends Plant Sci. **15:** 573–581.

Duroux, M., Houben, A., Růzicka, K., Friml, J., and Grasser, K.D. (2004). The chromatin remodelling complex FACT associates with actively transcribed regions of the *Arabidopsis* genome. Plant J. **40:** 660–671.

Endo, M., Shimizu, H., Nohales, M.A., Araki, T., and Kay, S.A. (2014). Tissue-specific clocks in Arabidopsis show asymmetric coupling. Nature **515:** 419–422.

Farinas, B., and Mas, P. (2011). Functional implication of the MYB transcription factor RVE8/LCL5 in the circadian control of histone acetylation. Plant J. **66:** 318–329.

Gardner, K.E., Allis, C.D., and Strahl, B.D. (2011). Operating on chromatin, a colorful language where context matters. J. Mol. Biol. **409:** 36–46.

Gray, J.A., Shalit-Kaneh, A., Chu, D.N., Hsu, P.Y., and Harmer, S.L. (2017). The REVEILLE clock genes inhibit growth of juvenile and adult plants by control of cell size. Plant Physiol. **173:** 2308–2322.

Greenham, K., and McClung, C.R. (2015). Integrating circadian dynamics with physiological processes in plants. Nat. Rev. Genet. **16:** 598–610.

Hajheidari, M., Koncz, C., and Eick, D. (2013). Emerging roles for RNA polymerase II CTD in Arabidopsis. Trends Plant Sci. **18:** 633–643.

Hetzel, J., Duttke, S.H., Benner, C., and Chory, J. (2016). Nascent RNA sequencing reveals distinct features in plant transcription. Proc. Natl. Acad. Sci. USA **113:** 12316–12321.

Hsu, P.Y., Devisetty, U.K., and Harmer, S.L. (2013). Accurate timekeeping is controlled by a cycling activator in Arabidopsis. eLife **2:** e00473.

Hyun, Y., Richter, R., Vincent, C., Martinez-Gallegos, R., Porri, A., and Coupland, G. (2016). Multi-layered regulation of SPL15 and cooperation with SOC1 integrate endogenous flowering pathways at the Arabidopsis shoot meristem. Dev. Cell **37:** 254–266.

James, A.B., Monreal, J.A., Nimmo, G.A., Kelly, C.L., Herzyk, P., Jenkins, G.I., and Nimmo, H.G. (2008). The circadian clock in Arabidopsis roots is a simplified slave version of the clock in shoots. Science **322:** 1832–1835.

Jin, H., and Martin, C. (1999). Multifunctionality and diversity within the plant MYB-gene family. Plant Mol. Biol. **41:** 577–585.

Jones, D.T., Taylor, W.R., and Thornton, J.M. (1992). The rapid generation of mutation data matrices from protein sequences. Comput. Appl. Biosci. **8:** 275–282.

Jonkers, I., and Lis, J.T. (2015). Getting up to speed with transcription elongation by RNA polymerase II. Nat. Rev. Mol. Cell Biol. **16:** 167–177.

Komarnitsky, P., Cho, E.-J., and Buratowski, S. (2000). Different phosphorylated forms of RNA polymerase II and associated mRNA processing factors during transcription. Genes Dev. **14:** 2452–2460.

Kumar, S., Stecher, G., and Tamura, K. (2016). MEGA7: Molecular Evolutionary Genetics Analysis version 7.0 for bigger datasets. Mol. Biol. Evol. **33:** 1870–1874.

Lee, Y.C., Park, J.M., Min, S., Han, S.J., and Kim, Y.-J. (1999). An activator binding module of yeast RNA polymerase II holoenzyme. Mol. Cell. Biol. **19:** 2967–2976.

Livak, K.J., and Schmittgen, T.D. (2001). Analysis of relative gene expression data using real-time quantitative PCR and the 2(-Δ Δ C (T)) method. Methods **25:** 402–408.

Lolas, I.B., Himanen, K., Gronlund, J.T., Lynggaard, C., Houben, A., Melzer, M., Van Lijsebettens, M., and Grasser, K.D. (2010). The transcript elongation factor FACT affects Arabidopsis vegetative and reproductive development and genetically interacts with HUB1/2. Plant J. **61:** 686–697.

Malapeira, J., Khaitova, L.C., and Mas, P. (2012). Ordered changes in histone modifications at the core of the Arabidopsis circadian clock. Proc. Natl. Acad. Sci. USA **109:** 21540–21545.

Margaritis, T., and Holstege, F.C.P. (2008). Poised RNA polymerase II gives pause for thought. Cell **133:** 581–584.

Mason, P.B., and Struhl, K. (2005). Distinction and relationship between elongation rate and processivity of RNA polymerase II in vivo. Mol. Cell **17:** 831–840.

McCracken, S., Fong, N., Yankulov, K., Ballantyne, S., Pan, G., Greenblatt, J., Patterson, S.D., Wickens, M., and Bentley, D.L. (1997). The C-terminal domain of RNA polymerase II couples mRNA processing to transcription. Nature **385:** 357–361.

Menet, J.S., Rodriguez, J., Abruzzi, K.C., and Rosbash, M. (2012). Nascent-Seq reveals novel features of mouse circadian transcriptional regulation. eLife **1:** e00011.

Mizuno, T., Takeuchi, A., Nomoto, Y., Nakamichi, N., and Yamashino, T. (2014). The *LNK1* night light-inducible and clock-regulated gene is induced also in response to warm-night through the circadian clock nighttime repressor in *Arabidopsis thaliana*. Plant Signal. Behav. **9:** e28505.

Näär, A.M., Lemon, B.D., and Tjian, R. (2001). Transcriptional coactivator complexes. Annu. Rev. Biochem. **70:** 475–501.

Nakagawa, T., et al. (2007b). Improved Gateway binary vectors: high-performance vectors for creation of fusion constructs in transgenic analysis of plants. Biosci. Biotechnol. Biochem. **71:** 2095–2100.

Nakagawa, T., Kurose, T., Hino, T., Tanaka, K., Kawamukai, M., Niwa, Y., Toyooka, K., Matsuoka, K., Jinbo, T., and Kimura, T. (2007a). Development of series of Gateway binary vectors, pGWBs, for realizing efficient construction of fusion genes for plant transformation. J. Biosci. Bioeng. **104:** 34–41.

Nallamsetty, S., Austin, B.P., Penrose, K.J., and Waugh, D.S. (2005). Gateway vectors for the production of combinatorially-tagged His6-MBP fusion proteins in the cytoplasm and periplasm of *Escherichia coli*. Protein Sci. **14:** 2964–2971.

Nawrath, C., Schell, J., and Koncz, C. (1990). Homologous domains of the largest subunit of eucaryotic RNA polymerase II are conserved in plants. Mol. Gen. Genet. **223:** 65–75.

Ng, H.H., Robert, F., Young, R.A., and Struhl, K. (2003). Targeted recruitment of Set1 histone methylase by elongating Pol II provides a localized mark and memory of recent transcriptional activity. Mol. Cell **11:** 709–719.

Orphanides, G., LeRoy, G., Chang, C.-H., Luse, D.S., and Reinberg, D. (1998). FACT, a factor that facilitates transcript elongation through nucleosomes. Cell **92:** 105–116.

Perales, M., and Más, P. (2007). A functional link between rhythmic changes in chromatin structure and the Arabidopsis biological clock. Plant Cell **19:** 2111–2123.

Pérez-García, P., Ma, Y., Yanovsky, M.J., and Mas, P. (2015). Time-dependent sequestration of RVE8 by LNK proteins shapes the diurnal oscillation of anthocyanin biosynthesis. Proc. Natl. Acad. Sci. USA **112:** 5249–5253.

Preker, P., Nielsen, J., Kammler, S., Lykke-Andersen, S., Christensen, M.S., Mapendano, C.K., Schierup, M.H., and Jensen, T.H. (2008). RNA exosome depletion reveals transcription upstream of active human promoters. Science **322:** 1851–1854.

Rawat, R., Takahashi, N., Hsu, P.Y., Jones, M.A., Schwartz, J., Salemi, M.R., Phinney, B.S., and Harmer, S.L. (2011). REVEILLE8 and PSEUDO-REPONSE REGULATOR5 form a negative feedback loop within the Arabidopsis circadian clock. PLoS Genet. **7:** e1001350.

Roberts, T.C., Hart, J.R., Kaikkonen, M.U., Weinberg, M.S., Vogt, P.K., and Morris, K.V. (2015). Quantification of nascent transcription by bromouridine immunocapture nuclear run-on RT-qPCR. Nat. Protoc. **10:** 1198–1211.

Rodriguez, J., Tang, C.H., Khodor, Y.L., Vodala, S., Menet, J.S., and Rosbash, M. (2013). Nascent-Seq analysis of Drosophila cycling gene expression. Proc. Natl. Acad. Sci. USA **110:** E275–E284.

Rugnone, M.L., Faigón Soverna, A., Sanchez, S.E., Schlaen, R.G., Hernando, C.E., Seymour, D.K., Mancini, E., Chernomoretz, A., Weigel, D., Más, P., and Yanovsky, M.J. (2013). LNK genes integrate light and clock signaling networks at the core of the Arabidopsis oscillator. Proc. Natl. Acad. Sci. USA **110:** 12120–12125.

Shukla, A., Chaurasia, P., and Bhaumik, S.R. (2009). Histone methylation and ubiquitination with their cross-talk and roles in gene expression and stability. Cell. Mol. Life Sci. **66:** 1419–1433.

Smolle, M., and Workman, J.L. (2013). Transcription-associated histone modifications and cryptic transcription. Biochim. Biophys. Acta **1829:** 84–97.

Takahashi, N., Hirata, Y., Aihara, K., and Mas, P. (2015). A hierarchical multi-oscillator network orchestrates the Arabidopsis circadian system. Cell **163:** 148–159.

Thain, S.C., Murtas, G., Lynn, J.R., McGrath, R.B., and Millar, A.J. (2002). The circadian clock that controls gene expression in Arabidopsis is tissue specific. Plant Physiol. **130:** 102–110.

Van Lijsebettens, M., and Grasser, K.D. (2014). Transcript elongation factors: shaping transcriptomes after transcript initiation. Trends Plant Sci. **19:** 717–726.

Vermeulen, M., Mulder, K.W., Denissov, S., Pijnappel, W.W.M.P., van Schaik, F.M.A., Varier, R.A., Baltissen, M.P.A., Stunnenberg, H.G., Mann, M., and Timmers, H.T.M. (2007). Selective anchoring of TFIID to nucleosomes by trimethylation of histone H3 lysine 4. Cell **131:** 58–69.

Wenden, B., Toner, D.L.K., Hodge, S.K., Grima, R., and Millar, A.J. (2012). Spontaneous spatiotemporal waves of gene expression from biological clocks in the leaf. Proc. Natl. Acad. Sci. USA **109:** 6757–6762.

Wu, Z., Ietswaart, R., Liu, F., Yang, H., Howard, M., and Dean, C. (2016). Quantitative regulation of FLC via coordinated transcriptional initiation and elongation. Proc. Natl. Acad. Sci. USA **113:** 218–223.

Xie, Q., et al. (2014). LNK1 and LNK2 are transcriptional coactivators in the Arabidopsis circadian oscillator. Plant Cell **26:** 2843–2857.

Xie, Z., and Grotewold, E. (2008). Serial ChIP as a tool to investigate the co-localization or exclusion of proteins on plant genes. Plant Methods **4:** 25.

Xin, H., Takahata, S., Blanksma, M., McCullough, L., Stillman, D.J., and Formosa, T. (2009). yFACT induces global accessibility of nucleosomal DNA without H2A-H2B displacement. Mol. Cell **35:** 365–376.

Xing, H., Wang, P., Cui, X., Zhang, C., Wang, L., Liu, X., Yuan, L., Li, Y., Xie, Q., and Xu, X. (2015). LNK1 and LNK2 recruitment to the evening element require morning expressed circadian related MYB-like transcription factors. Plant Signal. Behav. **10:** e1010888.

Yakir, E., Hassidim, M., Melamed-Book, N., Hilman, D., Kron, I., and Green, R.M. (2011). Cell autonomous and cell-type specific circadian rhythms in Arabidopsis. Plant J. **68:** 520–531.

Zhang, E.E., and Kay, S.A. (2010). Clocks not winding down: unravelling circadian networks. Nat. Rev. Mol. Cell Biol. **11:** 764–776.

Zielinski, T., Moore, A.M., Troup, E., Halliday, K.J., and Millar, A.J. (2014). Strengths and limitations of period estimation methods for circadian data. PLoS One **9:** e96462.

Targeted Recruitment of the Basal Transcriptional Machinery by LNK Clock Components Controls the Circadian Rhythms of Nascent RNAs in Arabidopsis

Yuan Ma, Sergio Gil, Klaus D. Grasser and Paloma Mas

Plant Cell 2018;30;907-924; originally published online April 4, 2018;
DOI 10.1105/tpc.18.00052